ABSTRACT

Title of Document:	USING RADIO-FREQUENCY IDENTIFICATION TECHNOLOGY TO MEASURE ASPHALT COOLING
	Grant Howard Pfeiffer, Master of Science, 2010
Directed By:	Associate Professor, Dr. Charles W. Schwartz, Department of Civil and Environmental Engineering

Realistic prediction of asphalt temperatures as a function of time during paving is essential for optimizing compaction operations. Continued compaction after the asphalt lift has dropped below a critical threshold temperature may result in particle breakage and degradation of the material properties. To address this issue, this study evaluates the feasibility of using Surface Acoustic Wave (SAW) based Radio-Frequency Identification (RFID) technology to measure HMA temperatures via wireless sensors during paving. The survivability and temperature measurement capabilities of the SAW RFID sensors are demonstrated in the field. The measured asphalt cooling curves (temperature versus time) are compared with predictions from previously developed theoretical models for mat cooling. The prediction accuracy of these models is improved via a field calibration procedure using measured temperatures from the SAW RFID sensors. The predictions from the calibrated theoretical model are reasonable and agree well with the measured temperatures in the field.

USING RADIO-FREQUENCY IDENTIFICATION TECHNOLOGY
TO MEASURE ASPHALT COOLING

By

Grant Howard Pfeiffer

Thesis submitted to the Faculty of the Graduate School of the
University of Maryland, College Park, in partial fulfillment
of the requirements for the degree of
Master of Science
2010

Advisory Committee:

      Dr. Charles W. Schwartz (Chair)
      Dr. Dimitrios G. Goulias
      Dr. Ahmet H. Aydilek

This page has been intentionally left blank.

Dedication

To my family, thank you for everything.

To the Professors of the Institute, thank you for the inspiration.

To Melanie, thank you for your love and guidance during this academic venture.

"No one ever stumbled over a mountain."

– *My Father*

Table of Contents

List of Tables

List of Figures

Chapter 1: Introduction

Since the late 1960s, there has been an initiative to model hot-mix asphalt (HMA) temperatures as a function of time to optimize compaction effort. Compacting asphalt, in conventional terms, is a densification process where the volume of air in an HMA mixture is reduced by external loading (commonly a vibratory steel-drum roller). By reducing air voids via mechanical vibration, the asphalt aggregate is reoriented to a more condensed formation. It has been widely recognized that compaction is a decisive factor in flexible pavement performance. Achieving optimal compaction for any particular mix is mostly dependent on temperature (for a given asphalt viscosity) and compactive effort.

Modeling these temperatures as a function of time allows one to gauge if the temperature of the in-place HMA is sufficiently high for the period of time necessary to complete compaction. This is particularly useful in areas with shorter construction seasons and has been an outlet for developmental research. Inadequate compaction may result in reduced pavement stiffness, fatigue life, and durability.

It is the objective of this thesis to evaluate traditional asphalt "mat" cooling models in conjunction with a study performed with the Federal Highway Administration Pooled-Fund Study on Intelligent Compaction (TGI, 2010). More specifically, the objectives of the study are as follows:

1. Evaluate the feasibility of using Surface Acoustic Wave (SAW) based Radio-Frequency Identification (RFID) technology to measure HMA temperatures via wireless sensors.

2. Demonstrate, in the field, the survivability and temperature measurement capabilities of the SAW RFID sensors during a pavement overlay.

3. Consolidate data and perform a regression analysis to develop asphalt cooling curves (temperature versus time); compare the results with previously developed (traditional) mat cooling models.

4. Perform a sensitivity analysis on input parameters that affect the traditional mat cooling models when comparing to the measured asphalt cooling curves. In addition, calibrate, via the sensitivity analysis, input parameters that provide reasonable and close agreement with the field measured temperatures.

Any conclusions drawn from these analyses are presented herein. In addition, any techniques or recommendations to further improve the usage of the traditional models or testing equipment are also presented.

This thesis shall be presented in seven chapters:

Chapter 1 – Introduction

States the objective of the thesis and presents a brief background to the topic of the study. In addition, also presents the framework for the body of the thesis.

Chapter 2 – Previous Work (Literature Review)

This chapter discusses a literature review of several journal articles and technical reports. The topics reviewed include mat cooling models, thermophysical properties of asphalt, and other parameters.

Chapter 3 – Applying RFID Technology in Pavements

This chapter discusses previous work applying RFID technology in pavement construction and provides background information on the SAW RFID technology used in this study.

Chapter 4 – Laboratory Evaluation

This chapter discusses the laboratory evaluation of the SAW RFID technology. More specifically, the chapter includes an evaluation of the readability, usability, and survivability of the equipment in preparation for field evaluation.

Chapter 5 – Field Evaluation

This chapter discusses the field evaluation of the SAW RFID technology. The field evaluation was performed on a MDSHA project site in Frederick, Maryland. The primary focus of the field evaluation is to demonstrate the usability of the SAW RFID technology and to develop measured asphalt mat cooling curves.

Chapter 6 – Comparisons Between Measured and Predicted Mat Cooling Response

This chapter discusses a comparison between the traditional mat cooling models (from Chapter 2) with the experimental cooling curves obtained through field evaluation (Chapter 5). In addition, this chapter presents a calibration, performed via a sensitivity analysis, on mat cooling model input parameters that may provide a reasonable and close agreement with the field measured temperatures.

Chapter 7 – Conclusions and Lessons Learned

This chapter presents a summary of conclusions, lessons learned, and recommendations for future studies involving RFID technology in pavements.

Chapter 2: Previous Work (Literature Review)

A literature review of all previous work related to the development mat cooling models was performed. Although numerous journal articles and technical reports were reviewed, only the most relevant to the present study are referenced herein. A significant number of these sources are based on work originally performed by J.S. Corlew and P.F. Dickson (University of Toledo, Ohio).

2.1. J.S. Corlew and P.F. Dickson, 1968

In 1968, Corlew and Dickson (Corlew and Dickson, 1968) performed a pioneering study to develop methods of predicting HMA temperatures, as a function of time, from when the asphalt leaves the paver to the end of compaction. The objective of this study was to explore ways to reduce the seasonality effects on HMA paving. In other words, the study aimed to provide a method of evaluating marginal and adverse environmental conditions with respect to optimizing HMA compaction. The authors intended for their work to minimize paving failures due to inadequate compaction while guiding further experimental research.

Corlew and Dickson developed their mat cooling model based on the principles of one-dimensional transient heat flow. These principles are illustrated in Figure 2.1. Transient heat flow is described by a partial differential equation (PDE) relating temperature (T), time (t), and depth (y).

$$\frac{\partial T}{\partial t} = \alpha \frac{\partial^2 T}{\partial y^2} \qquad (2.1)$$

The parameter α in Eq. (2.1) is thermal diffusivity – the ability of any given material to conduct thermal energy compared to its ability to store thermal energy. Thermal diffusivity is defined as:

$$\alpha = \frac{k}{\rho \, C_p} \tag{2.2}$$

in which k is the thermal conductivity of the material, ρ is material density, and C_p is the specific heat. Units for thermal diffusivity are area per unit of time (e.g. square-feet per hour).

Corlew and Dickson offer an analytical solution to the PDE. However, they state that the interaction of various modes of thermal-energy transfer at the pavement surface is more accounted for in a numerical solution (Corlew and Dickson, 1968).
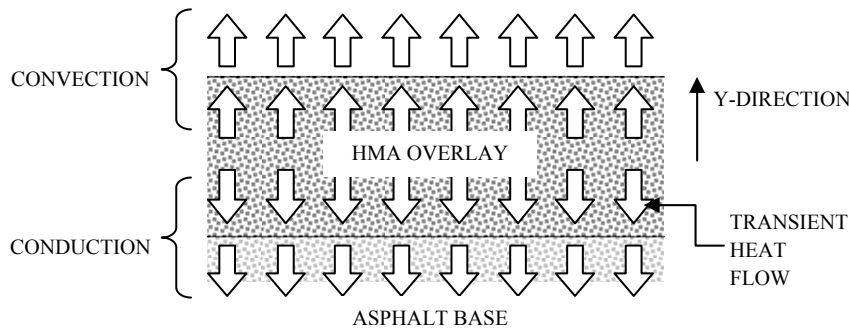
Figure 2.1 – Cross-section of an HMA overlay indicating directional flow of thermal energy

Figure 2.1 illustrates one-dimensional transient heat flow involving conduction through the mat and convection from the surface. Conduction is the heat transfer mechanism for a solid material in an energy transfer from a high-temperature region to a low-temperature region, according to Fourier's law of heat conduction. Convection is defined as the heat transfer

5

mechanism from a solid to either a liquid or gas at a surface. Convection is governed by

Newton's law of cooling (Holman, 2001).
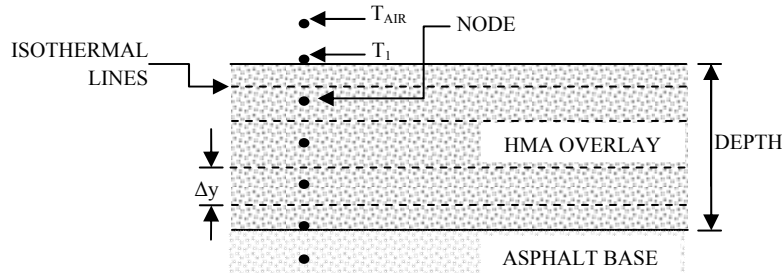
Figure 2.2 – Typical incremental elements of HMA overlay used in numerical solution

Figure 2.2 illustrates the numerical solution scheme for transient heat flow analysis. The

pavement thickness is divided into sublayers (sections divided by isothermal lines) and the PDE

in Eq. (2.1) is approximated using finite difference equations at the nodes (midpoints of each

sublayer). As shown in Figure 2.2, the nodes extend from the pavement surface boundary

through some depth of the asphalt base to the lower boundary. The boundary conditions consist

of a constant ambient air temperature (T_{AIR}) above the surface of the overlay and a constant base

temperature at the bottom of the analysis domain. The lower boundary is set at a sufficient depth

where conduction no longer affects the temperature of the base material over the duration of the

transient analysis. Equations (2.3) and (2.4) are the finite difference formulation of the heat

balance for conduction within the mat:

$$\frac{\partial T}{\partial t} = \alpha\ \frac{\partial^2 T}{\partial y^2} = \alpha \left(\frac{T_{i+1,j} - 2T_{ij} + T_{i-1,j}}{\Delta y^2} \right) = \frac{T_{i,j+1} - T_{ij}}{\Delta t} \qquad (2.3)$$

Rearranged to solve for $T_{i,j+1}$:

$$T_{i,j+1} = \frac{\alpha \, \Delta t}{\Delta y^2} \left[T_{i+1,j} - 2T_{ij} + T_{i-1,j} \right] + T_{ij} \qquad (2.4)$$

in which i is the node number, j is the time step, and T_{ij} is the temperature (°F) at node i and time j. Please note that the notation used in these equations is not identical to that presented by Corlew and Dickson.

These one-dimensional conduction equations are used to calculate temperatures within both the HMA overlay and asphalt base. Corlew and Dickson point out that the thermal diffusivity might be different for the two materials. However, this difference is expected to be small for most asphalt mixtures, and therefore for the purposes of this study, the thermal diffusivity shall be assumed uniform for the overlay and base material.

Similarly to conduction, convection is based on an energy balance equation:

$$(2.5)$$

$$T_{i,j+1} = T_{ij} \left[1 - \frac{2 \, \alpha \, \Delta t}{\Delta y^2} (N_{Bi} + 1) \right] + \frac{2 \, \alpha \, \Delta t}{\Delta y^2} (T_{i+1,j} + N_{Bi} \, T_{AIR}) + \underbrace{\frac{2 \, \alpha \, \Delta t}{k \, \Delta y} (a \, H_S - \varepsilon \, \sigma \, T'^4_{ij})}_{\text{Radiation Term}}$$

in which i is the node number, j is the time step, and T_{ij}, is the temperature (°F) at node i and time j, N_{Bi} is the Biot number (described below), k is thermal conductivity (BTU/ft^2-hr-(°F/ft)), T_{AIR} is the ambient air temperature (°F), a is solar absorptivity, H_S is solar heat flux (BTU/ft^2-hr), ε is emissivity, σ is the Stefan-Boltzman constant – 1.713 x 10^{-9} (BTU/ft^2-hr-°R^4), and T'_{ij} is the temperature (°R) at node i and time j.

The Biot number, N_{Bi}, is a dimensionless value commonly used in transient heat flow and mass transfer analysis (Holman, 2001). It is the ratio of heat transfer resistances *within* and *at the surface* of a mass undergoing convection. This number indicates whether temperatures within the body will vary significantly in space while the mass heats or cools over time due to thermal energy transfers at its surface. Mathematically, the Biot number is defined as (Holman, 2001):

$$N_{Bi} = \frac{h\,s}{k} \tag{2.6}$$

The convective heat transfer coefficient, h, in Eq. (2.6) relates convective heat flow with temperature difference and surface area (Newton's law of cooling). The effective length, s, is the ratio between volume and surface area, and k is the thermal conductivity. The radiation term in Eq. (2.5) includes parameters that account for the absorption of radiant solar energy (a H_S), and for radiant energy emitted by the pavement ($\varepsilon\,\sigma\,T_{ij}^{4}$).

Corlew and Dickson developed a computer program to simulate mat cooling based on this finite difference formulation. In addition, they performed field experiments to validate their models. Their field experimentation involved embedding thermocouples through the depth of an HMA overlay to measure mat cooling versus time. The purpose of the experimentation was to provide data for comparing actual temperatures to temperatures predicted by their modeling. Wind velocity, ambient air temperature, initial base temperature, solar radiation, and overlay thickness were also measured in their experiments.

Corlew and Dickson's testing found close correlations between actual and predicted temperatures. The following figure displays a sample of the test results from their field experimentation; Test No. 67-2, Evanston, Lyman (Corlew and Dickson, 1968):
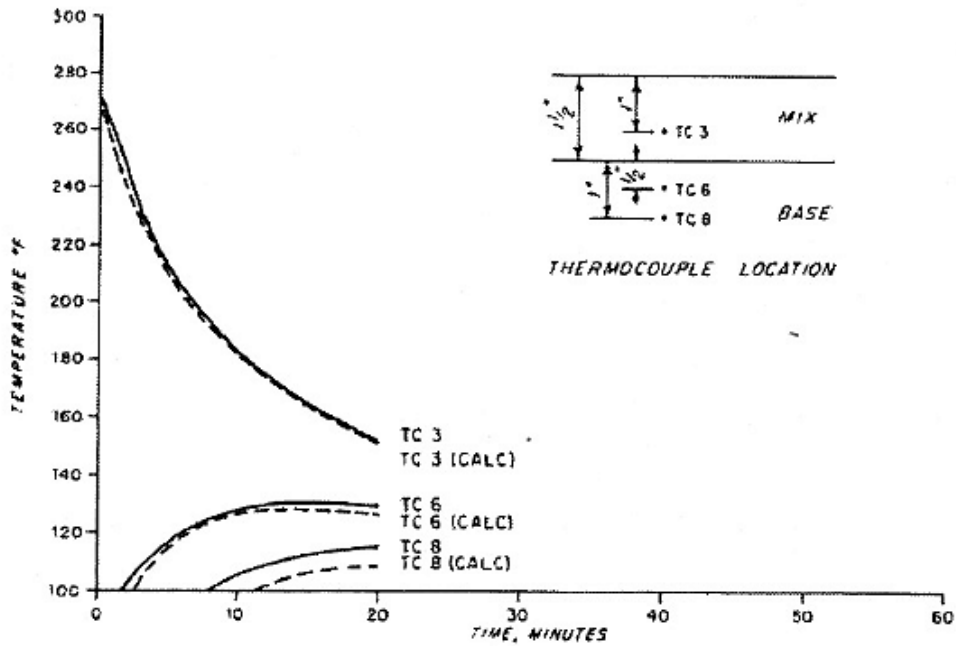
Figure 2.3 – Sample of Corlew and Dickson's test results (1968)

As shown above, there are close correlations between the measured curves and predicted curves (thermocouple or "TC" versus thermocouple-calculated or "TC (CALC)"). Note that "TC 3" was measured within the hot-mix asphalt while "TC 6" and 'TC 8" were measured within the base material.

Corlew and Dickson's computer program has been historically viewed as successful, provided that input parameters that best represent site conditions are used. Wolfe and Colony (1976) of the FHWA tested and confirmed Corlew and Dickson's computer procedure. However, as with all models, there are limitations due to the simplified PDE boundary conditions

and the assumption of constant physical properties. Nonetheless, in terms of mat cooling,

Corlew and Dickson's study suggested the following:

1. When considering proper environmental conditions, modeling mat cooling is feasible and
    accurate using finite difference analysis techniques.

2. The heat flux from the overlay into the underlying base layer is initially greater than the
    heat flux into the atmosphere. Therefore, the lower region of the overlay expels heat
    faster than the upper region. However, Jordan and Thomas (1976) found that with
    increasing time the cooling of the surface becomes dominant.

2.2. R.K. Wolfe and D.C. Colony, 1976, 1978, and 1983

Wolfe and Colony (1976) expanded on Corlew and Dickson's method and converted the

mat cooling models to a format that is suitable for a portable hand-held computer and for tabular

and graphical summary. In addition, they constructed a device that could be used during adverse

weather conditions to determine if compaction is feasible. However, the focus of this literature

review shall be on the development of their mat cooling model.

In an attempt to streamline the conductive heat flow calculation (Eq. 2.3), Wolfe and

Colony utilized "Saul'yev's Method for Conduction," a numerical technique based on forward

and backward finite differences. Saul'yev's method requires less memory than that needed by

Corlew and Dickson's formulation and thus was ideal for the comparatively primitive hand-held

computers available in the 1970s. Wolfe and Colony also developed an explicit form of

convective heat transfer energy balance at the mat surface.

Wolfe and Colony's finite difference energy balance equations are as follows:

$$(2.7)$$

$$-\varepsilon \sigma A (T_{ij} + 460)^4 + a H_S + \frac{k A (T_{i-1,j} - T_{ij})}{\Delta y} - h A (T_{ij} - T_{AIR}) = \frac{1}{2} \frac{A \Delta y \rho C_p (T_{i,j+1} - T_{ij})}{\Delta t}$$

In other words, there are energy losses due to radiation and convection, and a gain from solar energy and surface temperature. Eq. (2.7) can then be rearranged to solve for the temperature at the next time step, $T_{i,j+1}$:

$$(2.8)$$

$$T_{i,j+1} = T_{ij} + \frac{2 h \alpha \Delta t}{k \Delta y} (T_{AIR} - T_{ij}) + 2 \alpha \frac{\Delta t}{\Delta y^2} (T_{i-1,j} - T_{ij}) + \frac{2 a \alpha \Delta t H_S}{k \Delta y} - \frac{2 \varepsilon \sigma \alpha \Delta t}{k \Delta y} (T_{ij} + 460)^4$$

in which i is the node number, j is the time step, and T_{ij} is the temperature (°F) at node i and time j, h is the convective heat transfer coefficient (BTU/ft^2-hr-°F), k is thermal conductivity (BTU/ft^2-hr-(°F/ft)), T_{AIR} is the ambient air temperature (°F), a is solar absorptivity, A is pavement surface area, H_S is solar heat flux (BTU/ft^2-hr), ε is emissivity, σ is the Stefan-Boltzman constant – 1.713 x 10^{-9} (BTU/ft^2-hr-°R^4), and T'$_{ij}$ is the temperature (°R) at node i and time j.

Eqs. (2.4) and (2.8) are used in this study as the finite difference solution for conduction and convection. In other words, these equations shall be used as the "traditional mat cooling model" for comparison with the measured cooling curves in Chapter 5.

In addition to the numerical methods, Wolfe and Colony also present a thorough discussion of heat transfer mechanisms and thermophysical properties to be used as input parameters for the equations. These input parameters include the convective heat transfer coefficient (h), solar heat flux (H_S), and others.

2.2.1. Convective heat transfer coefficient (h)

According to Wolfe and Colony (1976 and 1978), for an open highway construction environment, both free and forced convection principles should be included when calculating the convective heat transfer coefficient. Free convection occurs when there is no wind velocity impact, as opposed to forced convection that includes wind velocity.

After studying various methods for determining the convective heat transfer coefficient h and performing laboratory tests (as described below), Wolfe, Colony, and Heath (1983) recommend for free convection that

$$h = 1.30 \qquad\qquad (2.9a)$$

when the wind velocity is less equal to zero miles per hour. When the wind velocity greater than zero miles per hour, they recommend the following relation for forced convection:

$$h = 1.3 + 0.62\,(V)^{3/4} \qquad\qquad (2.9b)$$

in which V is the wind velocity in miles/hour.

2.2.2. Solar heat flux (H$_S$)

Wolfe and Colony (1976) state that solar heat flux emitted by the sun can range up to about 400 BTU per hour at local solar noon. However, it is dependent on the time of the year,

the sun's declination, and location (latitude) of the surface being considered. Wolfe and Colony suggest the following equation for estimating solar heat flux (Wolfe and Colony, 1978):

$$H_S = R_i\,(1 - NW/100)$$

<div align="right">(2.10)</div>

in which R_i = incident radiation (direct and diffuse, in BTU/ft – hr); N = cloud base factor, which varies from 0.80 to 0.90; and W = percentage could cover, which is visually estimated. The value for incident radiation is obtained from historical data. The authors, however, offer a graph of solar heat flux versus time for incident radiation in Ohio between 38°–50' and 42°–00' latitude (the location of their study).

Alternative methods for determining solar heat flux have been proposed in the literature. Voller *et al*. (1998) performed a computer–modeling study for HMA cooling similar to Wolfe and Colony's. Rather than modifying solar radiation for cloud effects and cover, radiation is quantified in terms of the effective sky temperature (Kreith, 1980).

2.2.3. Other Thermophysical Properties

Wolfe and Colony (1976), based on a review of several sources, recommend the following material property values for asphaltic mixtures:

Table 2.1 – Thermophysical Properties, Wolfe and Colony, 1976

Property	Units	Symbol	Suggested	Min. Value	Max. Value
Thermal conductivity	BTU/ft^2-hr-(°F/ft)	k	0.80	0.58	1.01
Thermal diffusivity	ft^2/hr	α	0.0215	0.0215	0.0337
Absorptivity	Dimensionless	a	0.85	0.85	0.90
Emissivity	Dimensionless	ε	0.95	0.90	0.95
Stefan-Boltzman constant	BTU/ft^2-hr-°R^4	σ	1.713 x 10^{-9}	N/A	N/A

Wolfe and Colony performed a simulation study to generate mat cooling curves (temperature versus time) for different environmental conditions. Their objective was to generate cooling curves that could be compiled in a book for use in the field as well as to demonstrate that their numerical techniques were suitable for programming on a hand-held computer. The hand-held computer program could be used to generate unique cooling curves for individual project sites.

In 1979, Wolfe, Colony, and Heath (1983), performed laboratory and then field tests to demonstrate that their numerical techniques correlated favorably to measured mat cooling curves. The laboratory tests were performed to measure temperatures near and at the interface of newly placed HMA and its base layer. The laboratory tests involved designing and constructing a thermocouple temperature probe in a controlled environmental chamber with the capability of simulating wind effects. The results were generally positive with an acceptable percentage of error, justifying use of a similar probe in the field trials.

The field trials were performed in November 1979 at a project site in Ohio. The field instrumentation at the project site included: a radiation pyrometer to measure base surface temperatures, a pyrheliometer to measure solar insolation, an anemometer to measure wind speed, temperature probes (similar to those evaluated in the laboratory tests) for measuring temperatures within the mat, and recording devices. The field test measured temperatures near and at the interface of the newly placed HMA and its base layer. Surface temperatures were also measured but were dismissed due to instrumental inaccuracies. The field test found generally close correlations between calculated and measured temperatures. Figure 2.4 displays a sample of their comparative analysis between field-measured values and calculated values; average asphalt temperature versus time and calculated average temperature versus time:

Air Temperature   46 °F (8 °C)
Base Temperature   46 °F (8 °C)
Initial Asphalt Temperature   305 °F (152 °C)
Air Velocity   5 mph (2.24 m/s)
Insolation   80 Btu/($ft^2 \cdot h$) (252 J/($m^2 \cdot s$))
Mat Thickness   1·/4 inches (32 mm)
Thermal Conductivity   1.01 Btu/($ft \cdot °F \cdot h$) (1.75 J/($m \cdot °C \cdot s$))
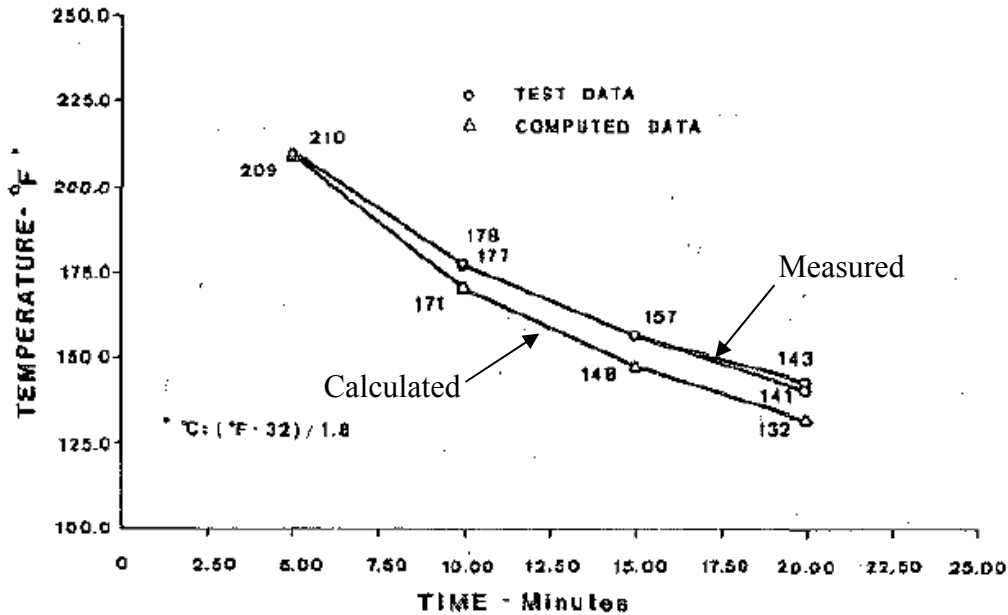
Figure 2.4 – Sample of Wolfe, Colony, and Heath's test results (1983)

Wolfe, Colony, and Heath determined, based on laboratory and field trial results (as shown in the above figure), that their predictive equations were adequate for the purpose of making "go/no-go" decisions in the field for placing and compacting HMA under adverse site conditions. Specific findings from the study included the following:

1. Based on the simulation results, solar radiation and cloud cover are not major influences on the placement of HMA. In other words, solar radiation should not be considered in making a "go/no-go" decision in the field.

15

2. The convective heat transfer coefficient is relatively difficult to measure in the field. There are numerous equations and experimental methods to estimate this parameter. However, the study generally confirmed the recommendations in Eq. (2.9) for this value.

3. Prior to the actual paving, the surface of the base material is subjected to heat from the paver as it passes. The authors suggest that, depending on the speed of the paver (and if it pauses), the interface temperature between the asphalt and base material may not be accurate. Temperatures should be recorded once the paver passes the test area.

2.3. Joseph Luca and Donath Mrawira, 2005

Luca and Mrawira (2005) performed a series of experiments to identify the thermal properties of Superpave asphalt-concrete. Through laboratory testing, they evaluated thermal diffusivity, α, and thermal conductivity, k, and compared their measured values with values reported previously in the literature. When comparing their measured values with the literature, the results are generally favorable; the values fit within a general range of 1.35×10^{-2} to 3.20×10^{-2} (ft^2/hr) for thermal diffusivity and 0.70 to 2.24 (BTU/ft-hr-°F) for thermal conductivity. The authors highlight that these parameters are generally difficult to measure. Tables 2.2 and 2.3 summarize Luca and Mrawira's findings.

Table 2.2 – Comparison of Thermal Diffusivity Values, Luca and Mrawira, 2005

Author	Year	Thermal Diffusivity, α, x 10^{-2} (ft^2/hr)
Luca and Mrawira	2005	1.56 – 2.13
Wolfe et al.	1980	1.99 – 3.20
Tan et al.	1997	2.07 – 2.24
Highter and Wall	1984	1.35 – 2.90
Corlew and Dickson	1968	2.27

16

Table 2.3 – Comparison of Thermal Conductivity Values, Luca and Mrawira, 2005

Author	Year	Thermal Conductivity, k, (BTU/ft-hr-°F)
Luca and Mrawira	2005	0.94 – 1.19
Wolfe et al.	1980	0.58 – 1.01
Tan et al.	1997	2.07 – 2.24
Highter and Wall	1984	0.75 – 0.82
Corlew and Dickson	1968	0.70

Chapter 3: Applying RFID Technology in Pavements

This chapter reviews recent research applications of RFID technology to HMA pavements. It also introduces the RFID equipment used in this study and provides a preface to their laboratory and field experimentation. The previously performed research was conducted by Schwartz and Khan (2008) using ultra high frequency (UHF) RFID technology, whereas the equipment used in this study is based on SAW RFID technology.

3.1. UHF RFID Technology

The study reported in this thesis is a continuation of the work performed by Schwartz and Khan (2008). Their work focused on improving the quality control of pavement construction by using RFID technology to track the placement of HMA during construction. The principal objective of this work was to provide a foolproof and non-intrusive method for linking material properties measured at the HMA production plant to pavement performance data on the roadway collected as part of pavement management activities.

The RFID technology employed in their study involved encoding a digital signature on a small microchip attached to a copper foil antenna – the "RFID tag." This passive tag receives energy from radio waves transmitted by a "RFID tag reader"; the tag harvests this incoming radio frequency energy to transmit back to the reader its encoded digital signature. These RFID tags, even though small, may be read several yards away from the reader's antenna. The primary objectives of Schwartz and Khan's study were to evaluate the feasibility of using UHF RFID tags in laboratory asphalt specimens and in the field during paving construction.

Schwartz and Khan also performed a literature review to determine the previous applications of RFID technology in construction. They found that RFID technology is widely used today for supply chain inventory management, security, equipment tracking, among others. However, in terms of construction, RFID technology is primarily used for tracking equipment and materials. General surveys of RFID applications in construction are provided by Jaselskis et al (1995), Jaselskis and El-Misalami (2003), and Sawyer (2004).

The laboratory tests and field trials performed by Schwartz and Khan consistently demonstrated the successful use of the RFID technology within HMA specimens and in-field placement. The primary findings of their study are as follows:

- The RFID tags should be encapsulated in an epoxy material as protection from thermal and physical damage.

- During the laboratory trials, the RFID tags were successfully read at ranges of several feet from antenna even while being encapsulated in epoxy and within HMA samples. During the field trials, 60-80% of the tags were successfully read after being paved and compacted in the mat.

- The application of RFID technology allows for minimal intrusion in the usual paving construction sequence.

3.2. SAW RFID Technology

As stated in Chapter 1, it is one of the objectives of this study to evaluate the feasibility of using SAW based RFID technology to measure HMA temperatures. SAW based RFID sensors are inherently capable of measuring and transmitting temperatures as well as a digital signature. This is in contrast to the conventional RFID technology used by Schwartz and Khan,

which was capable only of transmitting digital signatures. In addition, the SAW RFID technology is inherently capable of operating successfully at lower energy inputs than the conventional silicon-based integrated circuit RFID technology. Figure 3.1 provides an overview of the SAW RFID technology (RF SAW, 2010).
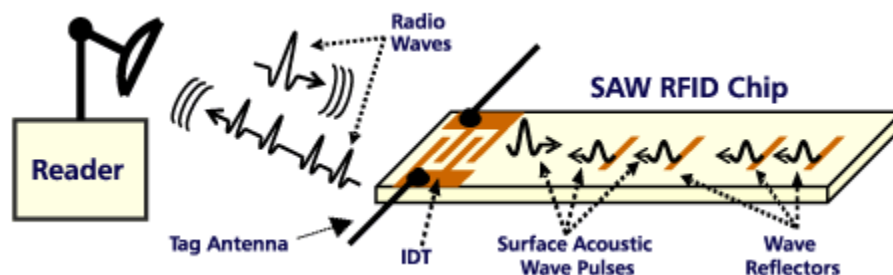
Figure 3.1 – Overview of the SAW RFID system (RF SAW, 2010)

As shown above, the SAW RFID tag consists of an interdigital transducer (IDT) and a series of acoustic reflector traps etched into a piezoelectric substrate. The tag reader emits a radio wave pulse to the IDT that is converted piezoelectrically into a nanoscale acoustic wave. The wave travels past the reflectors to produce a unique pattern of reflected pulses. These travel back to the IDT, where they are piezoelectrically converted into an encoded radio wave reply signal to the reader. The SAW chip operates in a purely passive mode and does not require supplementary DC power (i.e., battery).

Overall, the principal advantages of this technology for pavement construction include better inherent ruggedness, smaller formats, and longer read ranges for a given tag antenna size as compared to conventional RFID. Unlike conventional RFID tags, the incoming radio-frequency (RF) signal does not need to be converted to a direct current in SAW RFID. Therefore, the incoming RF signal strength does not need to exceed the minimum threshold

required for the rectifier operation. This is the principal theoretical reason for the inherently longer read ranges in the SAW RFID technology. Also, as stated before (and most relevant to this study), it is capable of wireless measurement of temperature.

The SAW RFID technology inherently measures temperature via the perturbation of the return wave signal caused by the influence of thermal strains on the spacing of the acoustic reflectors. The equipment manufacturer (RF-SAW Inc.) reports a tag temperature range of -100°C to over 200°C, more than adequate for HMA pavement applications.

Chapter 4: Laboratory Evaluation

To evaluate the suitability of SAW RFID technology for pavement applications, a series of laboratory tests were performed to demonstrate the following:

- An encapsulation process with a thermally conductive epoxy that will promote the transfer of thermal energy while protecting the tag from physical damage.

- A read range study that illustrates the signal strength/readability of the SAW RFID tags. The read range study includes testing for tag orientation (including rotation) to the antenna and position/distance from the antenna.

- A thermal sensitivity study that analyzes the thermal response of the tags, when exposed to elevated temperatures. More specifically, this study evaluates the time required for a tag to "heat up" and equilibrate to the temperature of the surrounding material/environment.

The following sections of this chapter detail the laboratory tests performed to evaluate the SAW RFID equipment used in this study.

4.1. Tag Encapsulation

Encapsulating the RFID tags with a thermally conductive epoxy protects them from paving and compaction stresses while only minimally interfering with heat transfer during mat cooling. Similarly, the work performed by Schwartz and Khan (2008) also included encapsulating their UHF RFID tags to survive thermal and physical damage during testing. The encapsulation media selected for this study is Durapot 865™ epoxy from Cotronics, Inc. This encapsulant has a thermal conductivity of about 1 BTU/hr-°F-ft and is electrically insulating. To

put this parameter into perspective: the thermal conductivity of copper is about 230, standard

epoxy is about 0.20, and asphalt is about 0.433 BTU/hr-°F-ft. For thermal diffusivity, copper is

about 4.89, standard epoxy is about 0.0012, and asphalt is about 0.015 ft^2/hr (material properties

sourced from www.engineeringtoolbox.com). It is a two-component epoxy (resin and hardener)

that cures at room temperature. The following encapsulation procedure was followed:

- The epoxy resin component is preheated for about 40 minutes at 50°C to reduce its
  viscosity.

- The epoxy components are then combined at 100 parts resin to 21 parts hardener and
  thoroughly mixed.

- The wooden mold (fabricated in advance) is lined with standard kitchen plastic wrap
  secured using masking tape.

- A layer of epoxy is poured at the bottom of the mold prior to tag placement to create a
  thin protective base layer.

- The tag is placed in the mold on top of the bottom epoxy layer and pressed downward
  into the encapsulant. The tag is then covered in the epoxy to completely encase it.

- The wood mold, with epoxy and tag, is then placed in a vacuum dessicator to remove any
  air-pockets in the epoxy.

- After removing the air and curing for 24 hours, the tags are removed and sanded for
  smoothness.

Figure 4.1 provides photographs of the unencapsulated tags used in this study. As will be

described more fully later, the larger tag on the left of Figure 4.1 is the single patch antenna tag

(with larger receiving antenna) approximately 1¾-inch by 1¾-inch in size. The tag on the right

is the monopole antenna tag approximately 1/3-inch by 1¾-inch in size. Figure 4.2 shows

photographs of the encapsulated tags prior to final sanding. Both the unencapsulated and encapsulated tags were evaluated in the read range and thermal sensitivity studies.
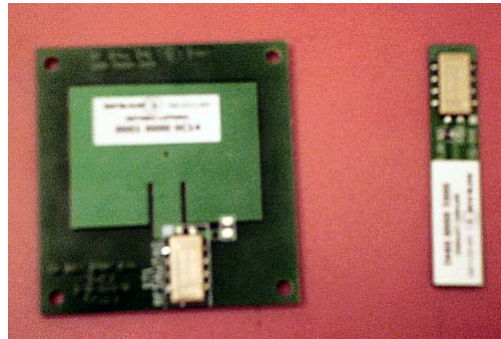
Figure 4.1 – Unencapsulated RFID tags (left: single patch, right: monopole)
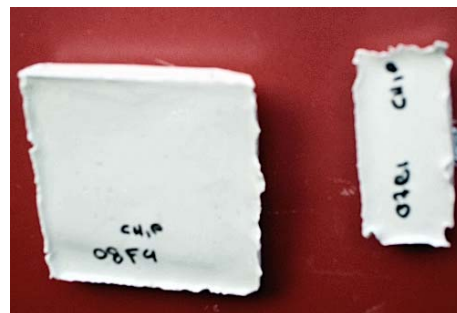
Figure 4.2 – Encapsulated RFID tags (left: single patch, right: monopole)

4.2. Signal Strength and Readability

A series of read range tests were performed to evaluate the signal strength and readability of the RFID tags in both the monopole and single patch antenna configurations. The monopole and single patch tag antennae differ primarily in the shape of their RF field distributions (for transmission) and sensitivities (for reception).

The monopole antenna is formed by replacing half of its dipole antenna with a ground plane, normal to the antenna axis. If the ground plane is sufficiently large, the monopole

24

behaves like a dipole with its reflection in the ground plane providing the missing symmetric

half. As shown in Figure 4.3, a dipole antenna has a toroidal field strength/sensitivity

distribution with omnidirectional field strength/sensitivity in the midplane, normal to the antenna

axis and dead zones at the ends of the dipole.
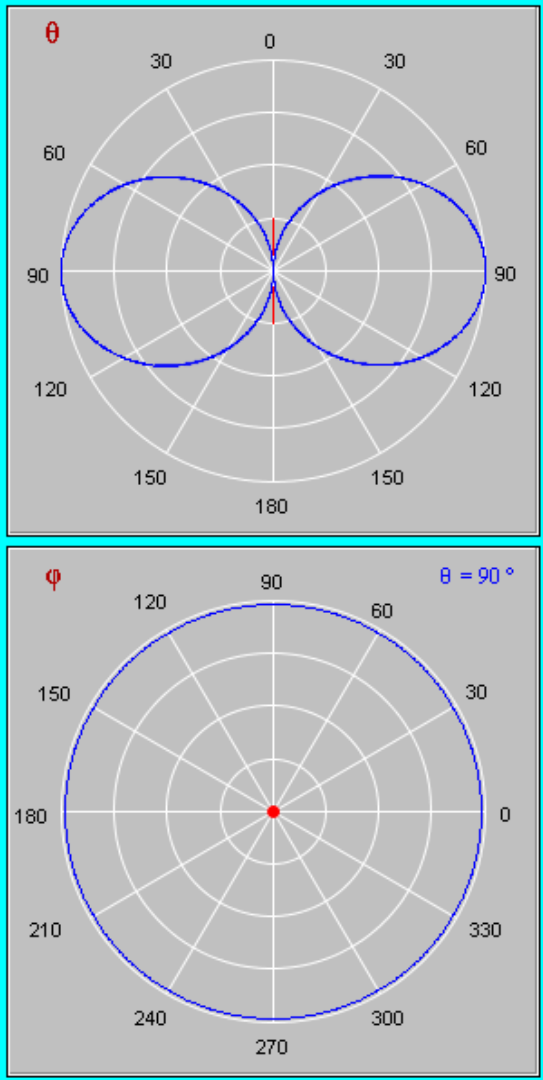
Figure 4.3 – RF field distribution for dipole antenna. Top figure is antenna plan view; bottom figure is along antenna axis (from http://www.amanogawa.com/archive/antennaA.html)

Patch antennae, on the other hand, are designed for a more directional RF

radiation/sensitivity. Its simple patch antenna consists of a metal patch one half-wavelength

long, separated by a constant thickness over a ground plane. The ground plane is typically only

modestly larger than the active patch. The simple patch antennae of this type radiate a linearly

polarized wave. The typical radiation pattern for a linearly-polarized patch antenna is shown in

plan view in Figure 4.4. The beam width angle is about 65°. An infinitely-large ground plane

would prevent any radiation toward the back of the antenna. But, with the more usual small

ground plane, power loss through the back side of the antenna is about -20 dB, as compared to

the front side.
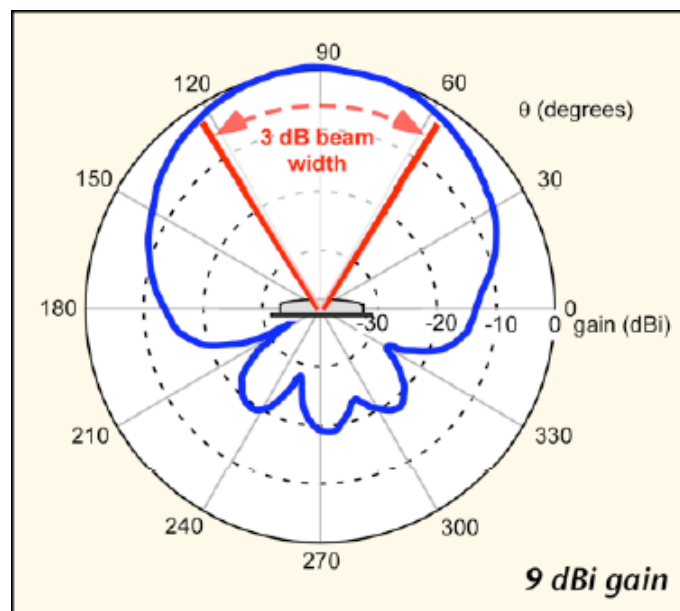
Figure 4.4 – RF field distribution for patch antenna (plan view—from Wikipedia)

Two types of reader antennae were supplied by the manufacturer – linearly and circularly

polarized antennae. Both reader antenna types were evaluated for the following tag

26

configurations: unencapsulated tags in air, encapsulated tags in air, and encapsulated tags in an asphalt specimen.

4.2.1. Unencapsulated Tags in Air

To determine the full read range capacity of the naked, unaltered/undisturbed RFID tags, an "open-floor" read range study was performed. The following tables illustrate the read range capacity for the unencapsulated tags in air. Each cell within the table represents a foot interval of lateral offset of distance ahead of the antenna. Note that the antenna is fixed one foot away from the test grid in front of cells L-A and R-A. For example, cell "-2, B" is located two feet to the left and three feet ahead of the face of the antenna. The numbers in each cell are the number of read responses from the tag at that location during a twenty-second interval.

A uniform tag orientation was utilized throughout this study; the tag was affixed to the back of a plastic board, antenna orientated vertically, facing towards the antenna (unless otherwise noted). Tables 4.1 and 4.2 display the results of the read range study performed on a single patch tag using a linearly polarized antenna and circularly polarized antenna, respectively. The green cells indicate strong reliable readings, yellow are more unpredictable, and red are zero or unlikely readings.

Table 4.1 – Unencapsulated Single Patch Tag, Linear Polarization

	-4	-3	-2	-1	L	R	1	2	3	0
A	0	0	0	32	53	56	0	0	0	0
B	0	0	0	34	51	48	33	0	0	0
C	0	0	0	32	50	53	33	0	0	0
D	0	0	23	33	48	49	5	32	0	0
E	0	0	32	0	50	50	33	0	0	0
F	0	0	17	0	52	50	38	0	0	0
G	0	12	0	17	34	52	34	0	0	0
H	0	0	0	29	33	52	33	27	0	0

Table 4.2 – Unencapsulated Single Patch Tag, Circular Polarization

	-4	-3	-2	-1	L	R	1	2	3	0
A	0	0	0	0	57	32	31	0	0	0
B	0	0	0	49	47	32	0	0	0	0
C	0	0	32	33	51	32	3	0	0	0
D	0	0	32	33	49	34	0	0	0	0
E	0	4	8	48	45	49	0	0	0	0
F	0	3	0	49	44	48	0	0	0	0
G	0	0	1	47	45	45	0	0	0	0
H	0	0	26	35	49	34	27	0	0	0

Tables 4.3 and 4.4 summarize the read range results for unencapsulated monopole tags using a linearly and circularly polarized antenna.

28

Table 4.3 – Unencapsulated Monopole Tag, Linear Polarization

	-4	-3	-2	-1	ANTENNA L	R	1	2	3	0
A	0	0	0	0	33	32	0	0	0	0
B	0	0	0	0	31	33	0	0	0	0
C	0	0	0	17	33	32	0	0	0	0
D	0	0	0	0	33	33	0	0	0	0
E	0	0	0	0	32	32	11	0	0	0
F	0	0	0	0	31	32	27	0	0	0
G	0	0	0	0	33	33	26	0	0	0
H	0	0	0	0	32	32	22	0	0	0

Table 4.4 – Unencapsulated Monopole Tag, Circular Polarization

	-4	-3	-2	-1	ANTENNA L	R	1	2	3	4
A	0	0	0	0	30	30	0	0	0	0
B	0	0	0	4	32	32	4	0	0	0
C	0	0	0	14	33	32	0	0	0	0
D	0	0	0	0	33	32	8	0	0	0
E	0	0	0	17	33	31	8	0	0	0
F	0	0	4	17	33	32	12	0	0	0
G	0	0	0	18	33	33	14	0	0	0
H	0	0	8	16	31	32	16	0	0	0

Comparing these four tables, it is apparent that the single patch tags have a stronger readability than the monopole tags, in terms of the number of reads and the width of the readable zone ahead of the antenna. This is due to the larger size and higher sensitivity of their antennae. However, all of the unencapsulated tags (patch and monopole) exhibited read ranges greater than eight feet in air.

4.2.2. Encapsulated Tags in Air

Similar read range testing was performed on encapsulated tags. The tags were encapsulated in thermally conductive epoxy to protect them from damage due to the asphalt paver and compactor. Tables 4.5 and 4.6 summarize the measured read ranges for the encapsulated single patch tag using linear and circular reader antenna polarization. Tables 4.7 and 4.8 summarize similar results for the encapsulated monopole tag using linear and circular polarization.

Table 4.5 – Encapsulated Single Patch Tag, Linear Polarization

	-4	-3	-2	-1	L	R	1	2	3	0
A	0	0	0	0	33	33	0	0	0	0
B	0	0	0	14	32	33	0	0	0	0
C	0	0	0	18	33	33	0	0	0	0
D	0	0	0	0	32	33	0	0	0	0
E	0	0	0	0	33	33	0	0	0	0
F	0	0	0	0	33	33	0	0	0	0
G	0	0	0	0	32	32	0	0	0	0
H	0	0	0	0	30	32	4	0	0	0

(Column L and R are under the ANTENNA heading.)

Table 4.6 – Encapsulated Single Patch Tag, Circular Polarization

	-4	-3	-2	-1	ANTENNA L	ANTENNA R	1	2	3	4
A	0	0	0	0	31	29	0	0	0	0
B	0	0	0	0	31	29	0	0	0	0
C	0	0	0	2	32	31	0	0	0	0
D	0	0	0	0	33	31	0	0	0	0
E	0	0	0	12	33	33	4	0	0	0
F	0	0	0	22	33	33	16	0	0	0
G	0	0	0	21	32	33	0	0	0	0
H	0	0	0	7	32	31	0	0	0	0

Table 4.7 – Encapsulated Monopole Tag, Linear Polarization

	-4	-3	-2	-1	ANTENNA L	ANTENNA R	1	2	3	0
A	0	0	0	0	10	10	0	0	0	0
B	0	0	0	0	11	35	0	0	0	0
C	0	0	0	0	0	18	0	0	0	0
D	0	0	0	0	0	0	0	0	0	0
E	0	0	0	0	0	0	0	0	0	0
F	0	0	0	0	0	0	0	0	0	0
G	0	0	0	0	0	0	0	0	0	0
H	0	0	0	0	0	0	0	0	0	0

Table 4.8 – Encapsulated Monopole Tag, Circular Polarization

	-4	-3	-2	-1	**ANTENNA** L	R	1	2	3	4
A	0	0	0	0	6	7	0	0	0	0
B	0	0	0	0	14	7	0	0	0	0
C	0	0	0	0	12	23	0	0	0	0
D	0	0	0	6	0	8	0	0	0	0
E	0	0	0	0	0	6	4	0	0	0
F	0	0	0	0	0	0	0	0	0	0
G	0	0	0	0	0	0	0	0	0	0
H	0	0	0	0	0	0	0	0	0	0

Overall, based on the above tables, it is again apparent that the single patch tags have a stronger readability than the monopole tags. In addition, the polarization of the reader antenna also has an influence on read performance. A linearly polarized antenna will have more directionality than the circularly polarized antenna. This means that, all else being equal, the linearly polarized antenna will have better read performance for some orientations of the tag (relative to the plane of the antenna polarization) and worse read performance for others as compared to the circularly polarized antenna. The circularly polarized antenna will in general have slightly lower read performance but with much less sensitivity to tag vs. antenna orientation. As a result, for the sake of readability, all subsequent testing is conducted using only the circularly polarized reader antenna.

It is also apparent from these tables that while encapsulating the RFID tags within epoxy increases their likelihood of survival in the field, it is detrimental to their readability in air.

Based on the read range results, the encapsulated monopole tags are likely to perform marginally for field use while the encapsulated patch tags are anticipated to perform well.

4.2.3. Encapsulated Tags within Asphalt

In an effort to simulate survivability and readability under field conditions, the SAW tags were placed in HMA (about 400°F) and compacted in a gyratory compactor. All specimens were compacted at about 600 kPa using over 150 gyrations. Initially, unencapsulated patch and monopole tags were positioned in specimens to evaluate their inherent survivability. Two of three unencapsulated tags were destroyed during compaction. Therefore, all subsequent tags evaluated in this read range study were encapsulated in thermally conductive epoxy.

The encapsulated tags were placed near the center of the gyratory plugs. As shown in Figure 4.5, a variety of tag orientations were explored to determine which would provide the best readability. In addition to these orientations, the encapsulated tags were also rotated about the cylinder's axis to evaluate any further signal disturbance. Figure 4.6 depicts the rotational positions of the asphalt sample.
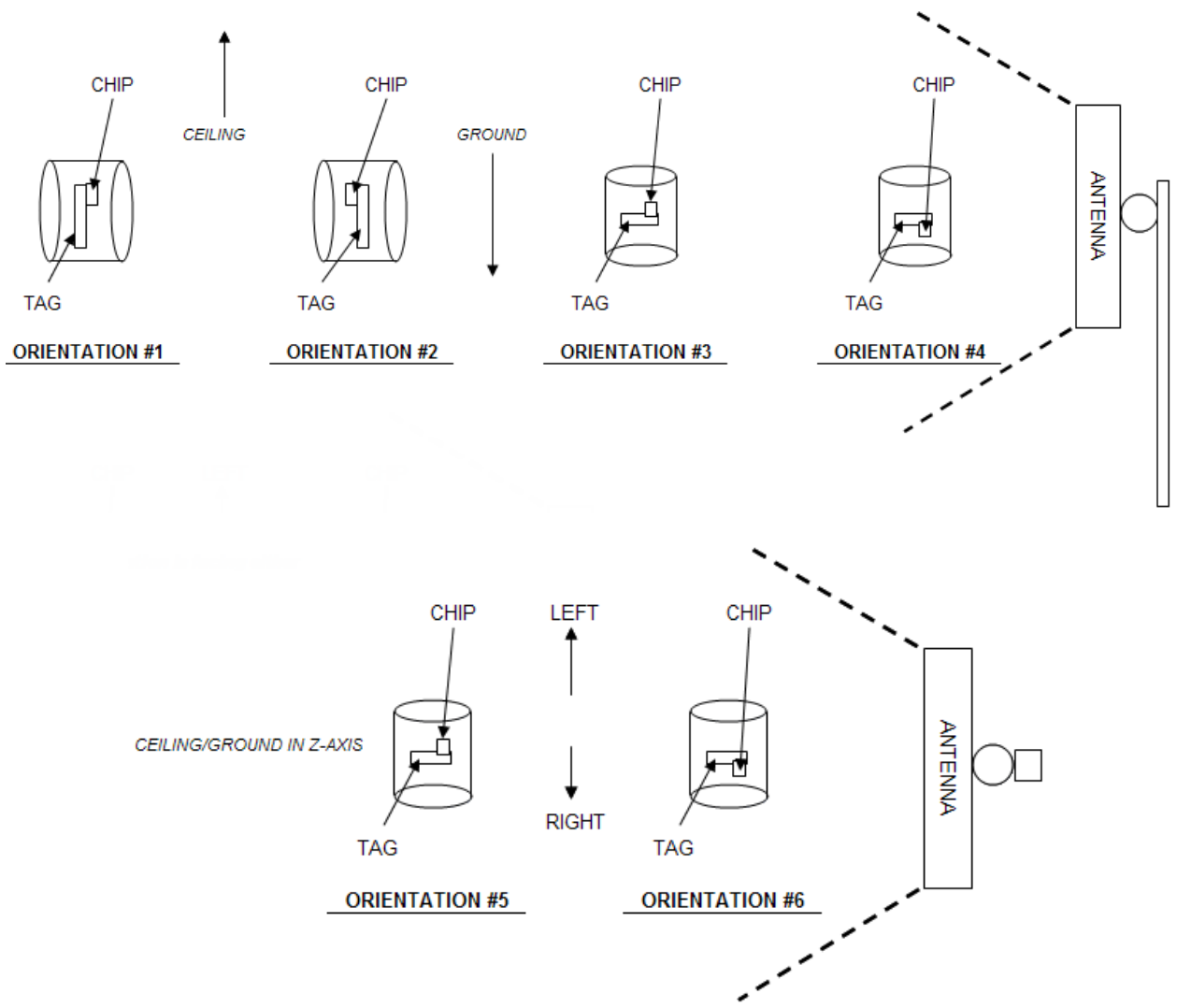
Figure 4.5 – Orientation guide for tags within asphalt specimens

PLAN VIEW OF SPECIMEN
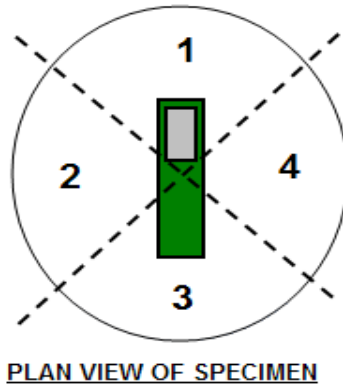
Figure 4.6 – Rotation scheme for tags within asphalt specimens (monopole and single patch)

Overall, the testing revealed that the strongest signal strength and readability was produced in orientation #1 (face side of the tag facing the antenna) for both the single patch and monopole tags. In this orientation, rotation #1 (Figure 4.6) provided the best and most consistent results. Figures 4.7 and 4.8 summarize the testing results for orientation #1 for both the monopole and single patch tags. Note that the single patch tag read up to about twelve feet from the antenna using this orientation. Orientations #2 and #4 were also considered strong and reliable. For the monopole tag, orientations #4 and #6 performed very well. Based on a comparison between Figures 4.7 the read range Tables 4.7 and 4.8, the readability of the monopole increased from encapsulating it in epoxy to placing the encapsulated tag within an asphalt specimen. In order to explain this phenomenon, further research is required. Additional figures summarizing these read range tests are included in an appendix.
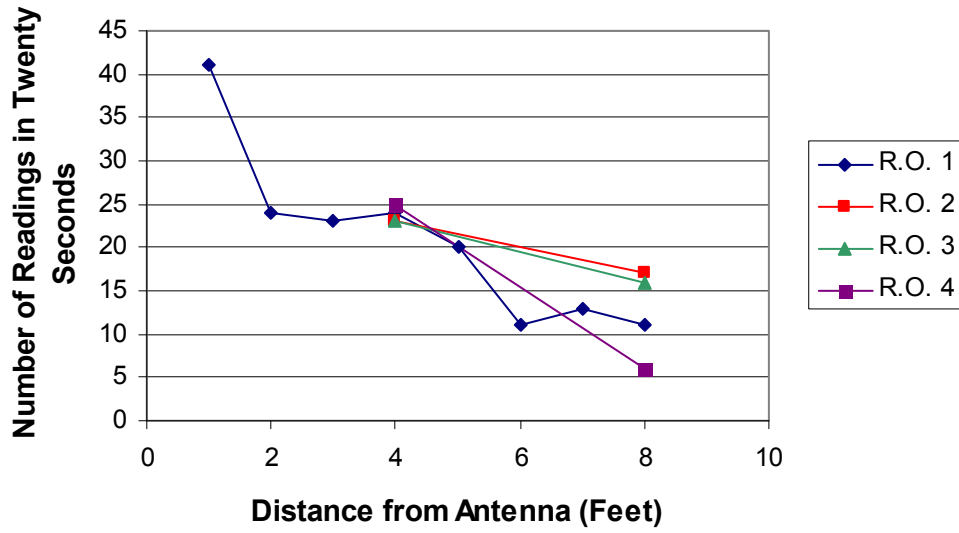
Figure 4.7 – Orientation #1 for monopole tag using circular polarization (R.O. = rotational orientation)
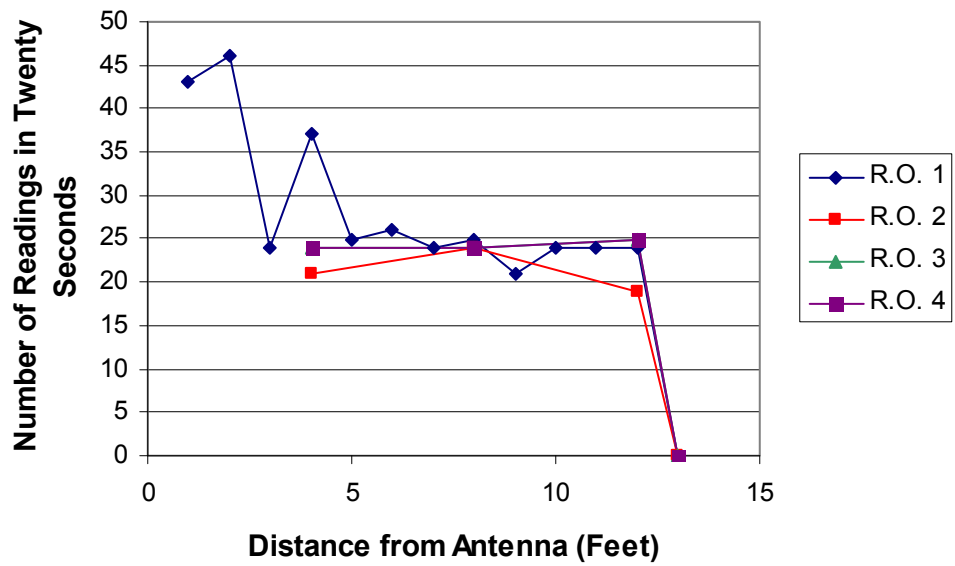
Figure 4.8 – Orientation #1 for single patch tag using circular polarization (R.O. = rotational orientation)

4.3. Conclusions: Signal Strength and Readability

Overall, both the encapsulated monopole and patch antenna tags showed acceptable performance when encased in HMA. The monopole tags, while more practical and compact in size, do not perform as reliably as the patch tags in terms of signal strength and readability. Based on the entire laboratory read performance testing, both the monopole and patch tags warrant further investigation in field trials. Since they are to be pre-positioned ahead of the asphalt paver, they can be placed in the optimum orientation #1/rotational position #1.

4.4. Thermal Sensitivity

In order to simulate field conditions within a laboratory, the testing apparatus shown in Figure 4.9 was developed for measuring the temperature sensitivity and transient response of the SAW RFID tags. As shown in the figure, the SAW RFID tags were pre-positioned on a flat wood plank covered in foil (to sustain temperatures and increase signal strength) and exposed to pre-heated materials. The selected materials used for testing included generically graded asphalt aggregate and HMA with about five percent binder content by weight. These materials were pre-heated to about 140-170°C (284-338°F) and placed over the test tag at room temperature. Upon exposure, tag temperatures were recorded over time (minutes) via the RF SAW computer software. Independent temperature measurements were collected using a Fluke thermocouple probe affixed to the foil adjacent to the tag. Because our initial small supply of SAW RFID tags was limited, the tags tested here were the same as those used previously for the survivability and read performance testing; they were recovered from the gyratory plugs after the completion of the survivability testing.
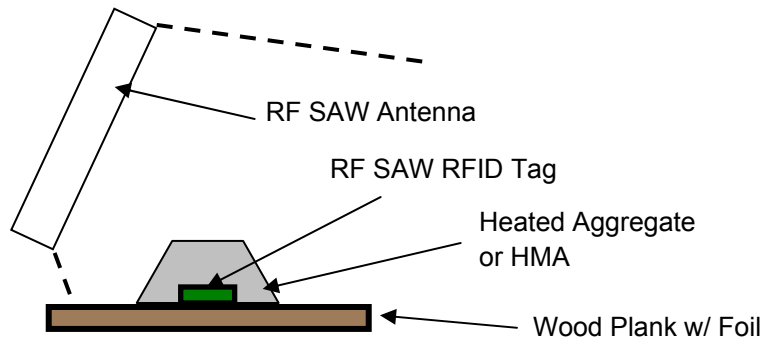
Figure 4.9 – Thermal testing apparatus

Table 4.9 describes the tags used for this study. Figures 4.10 through 4.12 summarize the thermal sensitivity study results for hot aggregate material. Time zero corresponds to ambient (room temperature) conditions immediately before covering the RFID tag and Fluke thermocouple with the hot aggregate. The test results show that the unencapsulated monopole tag (Tag 0A21—Figure 4.10) quickly matches the temperature readings from the thermocouple. The encapsulated monopole tag (Tag 0443—Figure 4.11) requires about five to six minutes to reach aggregate temperature, as measured by the thermocouple. This is assumed to be due to the additional thermal mass and low thermal conductivity from the encapsulating epoxy. This is even more pronounced for the encapsulated patch tag (Tag 09FE—Figure 4.12) due to its larger format and corresponding larger mass of encapsulating epoxy. Even after six minutes the encapsulated patch was 40°C cooler than the reference measurement. Note that no unencapsulated patch tag was evaluated in this thermal study because it had been destroyed in the gyratory compactor during the first stage of the testing.

Table 4.9 - Tags Employed in Thermal Testing

Tag Name	Type	Encapsulated
0A21	Monopole	No
0443	Monopole	Yes
09FE	Single Patch	Yes
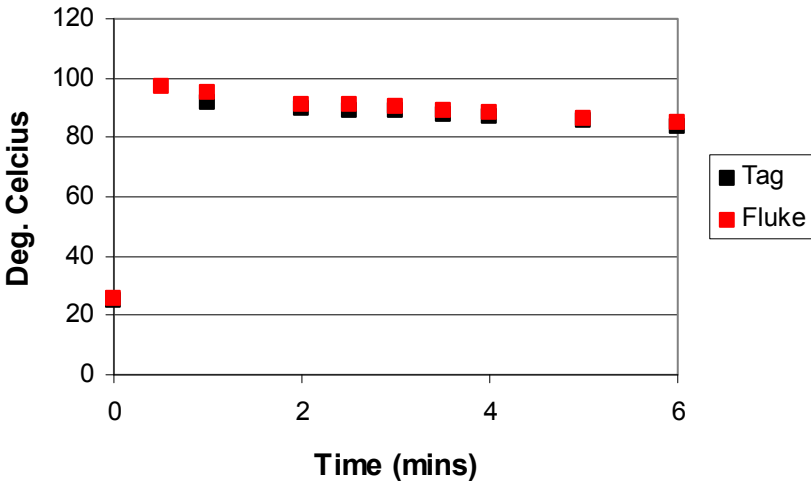
Figure 4.10 – Thermal response from Tag 0A21 using hot aggregate
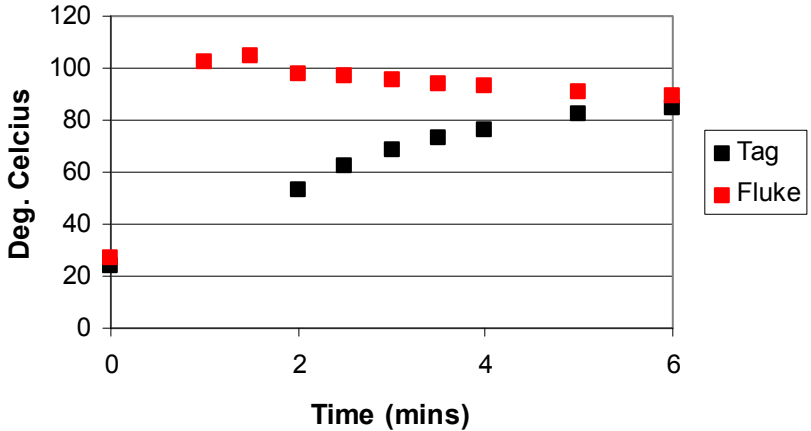
Figure 4.11 – Thermal response from Tag 0443 using hot aggregate
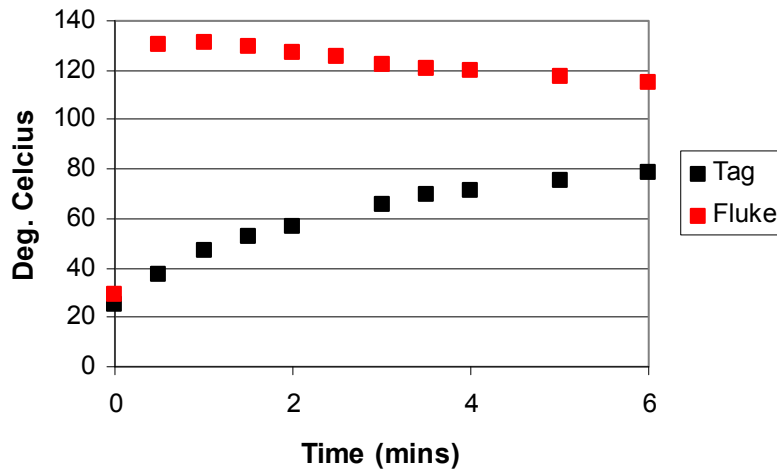
Figure 4.12 – Thermal response from Tag 09FE using hot aggregate

Figures 4.13 through 4.15 summarize the thermal sensitivity study results for the HMA material. Similar conclusions can be drawn here as for the hot aggregate: the unencapsulated monopole tag responds quickly and accurately; the encapsulated monopole tag responds with an acceptable time delay; and the encapsulated patch tag responds much more slowly, requiring approximately six to eight minutes to reach thermal equilibrium. This thermal lag may prove to be detrimental for field use.

Once the tags have equilibrated from the initial thermal shock (i.e., starting at ambient temperature and being covered with 140-170°C HMA), they then match the thermocouple measurements for the continued slow cooling with time. This is most evident for the monopole tags (Figure 4.13 and 4.14); readings were not continued for a long enough time period to completely confirm this for the encapsulated single patch tag (Figure 4.15).
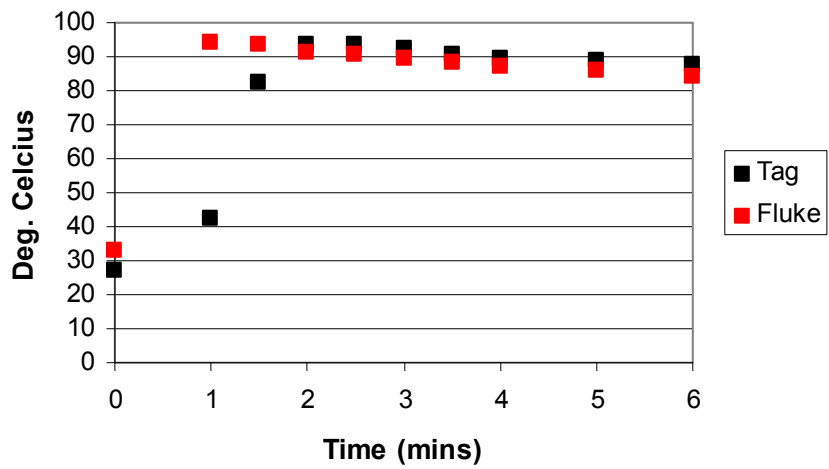
Figure 4.13 – Thermal response from Tag 0A21 using hot asphalt
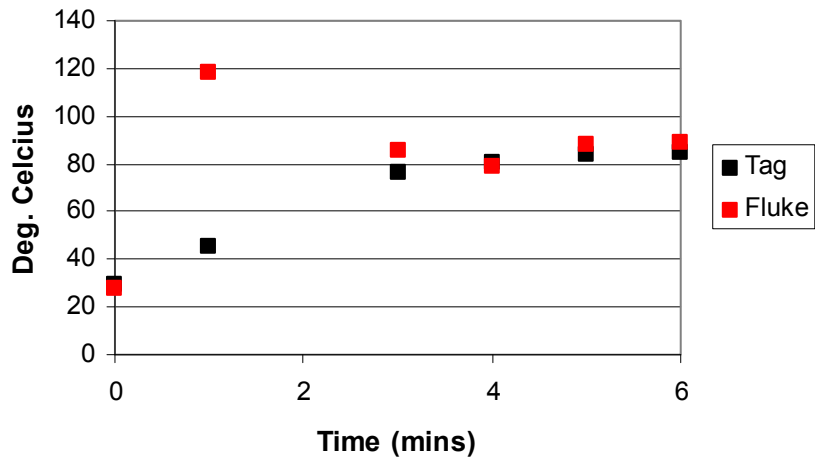
Figure 4.14 – Thermal response from Tag 0443 using hot asphalt
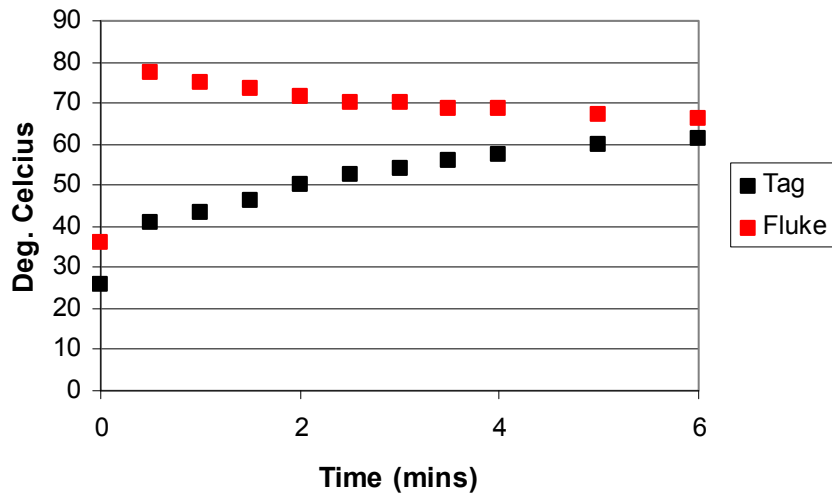
Figure 4.15 – Thermal response from Tag 09FE using hot asphalt.

4.5. Conclusions: Thermal Sensitivity

Overall, the thermal sensitivity study suggests that, given an adequate amount of time from asphalt exposure to compaction, all of the tested SAW RFID tags have transient thermal response sufficiently rapid for field use. The unencapsulated monopole tag performed more effectively than the others. Nonetheless, further field evaluation of all of the tags is justified.

Chapter 5: Field Evaluation

In conjunction with the FHWA Intelligent Compaction Pooled Fund Study (TGI, 2010), field trials were conducted to evaluate the suitability of SAW RFID technology for wireless measurement of in-place HMA temperatures during compaction. These trials, hosted by the Maryland State Highway Administration (MDSHA), were conducted on July 23, 2009 during placement of a 1½-inch pavement overlay of United States Route 15/Maryland Route 340 in Frederick County, Maryland.

5.1. Site Information

The project site for the field trials was located on United States Route 15/Maryland Route 340 in Frederick County, Maryland. More specifically, the site was located in the outer (right) northbound lane between Mt. Zion Road and the Jefferson Street Bridge. Figure 5.1 maps the general location of the project site.
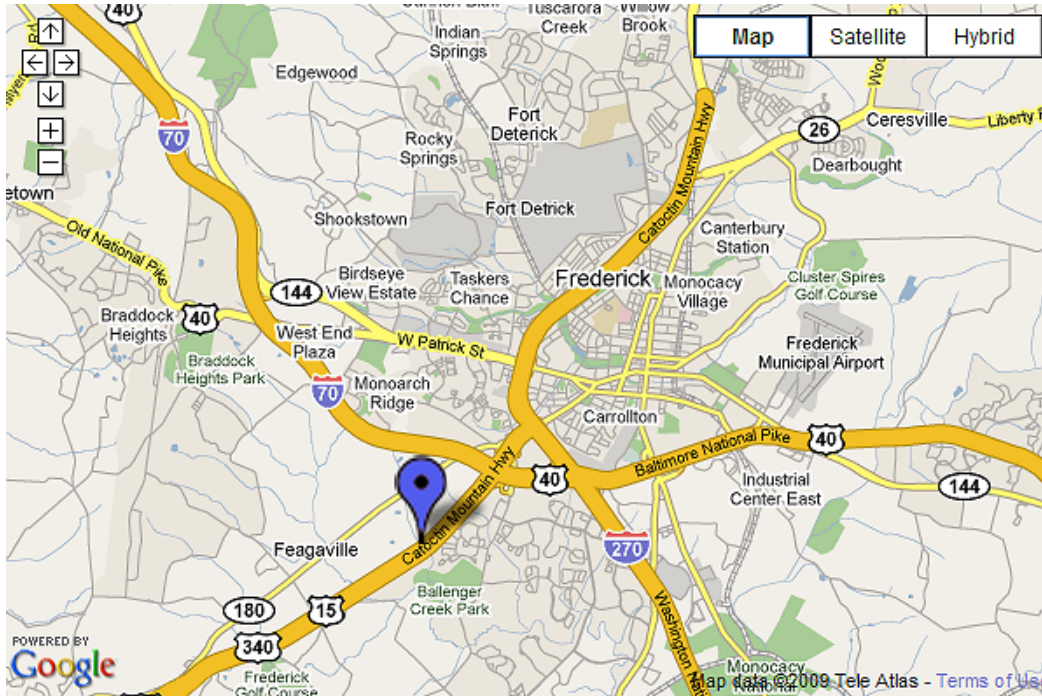
Figure 5.1 – Approximate extent of project site (source: googlemaps.com)

Construction and activities related to the Intelligent Compaction field trial were conducted at the project site from about July 20 to July 24, 2009. An initial attempt was made on the evening of July 22 to perform the field evaluation of the SAW RFID temperature measurement system. However, all construction activities were cancelled due to an unexpected rain storm. As described below, the encapsulated tags for the field trial had already been affixed to the milled paving surface using epoxy putty before the storm. After cancellation, the tags were pried of the road surface and the epoxy putty was carefully grinded off so that the tags could be reused on July 23. The field evaluation was completed on July 23 from about 0200 to 0300 hours. Weather conditions were clear, mild, and without wind. Table 5.1 summarizes weather data recorded just prior to testing from two nearby weather stations.

Table 5.1 – Weather data recorded near the project site for July 22-23, 2009

Time	Station	Temp (°F)	Dew Point (°F)	Relative Humidity (%)	Wind Speed (mph)
2055	Walnut Ridge	74.8	64	68	0
	Middletown	71.4	66	82	0
0053	Walnut Ridge	71.4	63	75	0
	Middletown	70.5	65	82	0
0147	Walnut Ridge	70.5	63	82	0
	Middletown	70.5	64	81	0

Note: Walnut Ridge and Middletown stations are about 8 and 37 miles from the project site, respectively (estimated from googlemaps.com).

5.2. Testing Procedure

The test section was about 51 feet long and was located near the interchange with Mt. Zion Road. Forty SAW RFID tags (10 single patch tags and 30 monopole tags) were prepositioned ahead of the paver. In an effort to measure temperature through the depth of the overlay, three elevations were considered: bottom of mat (elevation zero inches), middle of mat (elevation 0.75-inches), and surface of mat (elevation 1.5-inches). Please note, the middle of mat tags were prepared using a thicker layer of thermally conductive epoxy underneath the tag. Layout schematics for the test section are shown in Figures 5.2 and 5.3.

ROAD CENTERLINE

15-feet   15-feet   15-feet

WHEEL PATH

GROUP C   GROUP J

4-feet   12-feet   CENTERLINE

RF SAW RFID TAG

GROUP B   GROUP E   GROUP G   GROUP I

1-foot   DIRECTION OF PAVING

GROUP A   GROUP D   GROUP F   GROUP H

8-inches

SEE FIGURE NO. 3   LANE   GROUP OF TAGS

SHOULDER

NOT TO SCALE
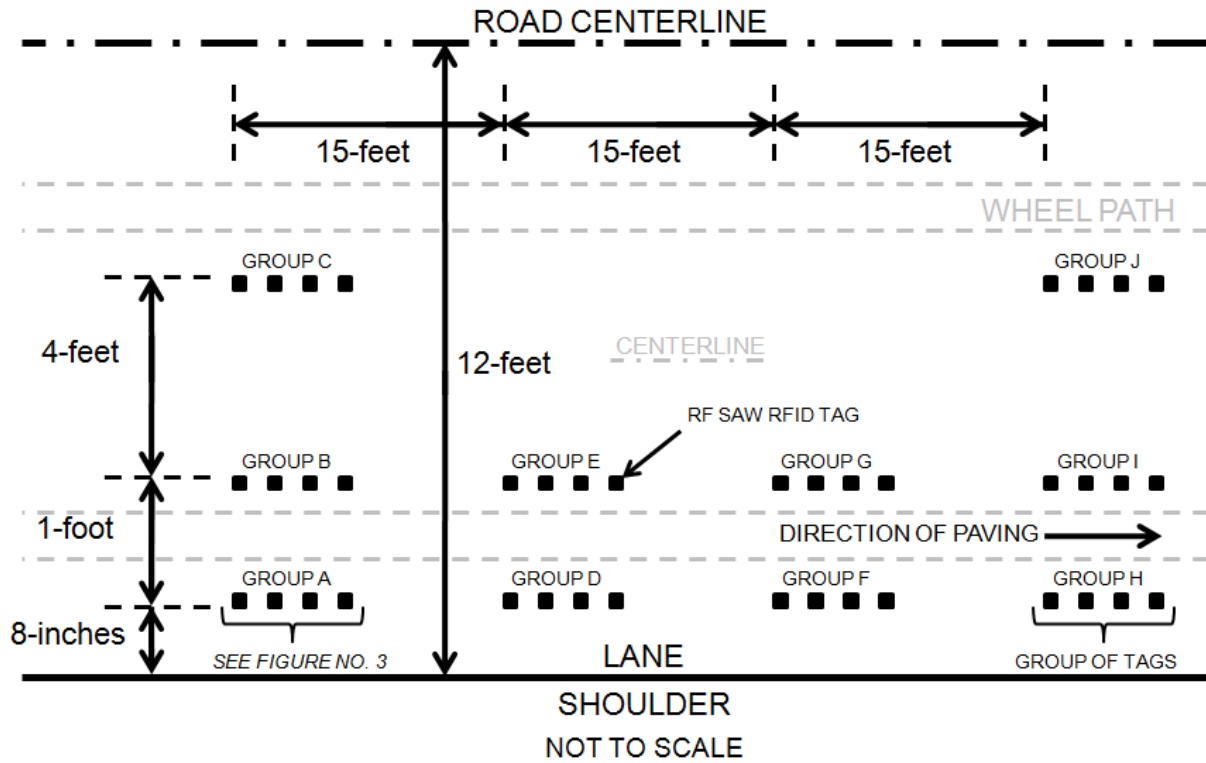
Figure 5.2 – Plan view of test section

GROUP A

SINGLE
PATCH   MONOPOLE   MONOPOLE   MONOPOLE

Elevated At: Bottom Of Mat   Middle Of Mat   Top Of Mat
(0-inch)   (0.75-inches)   (1.5-inches)

2-feet   2-feet   2-feet

NOT TO SCALE

NOTE: TYPICAL FOR ALL GROUPS
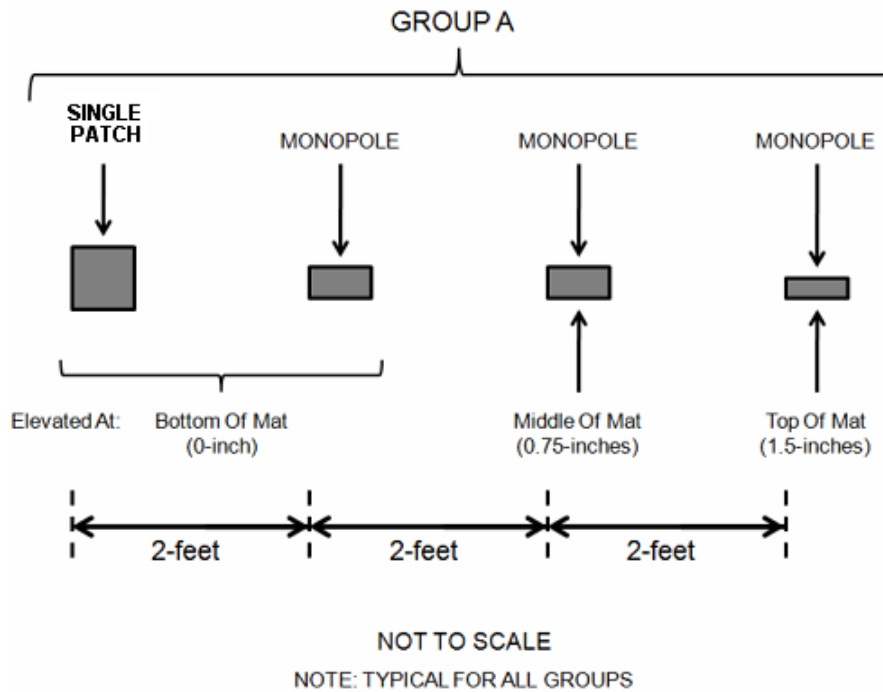
Figure 5.3 – Detailed plan view of a single group of SAW RFID tags

46

As previously described, all of the tags except for eight "top of mat" surface tags were encapsulated in a relatively rigid thermally conductive epoxy. All tags, other than those used for the surface, were affixed to the milled existing pavement surface using quick-hardening epoxy putty (Loctite 5-Minute Epoxy Putty). The mounted tags were oriented so that their ceramic chip and antenna were facing upward in order to enhance their readability (based on the recommended orientation and rotation from Chapter 4). The unencapsulated surface tags were placed face down into the asphalt by the Contractor immediately after the passing of the paver. Figure 5.4 shows the tags being placed on the milled surface.

Figure 5.4 – Placement of SAW RFID tags on surface of existing milled pavement

The RF SAW tag reader and circularly polarized antenna were mounted on a long-handled wheeled carriage in order to read the tags from the side of the road during compaction operations. The antenna was elevated (on the wheeled apparatus) about one-foot above the pavement surface. The wheeled apparatus was manually operated to minimize any disturbance to the hot asphalt or to the compaction operations while the lift was cooling and being compacted. The reader was cabled to a laptop that recorded temperature and tag signal strength during testing.

The reader software requires that the operator specify a temperature window prior to reading the tags. The manufacturer recommends a 30 degree temperature window, based on their calibration techniques at room temperature. This temperature window may be widened, however, the software signal processing time becomes longer. A longer signal processing time has been known to decrease the signal strength/response of the tag, especially when the tag is embedded in attenuating materials.

Thermal lag added another complication to getting initial reads from the encapsulated tags immediately after their covering with hot HMA. A thermal lag, as described in Chapter 4, is the time duration required for the encapsulated tags to "heat up" to the temperature of the surrounding material. Based on a previous laboratory study, it is suggested that the thermal lag for encapsulated tags to be about 3 to 8 minutes depending on the tag used; encapsulated single patch tags experience the most thermal lag, as shown in Chapter 4. The thermal sensitivity study also suggests that unencapsulated tags at the surface would exhibit only about 1 to 2 minutes of thermal lag.

The estimated temperature window immediately after placement of the overlay was set at 110-140°C. Initially, no response could be obtained from any tag. After the temperature

window on the reader was adjusted downward to 80-110°C, some tags were read successfully at about eight minutes after paving. The manufacturer-recommended temperature window of 30 degrees was used throughout the field trials. However, during the initial heating of the tags (thermal lag) and rapid cooling of the mat immediately after placement, it proved difficult to adjust the temperature window on the reader to successfully identify initial tag temperature.

The wheeled reader and antenna apparatus was initially passed over the "Group A" tags, then "Group B," then "Group C," and so on, after which the cycle was repeated. The data collected during testing included: the tag identification number; the time/date stamp of the tag's last reading during the antenna pass; the tag distance to the antenna of the tag's last reading; and temperature of the tag's last reading. Note that even if multiple reads were obtained from a tag during a given pass, the reader software saves only the data from the tag's last read. Four full cycles of readings from Groups A through I were performed until the mat had cooled sufficiently that the vibratory compactors moved on to other sections. Prior to each pass, the reader software temperature window was adjusted to the declining temperature conditions. Figure 5.5 shows the paving operation and test set up during construction.

Figure 5.5 – Paving operation and test set up during construction

5.3. Field Test Performance

After the hot-mix asphalt had been placed on the first groups of tags (Groups A through C), the vibratory compactors passed the testing area for a few minutes. In addition, as previously stated, additional time was required to provide the reader software with a proper temperature window to read the tags. Consequently, the first tag reads were obtained about eight minutes (± one minute) after the tags were covered with asphalt. Readings were than taken for approximately the next hour, continuing after the vibratory compactors had moved on to subsequent sections of pavement.

Overall, the temperatures at the bottom of the mat decreased from 92 to 57°C during the cooling period monitored in this study. At the middle of the mat and on the surface, temperatures generally decreased from 98 to 56 and from 104 to 44°C, respectively. Transcribed field data sheets documenting each tag's temperature and time of measurement are provided in an appendix.

Table 5.2 summarizes the read success rates for the tags. Five of the thirty pre-placed tags could not be read successfully during system testing prior to paving operations. This is likely due to damage caused by their removal from the roadway surface the night before and/or preparing them for reuse by grinding off the hardened epoxy putty. The read rates after asphalt placement and during compaction increased from 28% during the first pass to 52% in the fourth. This should not, however, be interpreted as an increase in the inherent read rate with time. Rather, this increase is because it was easier to set an appropriate temperature window in the reader software during the slower cooling of the later passes than during the rapid cooling in the first pass.

Table 5.2 – Tag read rates

Paver Pass	Tag Count	Total Possible	% Reading
Pre-Paving	25	30	83.33%
Pass 1	11	40	27.50%
Pass 2	19	40	47.50%
Pass 3	22	40	55.00%
Pass 4	21	40	52.50%

5.4. Field Test Results

Evaluations of the cooling HMA temperatures, with depth and over time, were performed at two transverse cross-sections: Groups A-D-F-H and B-E-G-I. Results from cross-section B-E-G-I are described here; the very similar results from cross-section A-D-F-H are provided in an appendix. Plots illustrating temperature versus time since paving are given in Figures 5.6 through 5.8 for the bottom, mid-thickness, and surface of the mat, respectively. "Time since paving" is the estimated elapsed time after the tags are covered with the asphalt by the paver.
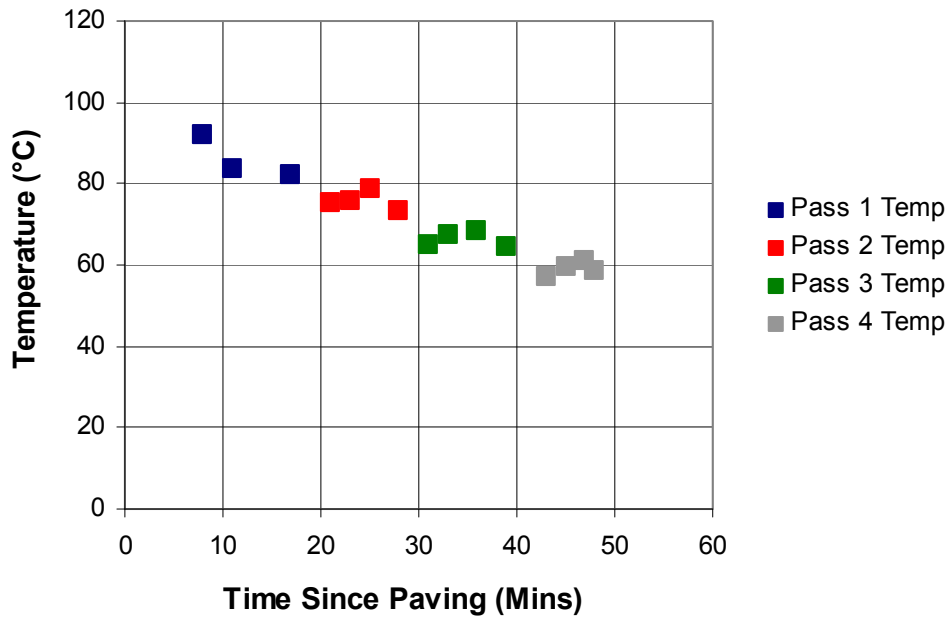
Figure 5.6 – Temperature versus time since paving, at bottom of mat (cross-section B-E-G-I)
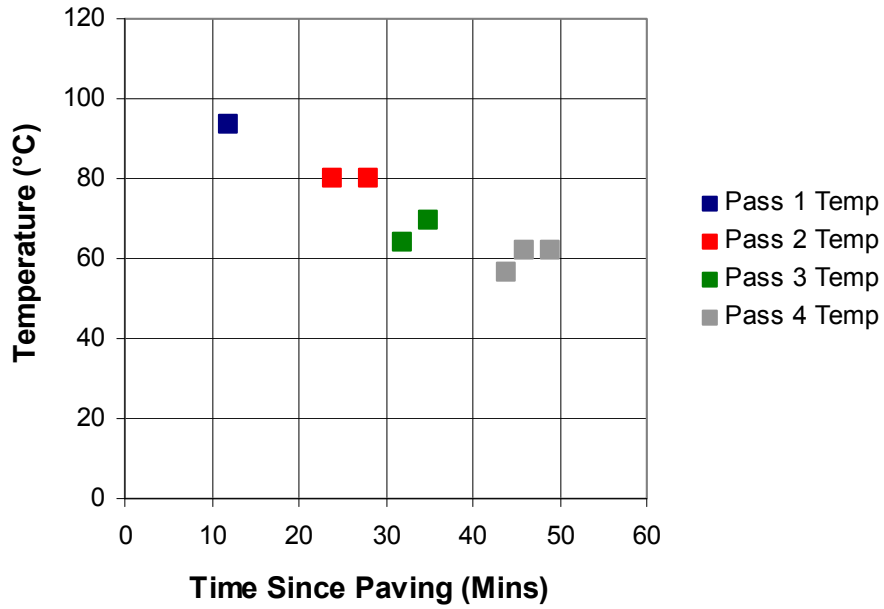
Figure 5.7 – Temperature versus time since paving, at mid-thickness of mat (cross-section B-E-G-I)
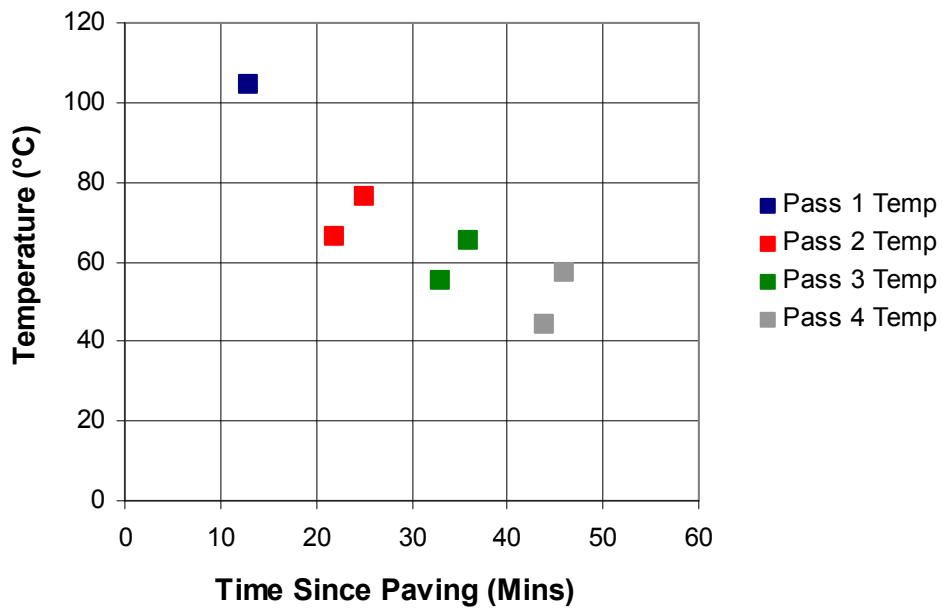
Figure 5.8 – Temperature versus time since paving, at surface of mat (cross-section B-E-G-I)

As shown in the above figures, the temperatures measured by the tags decreased with every pass of the testing area. Based on these test results and theoretical expectations for typical mat cooling trends, exponential regression lines were fit to the data. Figure 5.9 summarizes the cooling trends segregated by location within the mat thickness.
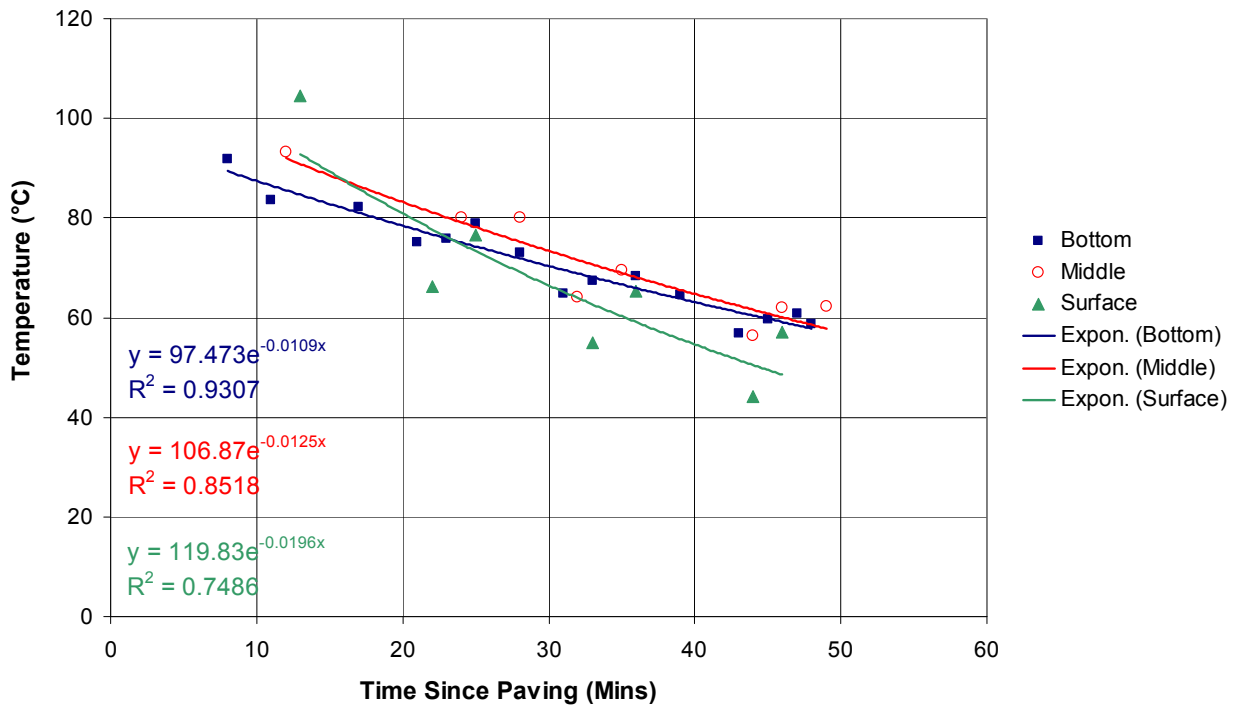
Figure 5.9 – Temperature versus time since paving, segregated by location (cross-section B-E-G-I)

The similarities between the regression lines shown on Figure 5.9 do not suggest any systematic variations in temperature through the depth of the mat. This is likely due to the thinness of the overlay (1.5-inches) and other limitations of the test (inaccuracies in the depth of the tags and nonuniformity of initial paving temperatures). Therefore, all depth locations were combined and a single exponential regression equation was fit to the combined data set (Figure 5.10). The regression equation for the combined data (along with that developed from cross-

section A-D-F-H in the appendix) shall be the basis for evaluating the traditional mat cooling

models from the literature.
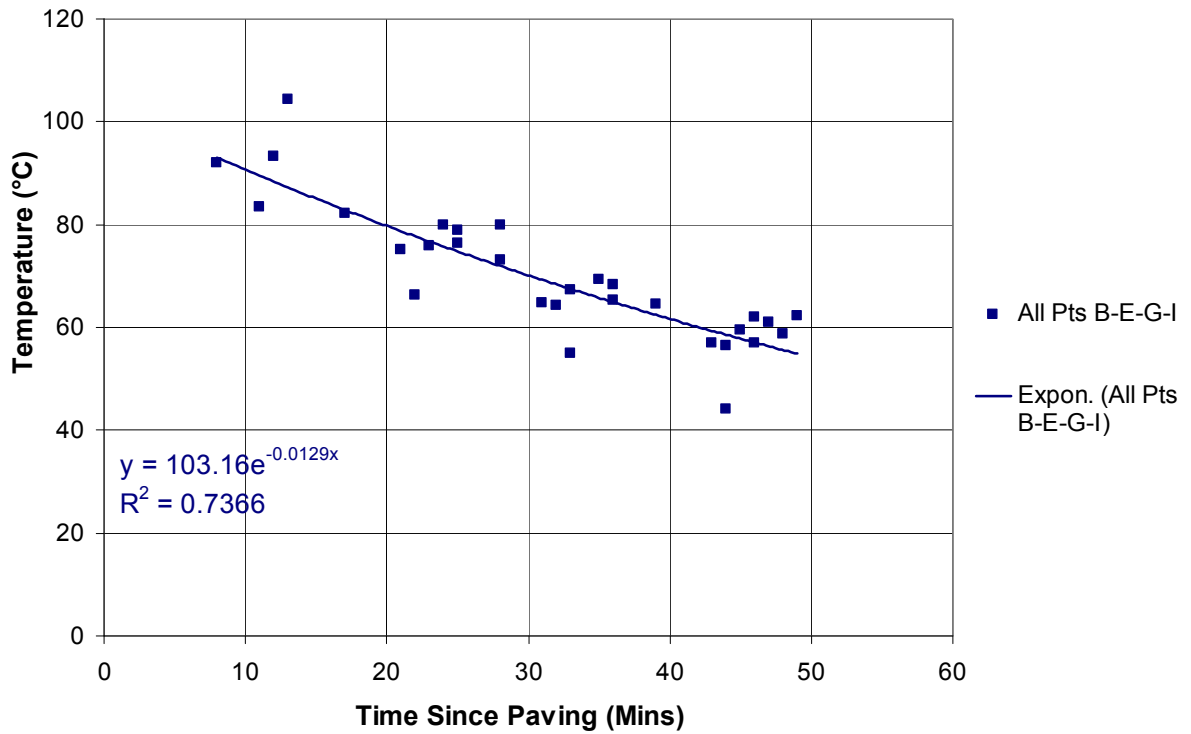
Figure 5.10 – Temperature versus time since paving, uniform with depth (cross-section B-E-G-I)

The exponential regression equation for the mat cooling at cross-section A-D-F-H is:

$$y(x) = 101.87 \, e^{-0.0096 \, x}$$
$$R^2 = 75.04\%$$

(5.1)

while for the cross-section B-E-G-I, the exponential regression is:

$$y(x) = 103.16 \text{ e}^{-0.013 \text{ x}} \qquad\qquad (5.2)$$
$$R^2 = 73.66\%$$

5.5. Variability & Reliability

In an effort to determine the reliability of the field test results and the consistency of the data collected, the following additional evaluations were made:

- Comparison of measured temperatures reported by single patch and monopole SAW RFID tags placed at the same location at the bottom of the mat.

- Comparisons of surface temperatures measured with the SAW RFID tags against independent measurements using a Fluke infrared thermometer.

- Additional laboratory testing to determine the variability of temperature measurements from the SAW RFID tags based on errors generated by the reader.

These variability and reliability analysis were performed on the temperature data recorded from cross-sections B-E-G-I and A-D-F-H.

To determine if there are any systematic differences between the single patch and monopole tags, pairs of each were placed at the bottom of the mat approximately two feet apart within each group (see Figures 5.11 and 5.12). A comparison between the temperatures measured by each tag type is presented in Table 5.3.
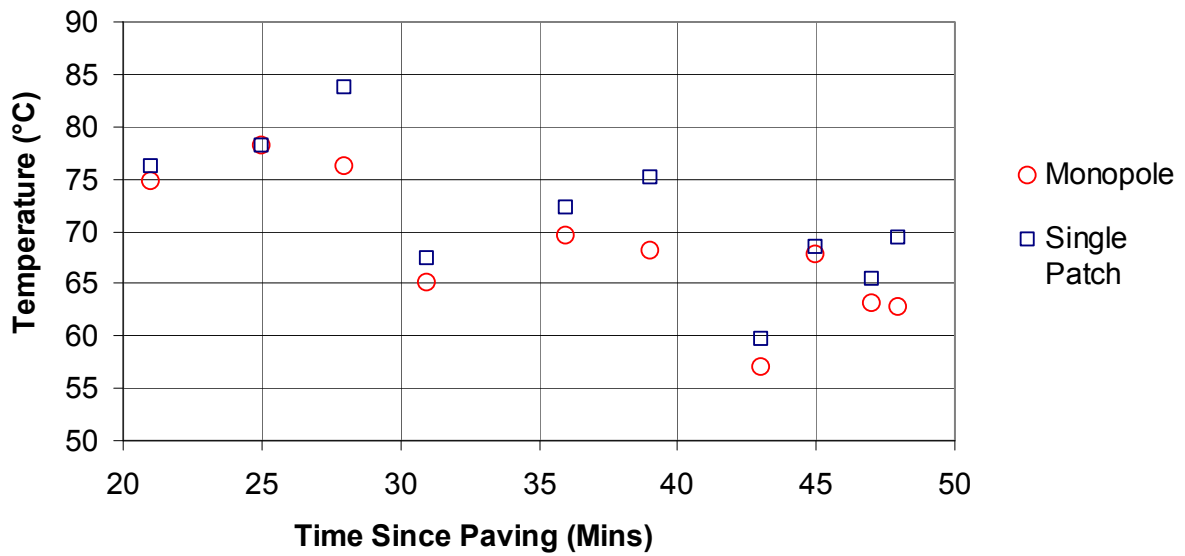
Figure 5.11 – Comparison of temperatures by tag type (cross-section A-D-F-H, bottom of mat)
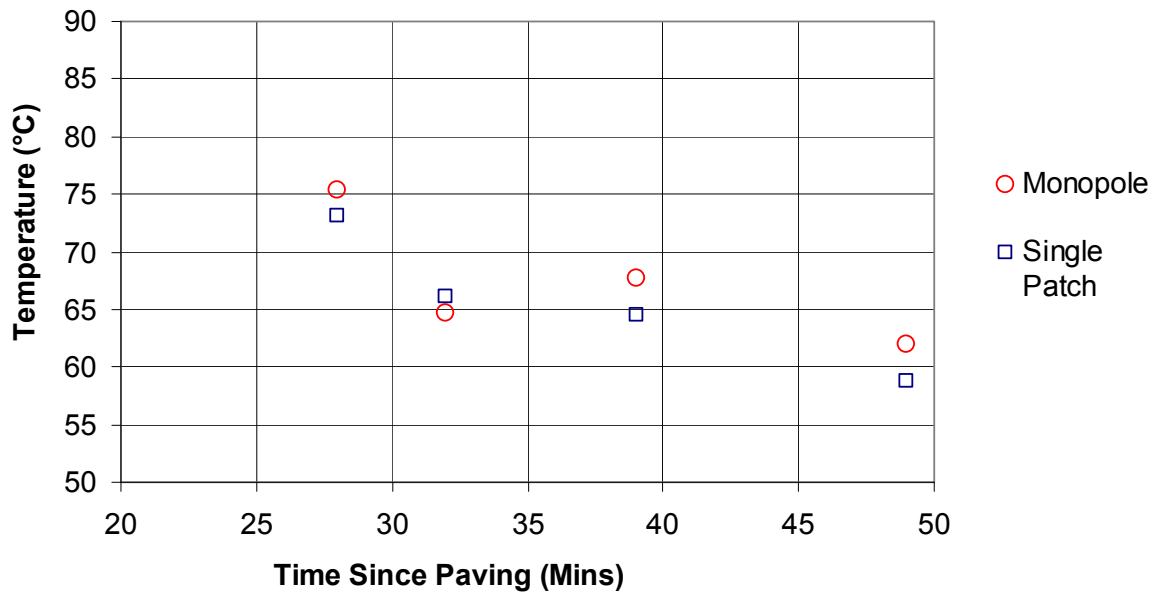
Figure 5.12 – Comparison of temperatures by tag type (cross-section B-E-G-I, bottom of mat)

Table 5.3 – Temperature comparisons at bottom of mat

Cross-Section A-D-F-H				Cross-Section B-E-G-I			
Monopole Temp	Single Patch Temp	Time (min)	**% Diff**	Monopole Temp	Single Patch Temp	Time (min)	**% Diff**
74.7	76.1	21	**1.84%**	75.3	73.1	28	**2.92%**
78.2	78.2	25	**0.00%**	64.7	66.1	32	**2.12%**
76.2	83.7	28	**8.96%**	67.7	64.5	39	**4.73%**
65	67.4	31	**3.56%**	61.9	58.7	49	**5.17%**
69.5	72.2	36	**3.74%**				
68.2	75.1	39	**9.19%**				
57	59.6	43	**4.36%**				
67.7	68.4	45	**1.02%**				
63.1	65.5	47	**3.66%**				
62.7	69.3	48	**9.52%**				

Note: temperature presented in degrees Celsius.

The maximum difference in temperature measured by the two types of tags at the bottom of the mat was about 9% for cross-section A-D-F-H at 28, 39, and 48 minutes since paving. The average temperature difference for all of the tags was 4.6% at cross-section A-D-F-H (standard deviation of 3.5%) and 3.7% at cross-section B-E-G-I (standard deviation of 1.4%). These differing temperatures may be due to a general functional inaccuracy of the tags (possibly a systematic bias) or to spatial variability. However, on average, the temperatures were consistent within a five percent difference.

In a similar fashion, comparisons were made between surface temperatures measured using the SAW monopole RFID tags and independent measurements using a Fluke infrared digital thermometer. Only general qualitative evaluations can be made as the location of the infrared readings may vary by several feet from the corresponding SAW RFID measurements. The comparisons between the two sets of measurements are summarized in Figure 5.13 and Table 5.4.
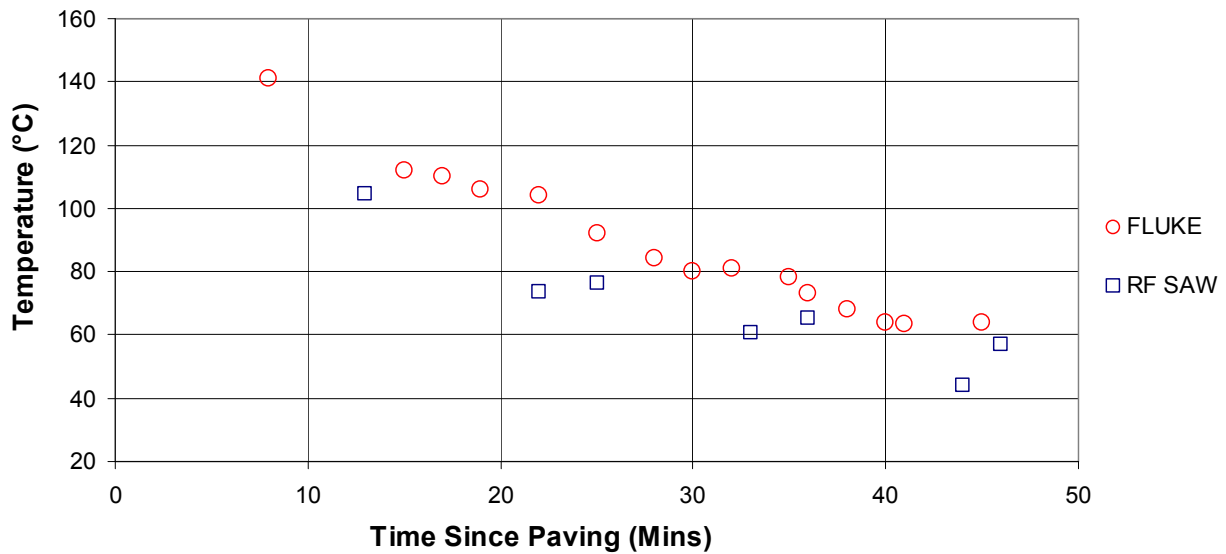
Figure 5.13 – Surface temperatures measured by SAW RFID tags vs. Fluke infrared thermometer

Table 5.4 – Temperature comparisons at top of mat

Fluke Readings		Surface Tag Readings		
Time (min)	Temp (°C)	Time	Temp (°C)	%Differ
8	141			
15	112	13	104.4	**6.79%**
17	110			
19	106			
22	104	22	73.4	**29.42%**
25	92.2	25	76.5	**17.03%**
28	84			
30	80			
32	81	33	60.85	**24.88%**
35	78			
36	73	36	65.4	**10.41%**
38	68			
40	64			
41	63.5			
45	63.8	44	44.2	**30.72%**

Note: temperature presented in degrees Celsius.

More significant temperature variations are exhibited from this comparison; the maximum temperature difference was about 30% at 22 and 45 minutes and about 25% at 32 minutes. In addition, the difference is widely sporadic and inconsistent (ranging from about 7% to about 30%). This may be the result of inconsistent technology between the Fluke

thermometer and the SAW RFID tags or non-uniform conditions (some of the Fluke thermometer measurements were recorded a few feet away from the surface tags). A more thorough explanation may require additional laboratory and/or field testing.

In order to determine the variability of temperature measurements from the tags based on computational errors generated from the RF SAW Reader, an additional laboratory study was performed. The study was performed at constant room temperature (70°F). Repeated readings were taken to determine any fluctuating temperature readings caused by the instrumentation rather than the environment. The result of the test found a negligible fluctuation of about ± 0.2 °C. The manufacturer also states that transmission interferences (wireless communication and magnetic fields) may contribute to inaccuracies. This, however, should not have been a factor in the field trials.

5.6. Conclusions: Field Evaluation

The overall findings from the field trials indicate that the SAW RFID tags can be used successfully for measuring mat cooling temperatures during HMA construction. It is important, however, to understand that this study is a part of a developing technology – certain provisions must be considered and imperfections exist, but improvements in the technology are to be expected.

5.6.1. Field Test Performance

- A temperature window must be specified in the RF SAW reader software in order to read the in-place tags. This may and did lead to operating issues in the field, particularly

during the early stages of mat cooling when the temperature dropped rapidly, causing difficulty in setting the correct temperature window.

- The manufacturer recommends a 30 degree temperature window based on their calibration techniques at room temperature. The temperature window may be widened, but the software signal processing time becomes longer and the signal strength/response of the tag decreases. The manufacturer's recommended temperature window of 30 degrees was used for all of the field trials.

- There was difficulty discerning physically damaged tags from those that simply could not be read immediately after paving/compaction. In other words, if a tag is nonresponsive to the reader, it might not be due to destruction by vibratory compaction. It may be that the reader cannot get a response because the temperature window is incorrect or the tag's signal is severely attenuated.

5.6.2. Field Test Results

- The field results generally show an exponential relationship between cooling temperatures and time. This generally agrees with theoretical considerations that suggest exponential cooling.

- No systematic temperature variations with depth were observed during mat cooling. In other words, the measured temperatures at the bottom, middle, and top of the asphalt mat, at any given location and time, were all within the variability range of the sensors. This may simply be a consequence of the thinness of the lift on this particular project.

5.6.3. Variability & Reliability

- Based on the comparative study at the bottom of the mat between two sets of tags (single patch and monopole) and previous laboratory testing, the temperatures recorded by the two tag types are reasonably consistent and accurate.

- The comparative study at the surface of the mat between the Fluke infrared thermometer and monopole tag found inconsistencies between the two sets of readings. This may due to a lack of testing at a uniform location and may require additional field and/or laboratory testing for further explanation.

Chapter 6: Comparisons Between Measured and Predicted Mat Cooling Response

This chapter compares the measured mat cooling response against predicted temperatures versus time from the theoretical/numerical models described in Chapter 2. As will be described later, this comparison will require some calibration of the model's input parameters, given that there are no laboratory measurements of the thermal properties for the mix placed at the field test site. The principal objectives of the comparisons between measured and predicted cooling response are to:

- Determine if the usage of RFID technology to measure HMA cooling temperatures was accurate and successful;

- Identify improvements in the overall process of measuring mat cooling temperatures using RFID technology; and

- Calibrate via a sensitivity analysis input parameters values that provide reasonable and close agreement with the field measured temperatures.

6.1. Analysis Inputs

As previously mentioned in Chapter 2, Corlew and Dickson (1968) developed a numerical solution for the one-dimensional transient heat flow in a cooling HMA layer (Eq. 2.4). Wolfe and Colony (1976) added computational improvements to Corlew and Dickson's convection model (Eq. 2.5) using a finite difference energy balance equation (Eq. 2.8). For this analysis, Eq. (2.4) was used for the conduction calculations and Eq. (2.8) was used for convection.

The input parameter values shown in Table 6.1 were used in for the model predictions. These were selected based on recommendations from previous investigations and the results of the input parameter optimization presented later in this chapter. Since the field construction was performed at night, the impacts of solar radiation (H_S) and absorptivity (a) are negligible. The convective heat transfer coefficient value corresponds to free convection, where wind velocity during mat cooling is zero miles per hour. This is consistent with weather station data at the time of paving construction that indicated near-zero wind velocity.

Table 6.1 – Input Parameters Used in Models

Property	Units	Symbol	Used
Thermal conductivity	BTU/ft-hr-°F	k	0.64
Thermal diffusivity	ft^2/hr	α	0.0213
Convective heat transfer coefficient	Dimensionless	h	1.30
Thermal emissivity	Dimensionless	ε	0.95

6.2. Predicted Mat Cooling Response

As previously discussed, the numerical model used in this analysis is based on the finite difference formulations by Corlew and Dickson and Wolfe and Colony. The depth and time increments for the finite difference calculations are summarized in Table 6.2.

Table 6.2 – Input Parameters Used in Finite Difference Solution

Calculation Parameter	Min. Value	Max. Value	Step Increment
Depth step, Δy (inches)	0	7½	¼
Time step, Δt (minutes)	0	60	~ 0.3

In Table 6.2, the depth increment indicates that temperatures are calculated through the depth of the newly placed asphalt mat every quarter-inch up to 1½ inches. In other words, there are seven temperature calculations through the depth of the HMA mat for each time step. The depth of the analysis also extends into the base layer to a sufficient depth at which conduction no longer influences the temperature of the base material. This depth is taken as six inches in these analyses, corresponding to twenty-four temperature locations in the base calculated at each time step. The time step increment was selected to satisfy the stability requirement for the Euler time-integration algorithm:

$$0.5 \quad \geq \quad \frac{\alpha \, \Delta t}{\Delta y^2} \qquad (6.1)$$

The boundary conditions consist of a fixed 81°F temperature at the bottom of the base layer (six-inch depth below the overlay, as previously described) and a fixed 71°F ambient air temperature. The initial conditions are a uniform 305°F temperature for the HMA in the overlay and a uniform 81°F temperature in the underlying base asphalt. The base course layer and ambient air temperatures were measured during the field trials. The initial HMA temperature in the overlay was provided by MDSHA.

Figure 6.1 illustrates conceptually the heat flows in the analysis. The hot HMA in the overlay loses heat via convection to the ambient air at the surface and via conduction to the underlying existing asphalt at the base.
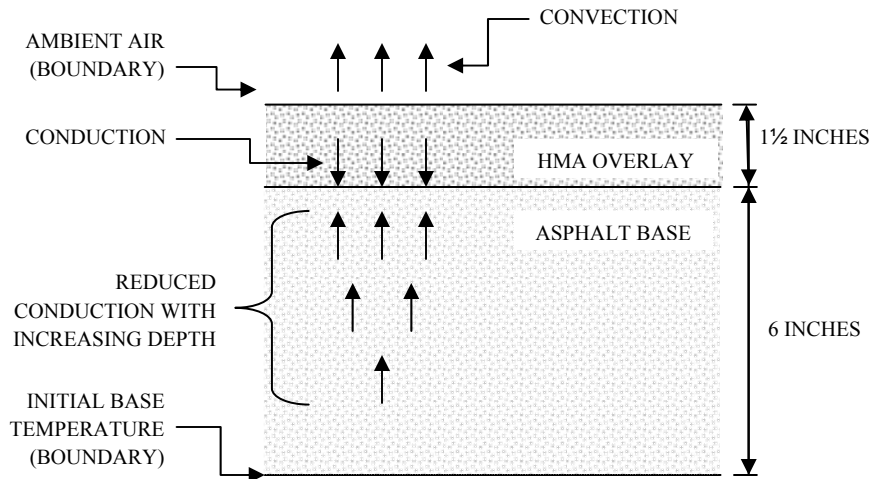

Figure 6.1 – General schematic for numerical solution

Figure 6.2 illustrates the predicted temperature versus time trends calculated in the finite difference solution at the bottom, middle, and surface of the HMA mat and the average temperature through the HMA thickness. As shown in the figure, the bottom of the mat expels the most heat initially. However, as time elapses the surface expels more heat than the bottom of the mat. These trends are consistent with those suggested by Jordan and Thomas (Jordan and Thomas, 1976). Figure 6.3 displays these cooling trends more explicitly. The y-axis on this figure is "change in temperature by time step", or in other words, the rate of temperature loss by "Δt" (from Table 6.2). The figure displays that initially the bottom of mat expels more than 20°F and then exponentially drops to about less than 1°F for the rest of the cooling process. The surface of the mat initially expels about 13°F and then, at about two minutes, begins to expel more heat than the bottom of the mat.
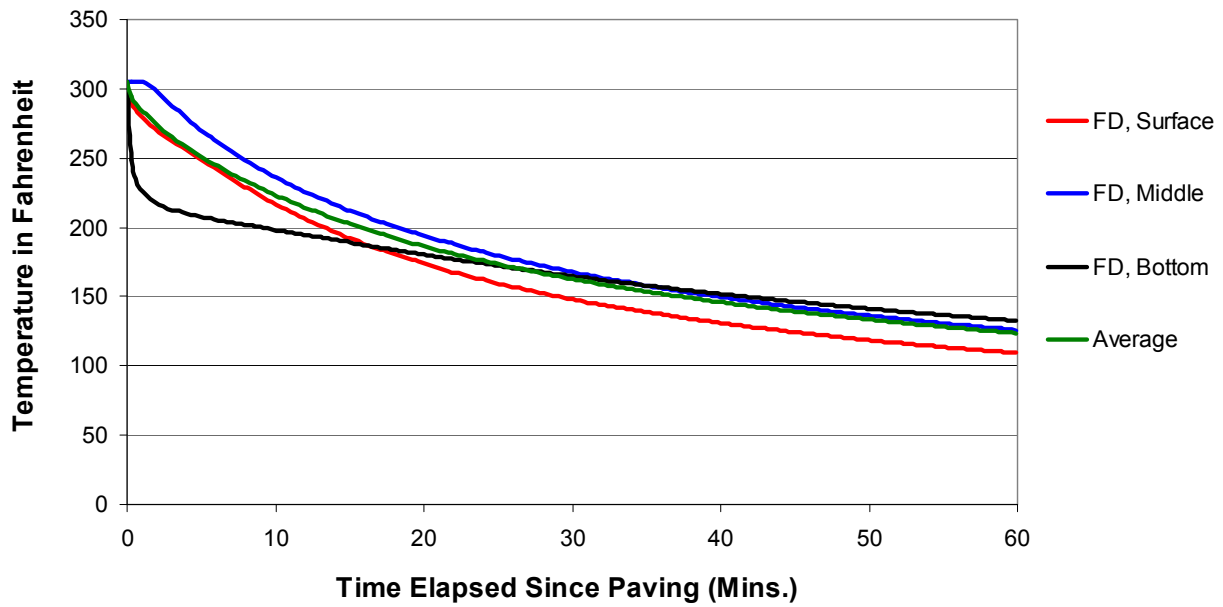
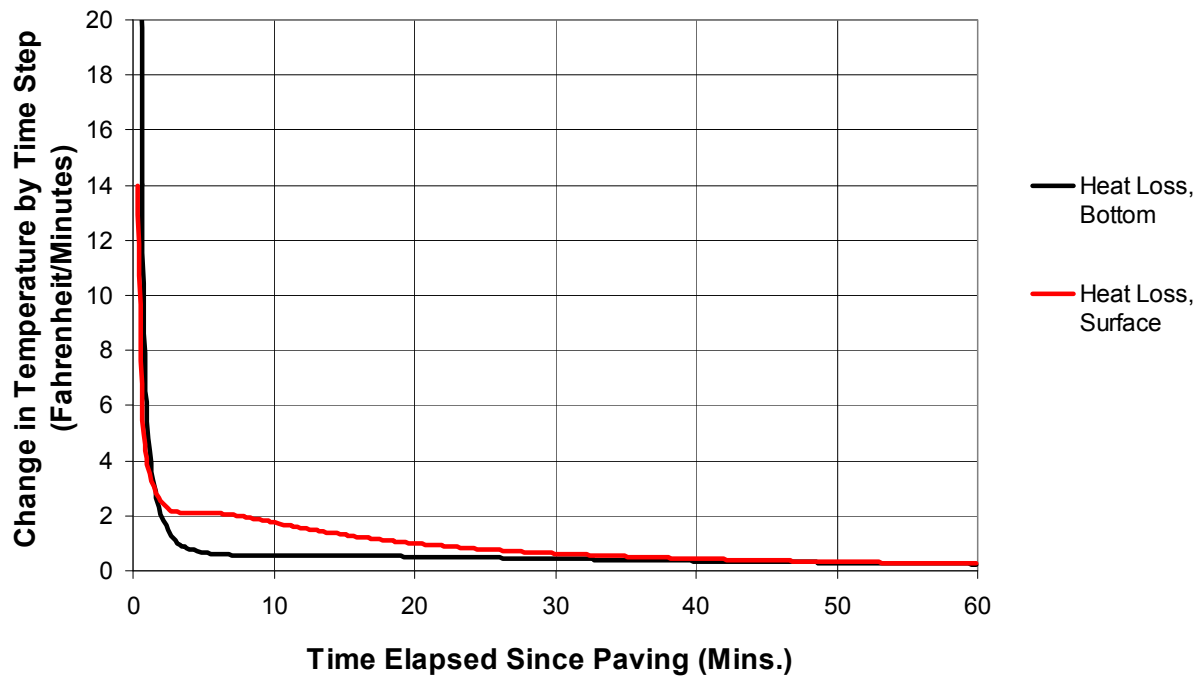Figure 6.2 – Finite difference solutions for bottom, middle, and surface of mat

Figure 6.3 – Cooling trends at the bottom and surface of the asphalt mat

Figure 6.4 displays the temperature trends of the base material as it heats and then cools due to conductive heat transfer from/to the HMA overlay. The asphalt base has an initial temperature of 81°F and, upon placement of the hot HMA overlay, rapidly heats up via conduction. Over time, as the HMA overlay cools mostly by convection, the heated base material cools along with the overlay. These cooling trends are logical and generally adhere to expectations for mat cooling.
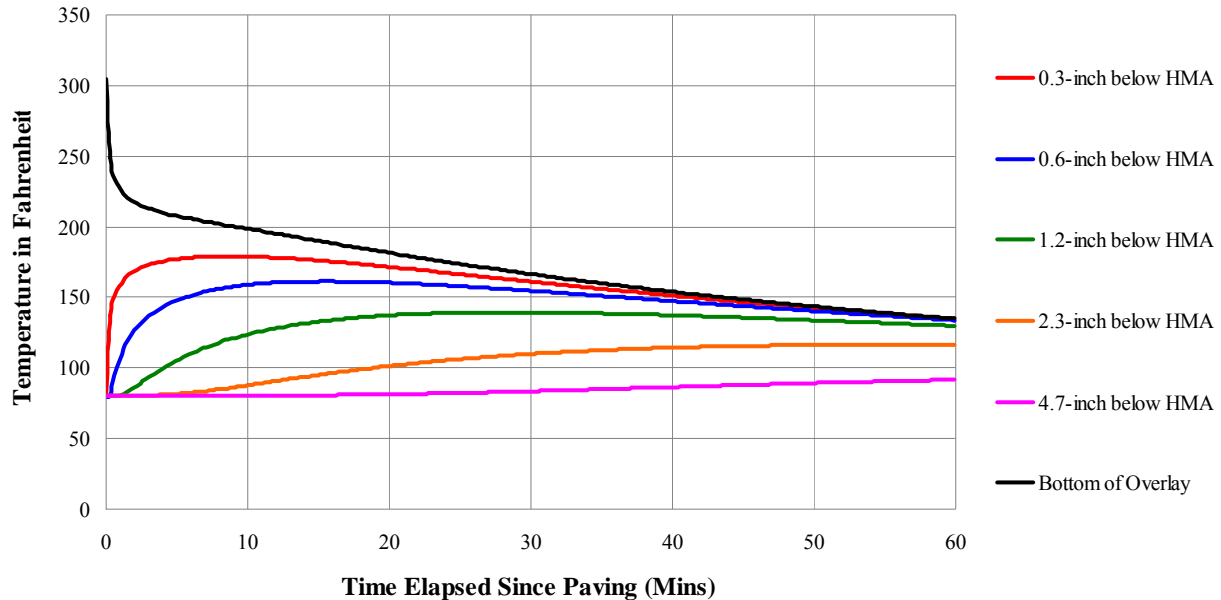
Figure 6.4 – Base material temperatures cooling over time due to convective heat transfer

Recall that the bottom fixed temperature boundary of the base layer is six inches below the bottom of the overlay. The decrease in temperature changes versus time at increasing depths within the base layer suggests that the arbitrary six inch depth for the lower fixed temperature boundary is sufficiently distant. As additional confirmation, Figure 6.5 compares predicted

cooling curves assuming 0, 1, 3, 6, and 8 inch base thicknesses. The cooling curves stabilize

once the base material has a thickness of 3-inches. This confirms that the 6 inch base material

thickness used in the analyses is sufficiently thick.
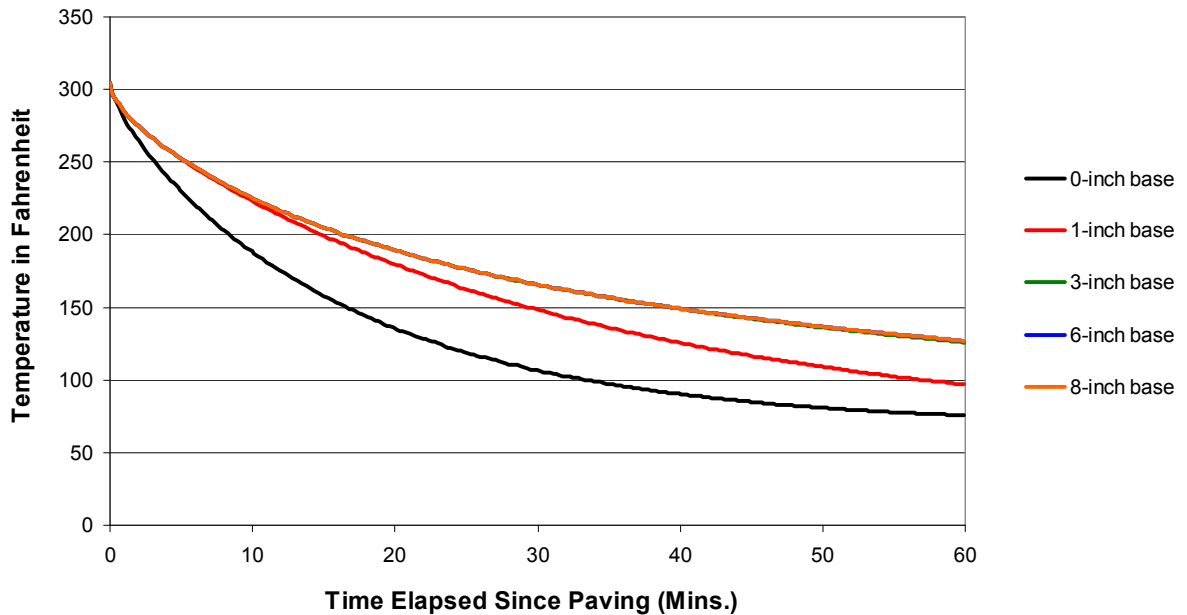
Figure 6.5 – Impact of altering thickness of base material to average predicted temperature profile

The results in Figures 6.3 through 6.5 all suggest that the finite difference solutions are

correct and a relatively accurate representation of field conditions.

6.3 Comparisons of Predicted vs. Measured Cooling Response

Figures 6.6 and 6.7 display a comparison between the calculated surface, middle, and

bottom of mat temperature trends with the raw data points from cross-sections A-D-F-H and B-

E-G-I, respectively. As an additional check on accuracy of the predictions, Figure 6.8 compares

the calculated temperatures at the surface against measured values obtained using the Fluke

infrared thermometer.

Figure 6.6 – Comparing predicted temperatures with raw data from cross-section A-D-F-H
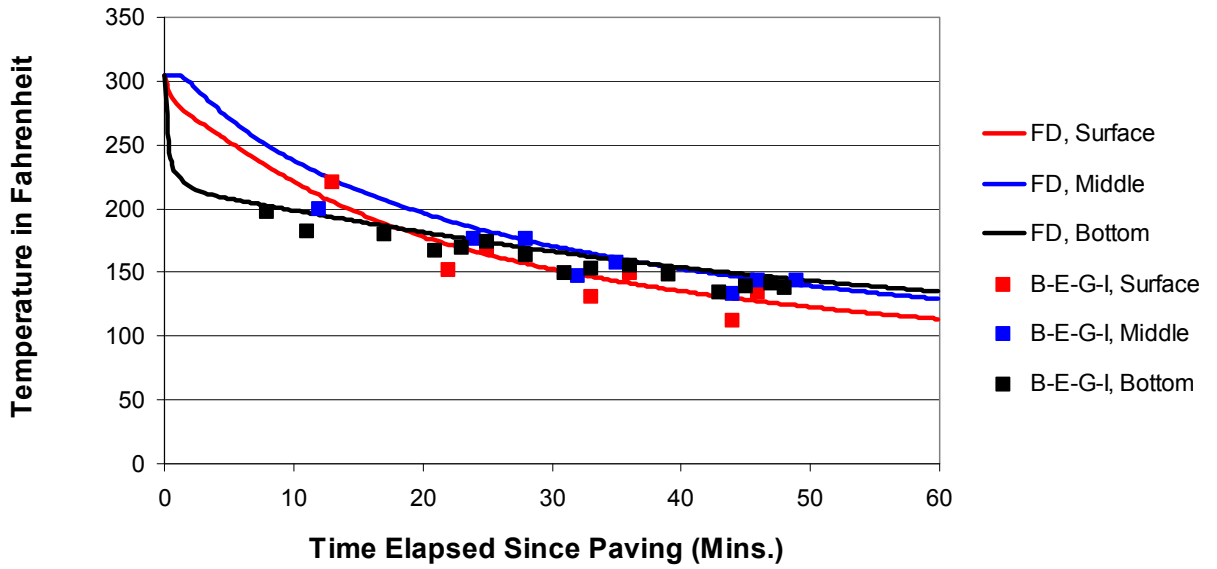
Figure 6.7 – Comparing predicted temperatures with raw data from cross-section B-E-G-I
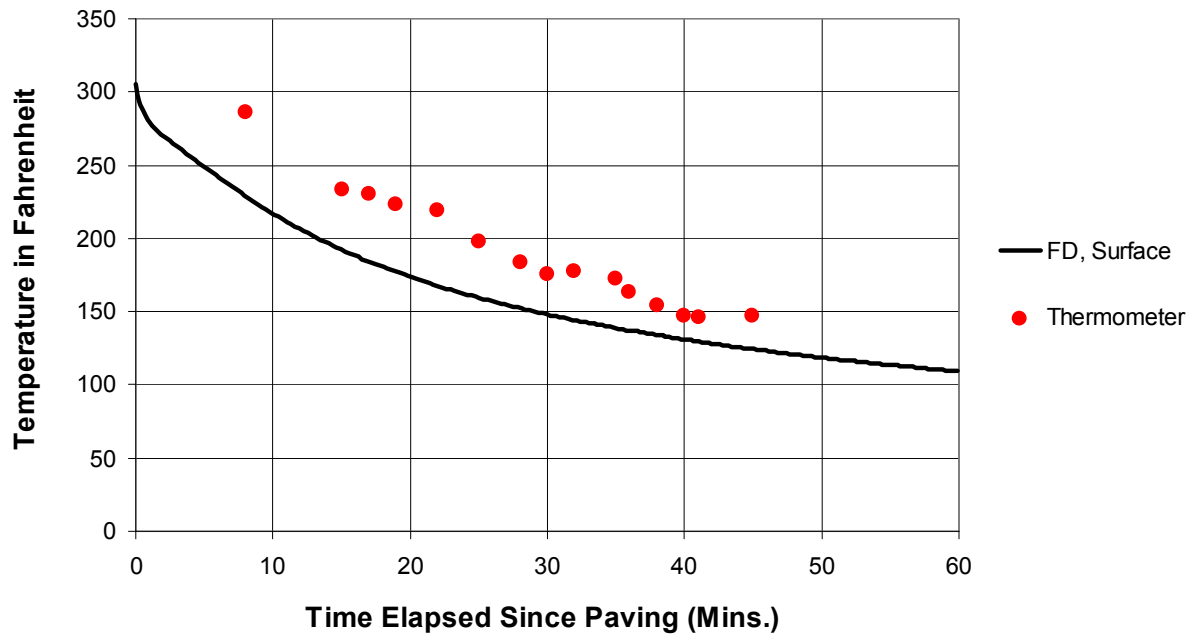
Figure 6.8 – Surface temperatures measured by thermometer compared to finite difference solution

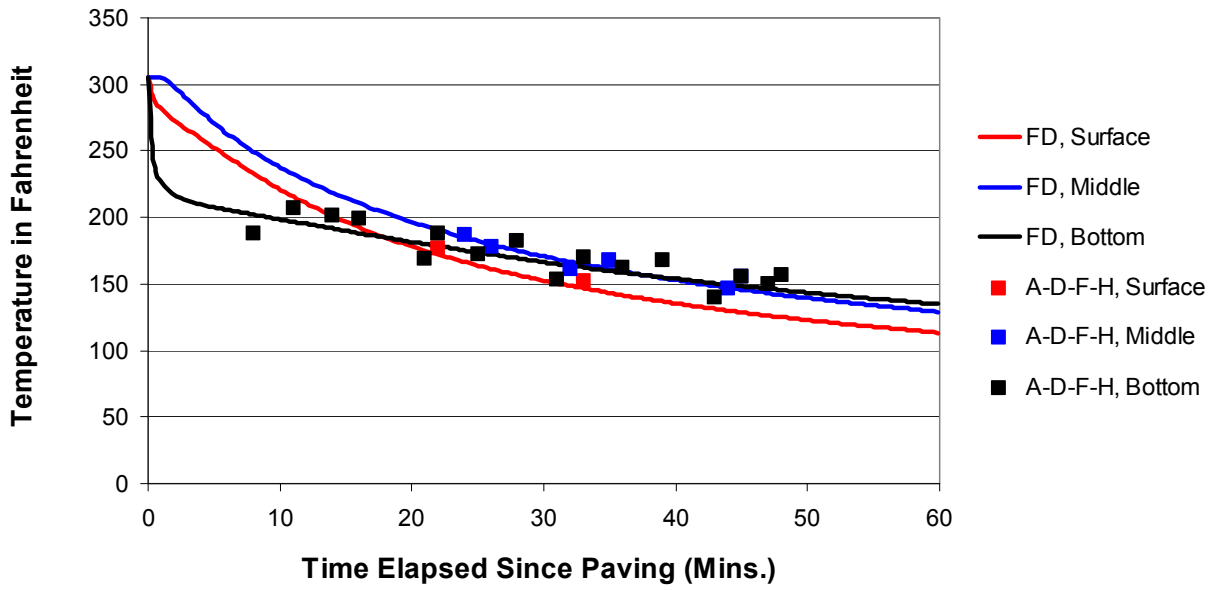The results in Figures 6.6 and 6.7 show generally good agreement between measured and predicted temperatures over time. However, it is difficult to discern any distinct correlations between the calculated curves and the raw temperature points as a function of depth. As described previously in Chapter 5, the thinness of the overlay and the imprecision in locating the RFID temperature sensors at specific depth locations make it impossible to detect any systematic trends in measured temperatures versus depth. The results in Figure 6.8 for the finite difference predictions at the surface and the actual measures as obtained by the infrared thermometer correlate generally well in terms of curvature, but the measured temperatures are consistently higher than the predicted values This may indicate either errors in the finite difference predictions at the surface or, as addressed previously in Chapter 5, inaccuracies in the infrared temperature measurements. Further research is required to analyze this issue completely.

As previously discussed in Chapter 5, it was impossible to detect any systematic variations in measured temperatures through the depth of the mat for either cross-section. Therefore, all depth locations were combined and a single exponential regression equation was fit to the combined data set for each cross-section. The following relation at cross-section A-D-F-H was developed:

$$y(x) = 101.87 \, e^{\,-0.0096 \, x} \tag{6.1}$$

The corresponding result at cross-section B-E-G-I is:

$$y(x) = 103.16 \, e^{\,-0.013 \, x} \tag{6.2}$$

Figures 6.9 and 6.10 show the comparisons between the predicted temperatures from the finite element analysis and the thickness-averaged measured temperatures at cross sections A-D-F-H and B-E-G-I, respectively. Figure 6.11 shows the combined results for the thickness-averaged measurements from the two cross sections and the thickness-averaged predictions from the finite difference model. In all cases, the predicted cooling curves follow an exponential decay very similar to the measured response.
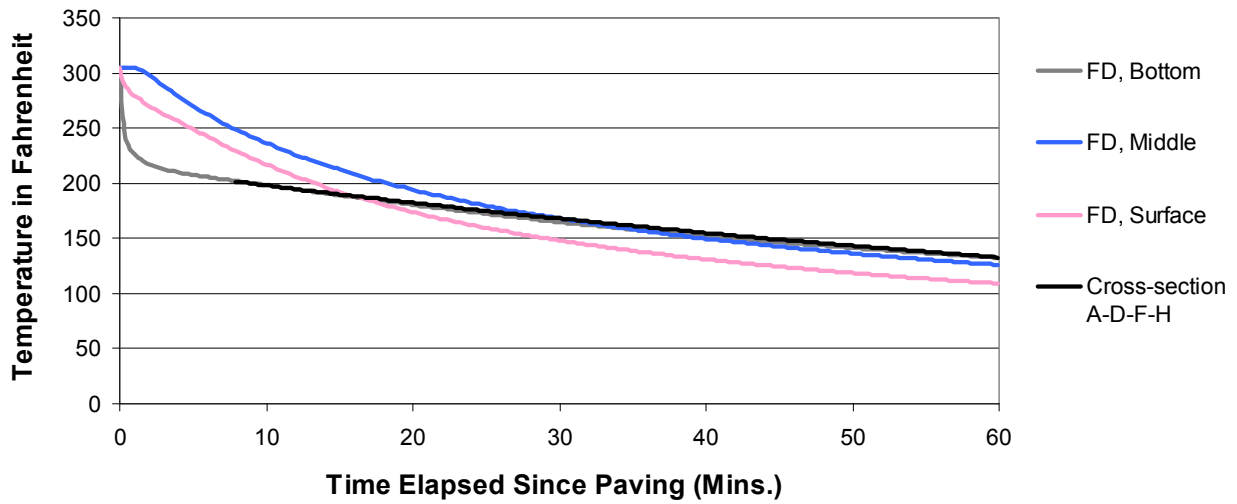
Figure 6.9 – Average measured mat cooling response at cross-section A-D-F-H compared to finite difference solutions
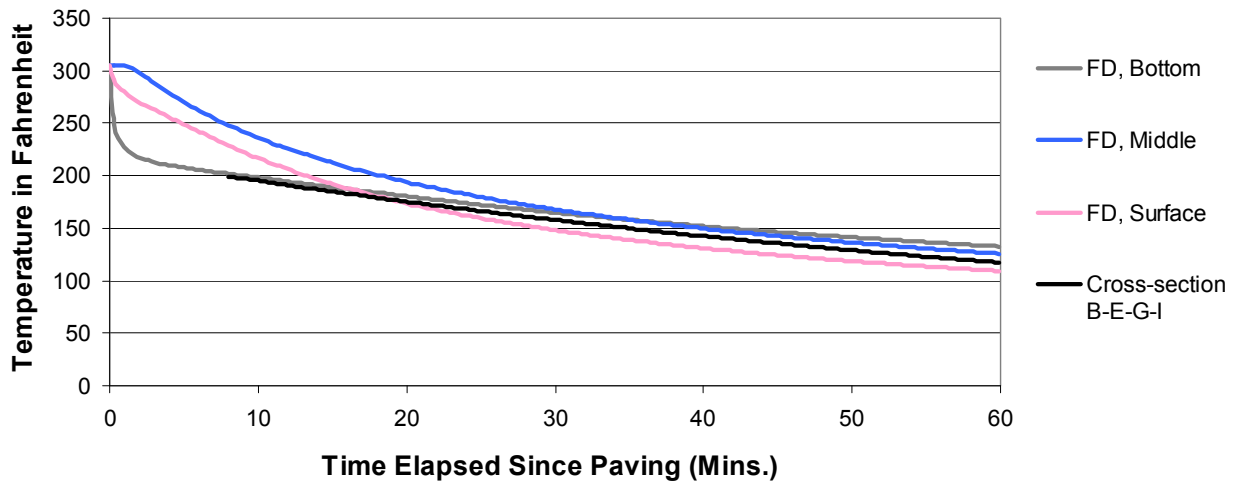
Figure 6.10 – Average measured mat cooling response at cross-section B-E-G-I compared to finite difference solutions
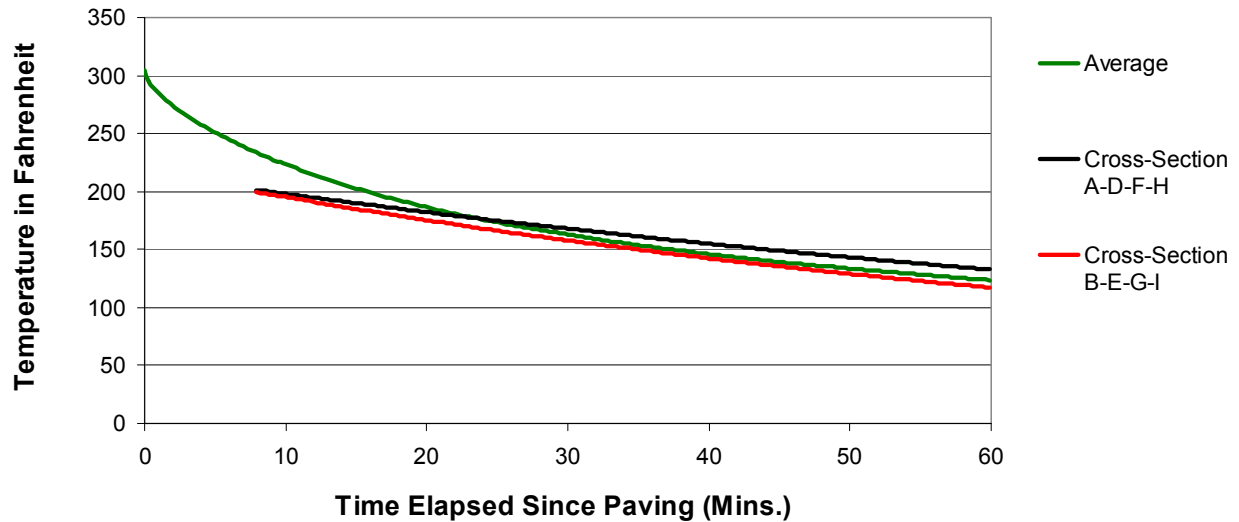
Figure 6.11 – Exponential curves from field trials compared to average finite difference solution

Based on the results in Figures 6.9 to 6.11, the following is observed:

- The curvatures of the measured exponential curves are relatively close to the calculated curve, with the exception of the early portion of the response. However, in terms of temperature accuracy, the average curve and exponential curves begin to show a close correlation only after about 15 to 20 minutes after paving. The early-stage comparisons are complicated by the fact that the tags did not return any data until about 8 minutes after paving. Nonetheless, it seems clear that the tag and calculated temperatures are not consistent in trend and curvature during the early stages of cooling. Further field investigations may be required determine the causes for this.

- Dempsey and Taylor (1973) and others state that an average mat temperature of 175°F is the threshold below which compaction is no longer economical or may even be injurious to the pavement (e.g., because of aggregate breakage). Therefore, temperature data from the time of initial paving to when it reaches 175°F are considered the most valuable.

Figure 6.12 superimposes the 175°F line on the data from Figure 6.11. The predicted and measured temperature data show close agreement only for about the last 5 to 10 minutes before the curves meeting the 175°F threshold.
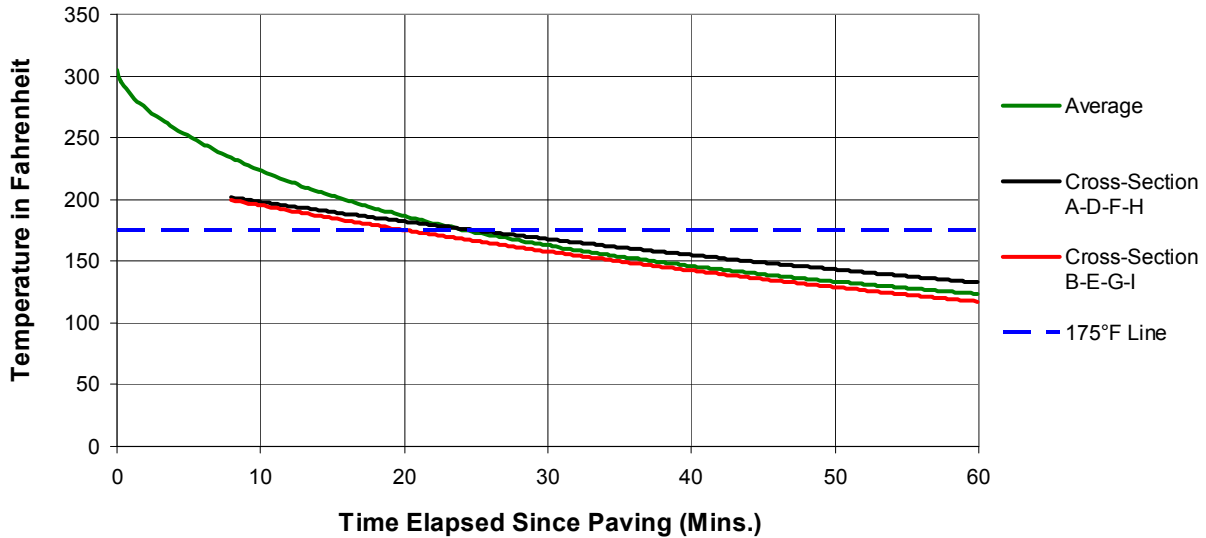
Figure 6.12 – Measured curves compared to calculated average curve with 175°F line

6.4. Conclusions: Comparison of Cooling Curves

As previously stated, the SAW RFID tags and equipment were successful in measuring the mat cooling temperatures during hot-mix asphalt placement. Comparisons with predictions from the finite difference computational models are generally favorable. However, there are inconsistencies between the predicted and measured temperatures, particularly during the early stages of the cooling response that may be due to limitations in technology, operator error, modeling error, or other causes. Therefore, further study is recommended to investigate and/or address the following:

- Recording temperature data immediately after paving rather than a few minutes afterward. This may be accomplished by preheating the tags to the initial asphalt temperature. The RF SAW Reader software can then be adjusted more easily to read the tags immediately after paving.

- The RF SAW Reader and software should be further improved so that one doesn't require setting a temperature window. The elimination of the temperature window would have allowed those tags experiencing a thermal to be read at that time.

- Perform more field trials that incorporate traditional temperature measuring instrumentation (e.g. thermocouples). Comparing the SAW RFID with the traditional instrumentation should identify any limitations or inaccuracies in the SAW RFID technology when being used in this application.

- Determine an encapsulation method and material that may optimize the functionality of the tag in terms of readability, thermal response, and physical survivability. During the field trials, a significant number of tags could not be read.

6.5. Sensitivity Analysis and Calibration Techniques

Laboratory tests to determine the input parameter values for the mat cooling model were not performed in conjunction with this study. Typical input parameters were obtained from the literature review. However, these values varied widely between citations and some of the recommended values were not expected to be sufficiently accurate. Therefore, in order to determine the proper input parameters for the numerical simulations described in the preceding section, a series of sensitivity and calibration analyses were performed. These analyses provided additional confidence and validation that the numerical solutions are logical and correct as well

as producing field-calibrated values for the inputs. The following subsections (6.5.1., 6.5.2., and 6.5.3.) detail sensitivity analyses for the following inputs: thermal diffusivity and conductivity, convective heat transfer coefficient, and emissivity, respectively. A calibration procedure is presented in subsection 6.5.4. to determine the input parameter values that produce the best fit between the measured and calculated temperatures. This field calibration technique enables accurate predictions from the mat cooling model in the absence of laboratory measured input parameters.

6.5.1. Thermal Diffusivity and Conductivity

As stated in Chapter 2, Luca and Mrawira (2005) conducted laboratory experiments to identify Superpave asphalt-concrete thermal properties. They measured thermal diffusivity, α, and thermal conductivity, k, and compared their measured values with ranges cited in the literature (Tables 2.2 and 2.3, respectively).

The sensitivity analyses aim to determine how changes in thermal diffusivity and conduction affect the curvature, rate of cooling, and other characteristics of the predicted cooling response. Note that changes in thermal diffusivity also imply changes in the analysis time step in order to satisfy the stability requirement for the Euler time-integration algorithm (Eqn. 6.1).

As shown on Table 2.2, Luca and Mrawira found that thermal diffusivity may range from 1.35×10^{-2} to 3.20×10^{-2} ft^2/hr. Five sample values within this range were therefore selected for the sensitivity analysis: 1.35×10^{-2}, 1.56×10^{-2}, 2.13×10^{-2}, 2.24×10^{-2}, and 3.20×10^{-2} ft^2/hr. Similarly, Luca and Mrawira found that thermal conductivity may range from 0.58 to 2.24 BTU/ft ̄hr-°F (Table 2.3). Four sampled values within this range were therefore selected for the sensitivity analysis: 0.58, 0.64, 1.01, 1.19, and 2.24 BTU/ft ̄hr-°F. Luca and Mrawira emphasized that

thermal diffusivity and conductivity are generally difficult to predict and measure. Therefore, parameters value that fall outside the ranges in Tables 2.2 and 2.3 should not be considered infeasible.

Figures 6.13 and 6.14 illustrate the results of the sensitivity analyses for thermal diffusivity and conductivity. Changing either the thermal diffusivity or the thermal conductivity values significantly affects the curvature and rate of cooling of the predicted mat cooling response. In order to understand fully the results in Figures 6.13 and 6.14, it is important to remember that thermal diffusivity and conductivity are interrelated:

$$\alpha \quad = \quad \frac{k}{\rho \, C_p} \tag{6.3}$$

in which ρ is the mass density and c_p is the specific heat capacity. Figure 6.13 shows that the rate of cooling increases with increasing thermal diffusivity. This is sensible; from Eq. (6.3), increasing α at constant k implies a decreasing specific heat capacity—i.e., decreasing thermal inertia, hence a faster cooling rate. Figure 6.14 shows that the rate of cooling decreases with increasing thermal conductivity. At first glance this appears paradoxical, as one would intuitively expect that an increased ability to conduct heat would lead to faster cooling. However, the observed behavior is indeed sensible given the relationship in Eq. (6.3): increasing k at constant α implies increasing specific heat capacity—i.e., increasing thermal inertia, hence a slower cooling rate.
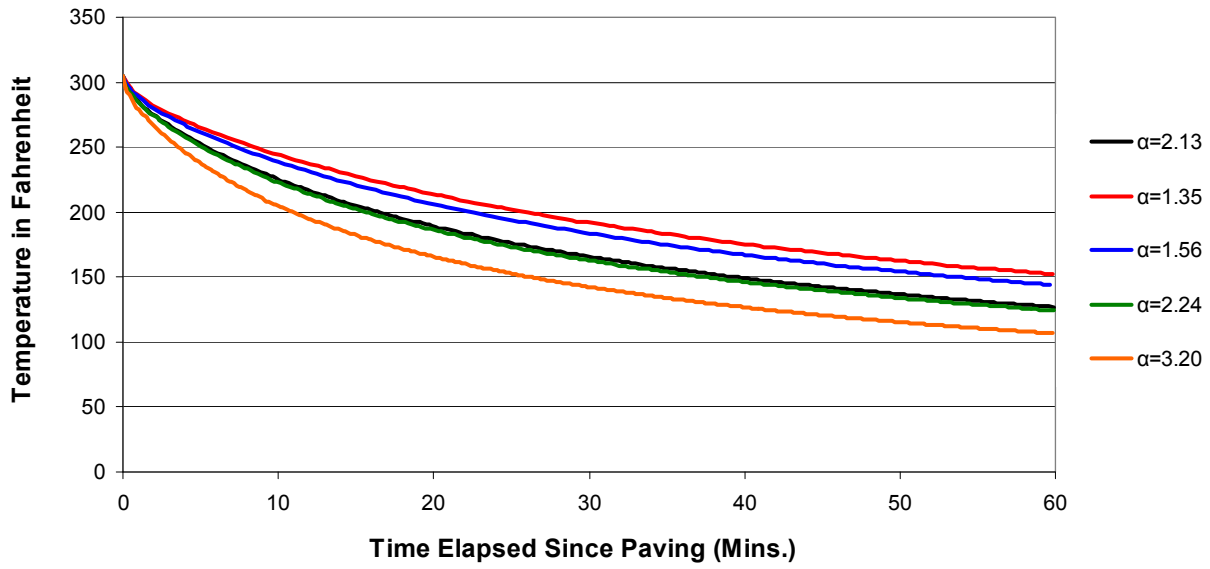
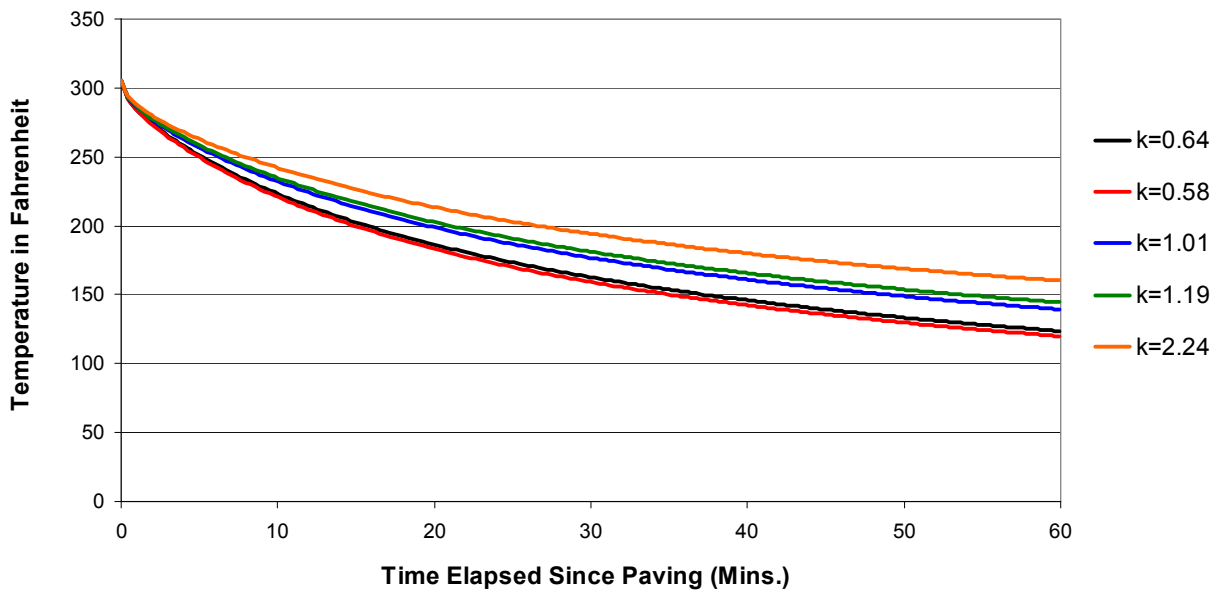Figure 6.12 – Sensitivity analysis for thermal diffusivity (k=0.64 BTU/ft-hr-^{o}F).

Figure 6.13 – Sensitivity analysis for thermal conductivity (α=2.13x10^{-2} ft^{2}/hr).

6.5.2. Convective Heat Transfer Coefficient (h)

Wolfe and Colony (1976 and 1978) developed a relation for estimating convective heat transfer coefficients for an open highway construction environment that considered both free and forced convection principles. After studying various methods for determining the convective heat transfer coefficient h and performing laboratory tests, Wolfe, Colony, and Heath (1983) recommend Eqs. (2.9a) and (2.9b). For this study, there was no wind impact during paving construction.

The sensitivity analysis for the convective heat transfer coefficient aims to determine how changes in convection affect the curvature, rate of cooling, and other characteristics of the predicted cooling response. Table 6.3 displays a series of increasing wind velocities and their correlating value for the convective heat transfer coefficient when using Eqs. (2.9a) and (2.9b). These convective heat transfer coefficients are used as input parameters for the sensitivity analysis. Figure 6.14 illustrates the results.

Table 6.3 – Comparison of Convective Heat Transfer Coefficients

Wind Velocity, mph	Conv. Heat Coeff. (h) $(BTU/ft^2\text{-}hr\text{-}°F)$
0	1.30
2	2.34
4	3.05
6	3.68
8	4.25
10	4.79
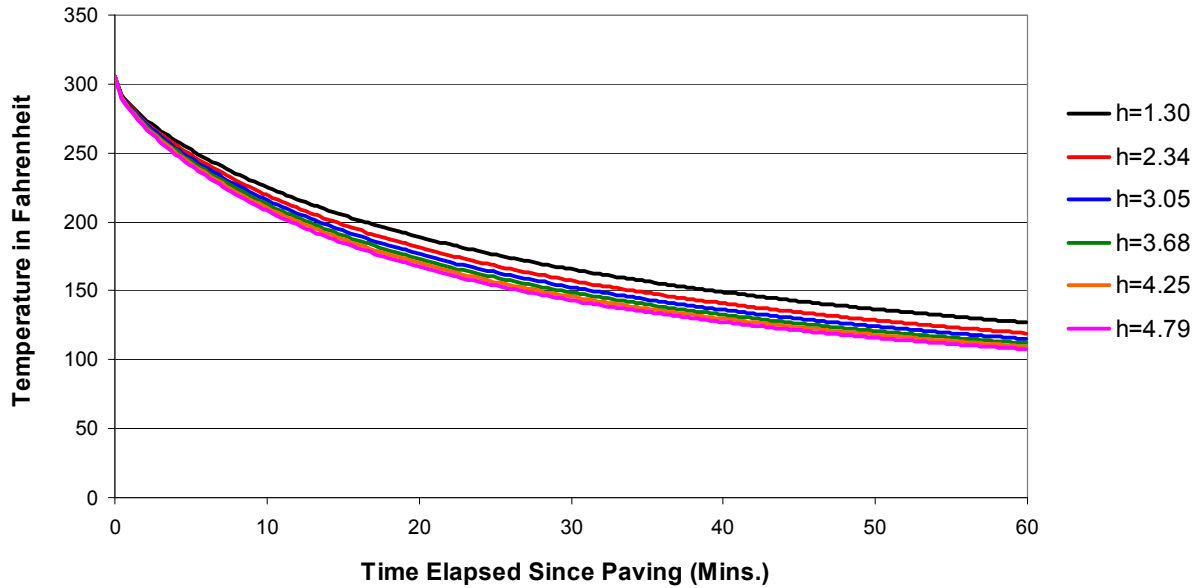
Figure 6.14 – Sensitivity analysis for the convective heat transfer coefficient

Based on the results shown on Figure 6.14, altering the input parameter for the

convective heat transfer coefficient does affect the curvature and rate of cooling of the mat

cooling model. However, it is less significant than the case of thermal diffusivity (Figure 6.12)

or thermal conductivity (Figure 6.13). As the convective heat transfer coefficient increases, the

curvature and rate of cooling increases. This is sensible; an increasing convective heat transfer

coefficient means that more heat is lost via convection through the surface, which in turn will

cause the mat to cool more quickly.

6.5.3. Emissivity (ε)

Emissivity is the pavement surface's relative ability to emit heat energy via radiation. It

is defined as the ratio of the actual heat energy radiated by the pavement to the heat energy

radiated by an idealized object that emits all radiation at the given temperature—i.e., a "perfect

radiator." (Holman, 2001). Wolfe and Colony (1968) recommend a relatively narrow range of 0.90 to 0.95 for the emissivity of an asphalt surface. Therefore, a sensitivity analysis comparing values 0.90 through 0.95 was performed to determine its affect on the curvature, rate of cooling, and other characteristics of the predicted temperature response. Figure 6.16 displays the results from the sensitivity analysis.
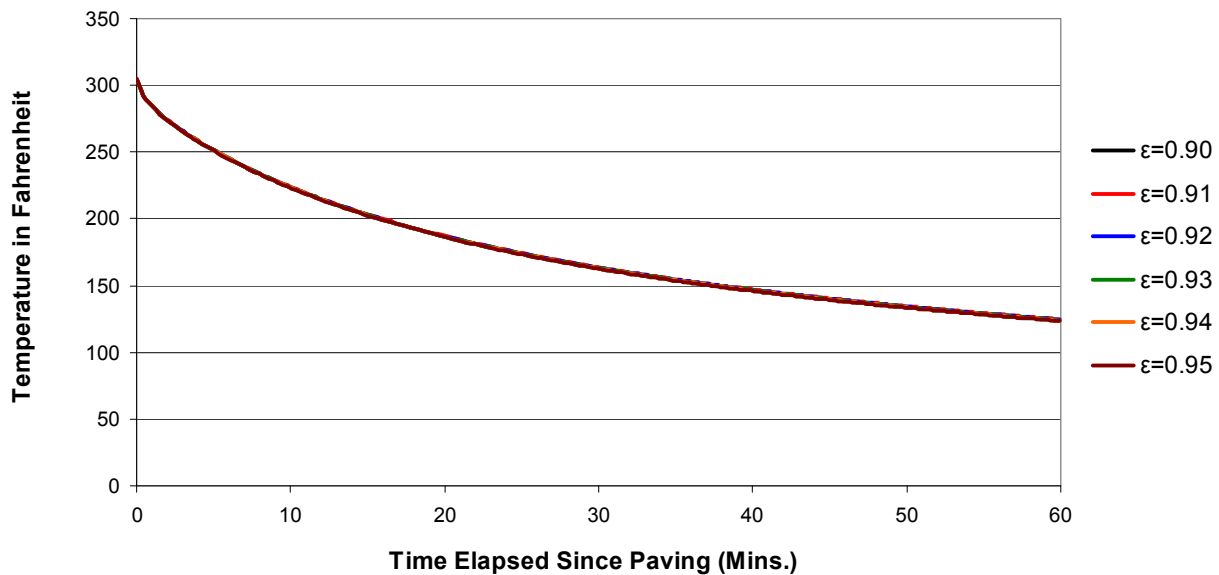
Figure 6.15 – Sensitivity analysis for solar emissivity

Based on the results shown on Figure 6.15, altering the input value for emissivity has little impact to the curvature and rate of cooling of the predicted cooling response.

6.5.4. Input Parameter Optimization and Calibration Techniques

An optimization was performed on the input parameters using Microsoft Excel Solver to determine the input values providing the best agreement between the field measured and calculated temperatures. Based on the literature, it is known that the input parameters (thermal

diffusivity, thermal conductivity, convective heat transfer coefficient, and emissivity) are not easily predicted or measured. Determination of these values through a field calibration process is required to expedite usage of the mat cooling models without requiring laboratory testing to determine the input parameters.

To perform the optimization, the predicted temperatures from the mat cooling model are compared with the actual field-measured temperatures. The sum of the squared residual values between the predicted and measured temperatures is minimized in the Microsoft Excel Solver program by changing the input parameters for thermal diffusivity, thermal conductivity, convective heat transfer coefficient, and emissivity. Constraints are set within the Solver program to prevent negative values for the inputs.

Two optimizations are performed: one that holds the convective heat transfer coefficient h constant at 1.3 (Eqn. 2.9a) and one that also optimizes h through the Solver program. Tables 6.4 and 6.5 summarize the results from both optimizations. Figure 6.16 compares the predicted cooling curves using the input values from the two optimizations.

Table 6.4 – Results of Optimization #1; "h" is constant

Property	Units	Symbol	Used
Thermal conductivity	BTU/ft-hr-°F	k	0.64
Thermal diffusivity	ft^2/hr	α	0.0213
Convective heat transfer coefficient	Dimensionless	h	1.30
Thermal emissivity	Dimensionless	ε	0.95

Table 6.5 – Results of Optimization #2; "h" is optimized

Property	Units	Symbol	Used
Thermal conductivity	BTU/ft-hr-°F	k	0.49
Thermal diffusivity	ft^2/hr	α	0.0212
Convective heat transfer coefficient	Dimensionless	h	0.42
Thermal emissivity	Dimensionless	ε	0.93
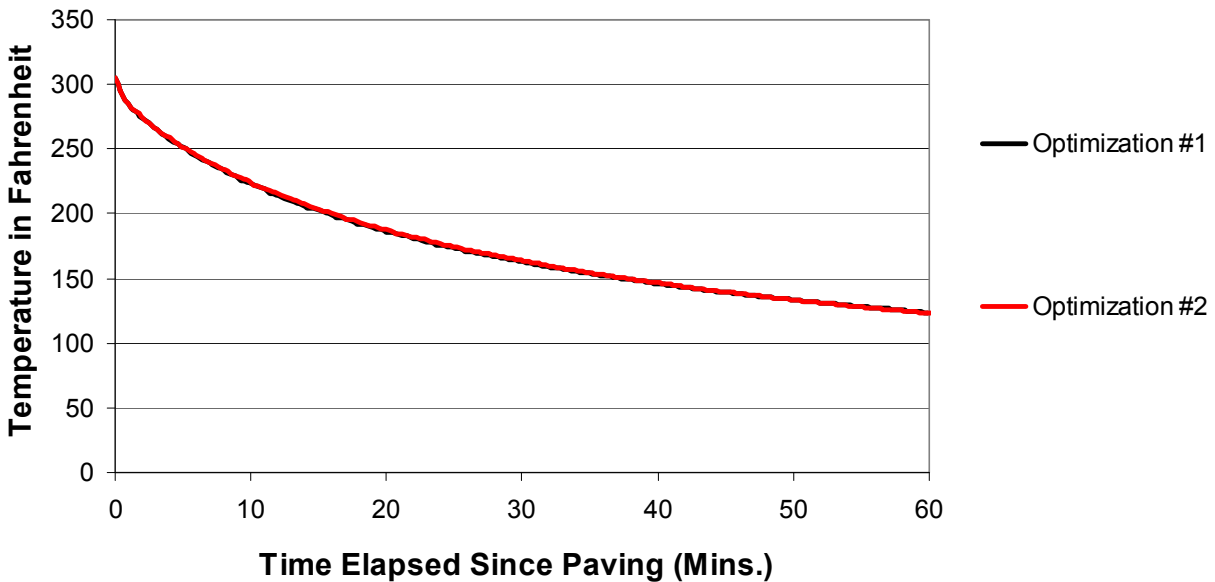
Figure 6.16 – Comparing both sets of optimized input parameters with mat cooling model

As is clear in Figure 6.16, both sets of optimized input parameters produce nearly identical calculated average cooling curves. Therefore, as a result of the sensitivity analysis and recommendations from the literature, the selected input parameters for usage in this study shall be taken from Table 6.4, with the value of the convective heat transfer coefficient as

recommended by Wolfe, Colony, and Heath (1983). However, Table 6.5 would have sufficed as well.

As demonstrated by these successful optimizations, Microsoft Excel Solver may be used to accurately field-calibrate thermal diffusivity, thermal conductivity, convective heat transfer coefficient, and emissivity. For any specific paving construction project, these input parameters may be determined by field calibration to limited field temperature measurements at the beginning of the project, eliminating the need for complex laboratory testing.

6.6. Conclusions: Sensitivity Analysis and Calibration Techniques

Each of the major input parameters was analyzed for its individual impact on the predicted cooling response. These sensitivity analyses provide added confidence that the numerical solutions are logical and correct. The following results were obtained:

- For thermal diffusivity: based on the results shown on Figure 6.12, altering the input parameter for thermal diffusivity does significantly affect the curvature and rate of cooling of the predicted response. As the value for thermal diffusivity increases, the curvature and rate of cooling increases.

- For thermal conductivity: based on Figure 6.13, altering the input parameter for thermal conductivity does significantly affect the curvature and rate of cooling of the model. As the value for thermal conductivity increases, the curvature and rate of cooling decreases.

- For the convective heat transfer coefficient: based on the results shown on Figure 6.14, altering the input parameter for the convective heat transfer coefficient does affect the curvature and rate of cooling of the mat cooling model. As the value for the convective heat transfer coefficient increases, the curvature and rate of cooling increases.

86

- For solar emissivity: based on the results shown on Figure 6.15, altering the input

   parameter for solar emissivity has little impact to the curvature and rate of cooling of the

   mat cooling model.

An optimization process was performed to determine the best input parameter values for
this study. That Microsoft Excel Solver analysis tool may be used to field-calibrate thermal
diffusivity, thermal conductivity, convective heat transfer coefficient, and solar emissivity
values. For any specific paving construction project, these input parameters may be determined
by field calibration to limited field temperature measurements at the beginning of the project,
eliminating the need for complex laboratory testing.

Chapter 7: Conclusions and Lessons Learned

As stated in Chapter 1, the overall purpose of this thesis was to evaluate RFID-based wireless temperature sensors and traditional asphalt mat cooling models in conjunction with the Federal Highway Administration Pooled-Fund Study on Intelligent Compaction (TGI, 2010). More specifically, the objectives are as follows:

1. Evaluate the feasibility of using Surface Acoustic Wave (SAW) based Radio-Frequency Identification (RFID) technology to measure HMA temperatures via wireless sensors.

2. Demonstrate, in the field, the survivability and temperature measurement capabilities of the SAW RFID sensors during a pavement overlay.

3. Consolidate data to develop asphalt cooling curves of measured temperature versus time.

4. Compare measured cooling response with predictions from theoretical mat cooling models.

5. Perform a sensitivity analysis of the effect of relevant input parameters in the theoretical mat cooling models on the predicted cooling response. From the sensitivity analysis, explore field-calibration techniques to expedite the usage of the mat cooling models without requiring laboratory measured input parameters.

Based on the evaluations and experiments performed in this thesis, the following conclusions were reached regarding the above-mentioned objectives:

7.1. Laboratory Evaluation

Through laboratory analysis and information from the literature, an encapsulation process was developed to protective the SAW RFID tags from physical damage (during construction) while promoting heat transfer. Details of this process are given in Chapter 4. It is recommended that additional work be performed to determine the minimum thinness of the epoxy coating to optimize tag readability while ensuring survivability.

In terms of signal strength and readability, both the encapsulated monopole and patch antenna tags showed acceptable performance when encased in HMA specimens. The monopole tags, while more practical and compact in size, do not perform as reliably as the patch tags in terms of signal strength and readability. Both tags performed the best when aligned closely to "orientation #1/rotation #1" (see Figures 4.5 and 4.6). Regarding thermal response, a thermal lag was observed after exposing the encapsulated tags to hot material. This lag is defined as the time required for the tag to "heat up" to match its environment. The encapsulated single patch tags required the longest thermal lag of about 5 minutes.

7.2. Field Evaluation

Overall, the findings from the field evaluation were that the RF SAW RFID tags can successfully measure asphalt mat cooling temperatures during paving and compaction. It is important to note SAW RFID is a developing technology – certain constraints and imperfections exist, and improvements in the technology are expected in the future. The following subsections summarize the conclusions from the field evaluation in terms of field test performance, field test results, and variability and reliability:

7.2.1. Field Test Performance

The RF SAW tag reader requires a narrow temperature window in order to read the in-place tags. The lead to operation issues in the field, especially during the early stages of the asphalt cooling when temperatures dropped rapidly. The manufacturer recommends a 30 degree temperature window based on their calibration techniques at room temperature. It is recommended that additional future field tests be performed to more closely monitor the initial temperature of the HMA, perhaps by pre-heating the tags so that they may be read immediately after paving. Alternatively, the manufacturer of the SAW RFID technology could eliminate the use of a temperature window from the reader software.

There was also difficulty discerning permanently damaged tags from those that simply could be read immediately after paving/compaction. In other words, if a tag is nonresponsive to the RF SAW reader, it might not be due to being destroyed due to high temperatures or vibratory compaction. It may be that the reader cannot get a response because the temperature window is incorrect or the tag's signal is severely attenuated.

7.2.2. Field Test Results

The field results generally show an exponential relationship between cooling temperatures and time. This generally agrees with theoretical considerations that suggest exponential cooling. No systematic temperature variations with depth were observed during mat cooling. In other words, the measured temperatures at the bottom, middle, and top of the asphalt mat, at any given location and time, were all within the variability range of the sensors. This may simply be a consequence of the thinness of the lift on this particular project.

7.2.3. Variability & Reliability

Based on the comparative study at the bottom of the mat between two sets of tags (single patch and monopole) and previous laboratory testing, the temperatures recorded by the two tag types are reasonably consistent and accurate. The comparative study at the surface of the mat between the FLUKE infrared thermometer and monopole tag found larger inconsistencies between the two sets of readings. This may due to testing at different locations on the mat surface. Additional field and/or laboratory testing are recommended to resolve this issue.

7.3. Comparisons Between Measured and Predicted Mat Cooling Response

RF SAW RFID tags and equipment can be used successfully for measuring the mat cooling temperatures during hot-mix asphalt placement. Predicted temperatures from the theoretical heat transfer model (using input parameters obtained from the literature and through field calibration) agreed favorably with field measurements. However, there are inconsistencies between the two that may either be due to limitations in the technology or to operator error. Further testing is recommended to investigate and remediate the following:

- Recording temperature data immediately after paving rather than a few minutes afterward. This may be accomplished by preheating the tags to the initial asphalt temperature – during laboratory testing, the tags exhibit a thermal lag to meet their intended temperature. The RF SAW Reader software may then be adjusted to read the tags accordingly; or simply improved by the manufacturer.
- Incorporate traditional thermocouple temperature sensors that have been used successfully in the past. Comparing the SAW RFID with the traditional equipment can better identify any limitations in the SAW RFID technology for this application.

- Refine the encapsulation process to optimize readability and survivability. During the field trials, there was difficulty discerning physically damaged tags from those that simply could not be read immediately after paving/compaction. In other words, if a tag is nonresponsive to the reader, it might not be due to destruction by vibratory compaction. It may be that the reader cannot get a response because the temperature window is incorrect or the tag's signal is severely attenuated.

7.4. Sensitivity Analysis and Calibration Techniques

Sensitivity analyses were performed on key input parameters and a field calibration procedure was developed to optimize the accuracy of the theoretical cooling response predictions. The following conclusions were drawn from these analyses:

- Increasing thermal diffusivity increases the curvature of the cooling curve and the rate of cooling.

- Increasing thermal conductivity reduces the curvature of the cooling curve and the rate of cooling.

- Increasing the convective heat transfer coefficient increases the curvature of the cooling curve and the rate of cooling.

- Emissivity has little impact on the predicted cooling response.

- The input parameter values for this study were determined through a field calibration process. Microsoft Excel Solver may be used to optimize the thermal diffusivity, thermal conductivity, convective heat transfer coefficient, and emissivity values to minimize the discrepancies between predicted and measured temperatures. For any specific paving construction project, these input parameters may be determined by field calibration to

limited field temperature measurements at the beginning of the project, eliminating the need for complex laboratory testing.

7.5. Lessons Learned

Based on the experiences and results of this study, the following lessons were learned:

- The encapsulation of the tags should be uniformly and minimally thin. In this study, the thickness of the encapsulant for each tag varied slightly, causing variability in the laboratory and field test results.

- To determine if there is the possibility of systematic variation within a pavement layer, future testing should be performed on thicker pavement overlays. It was difficult to discern systematic variations in temperature vs. depth for the very thin 1.5 inch overlay examined in this study.

- Future field trials should be performed under daytime condition so that the solar absorption terms in the mat cooling models can be exercised and evaluated.

Appendix A

This appendix serves to present work in conjunction with that stated in Chapter 4.

In reference to the read range study performed on encapsulated tags within asphalt specimens, the following figures display results using Orientations #2 through #6 for both monopole and single patch tags:
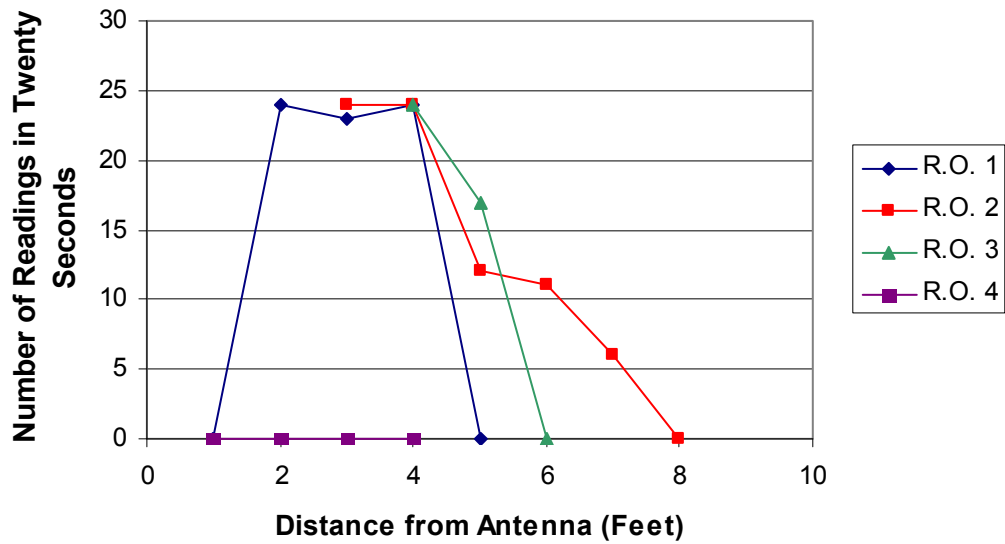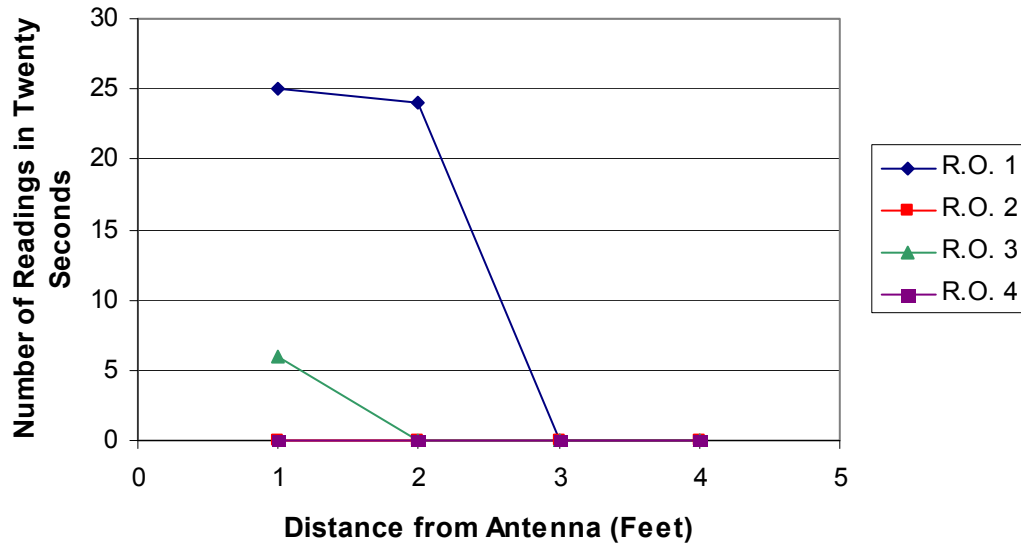
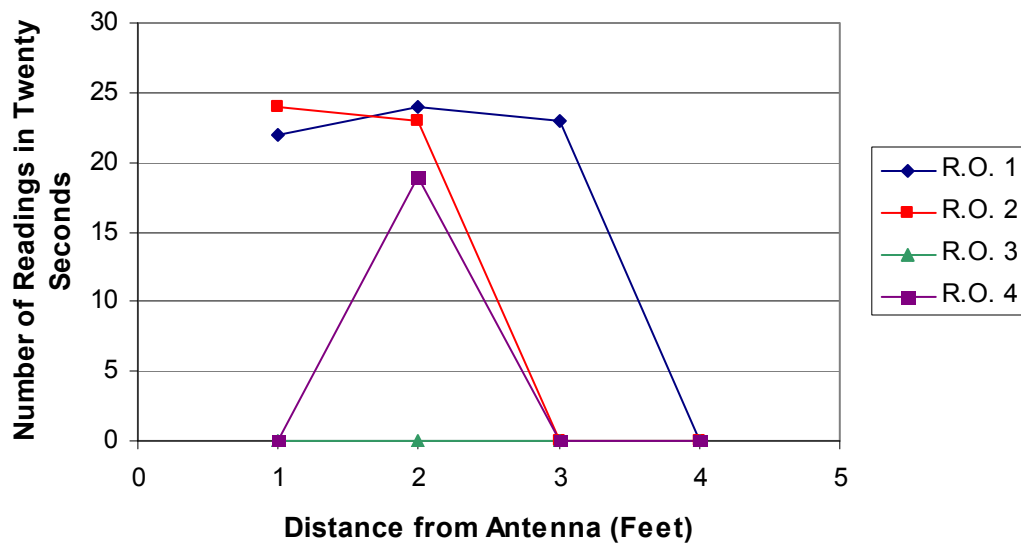**Monopole Tag, Circular Polarization, Orientation #2**
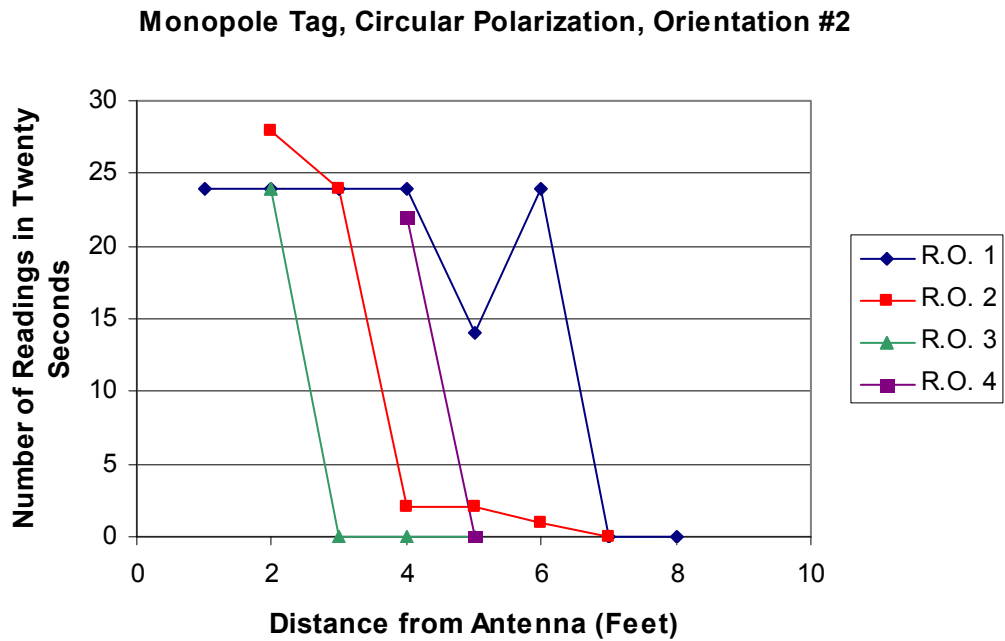
Monopole Tag, Circular Polarization, Orientation #3
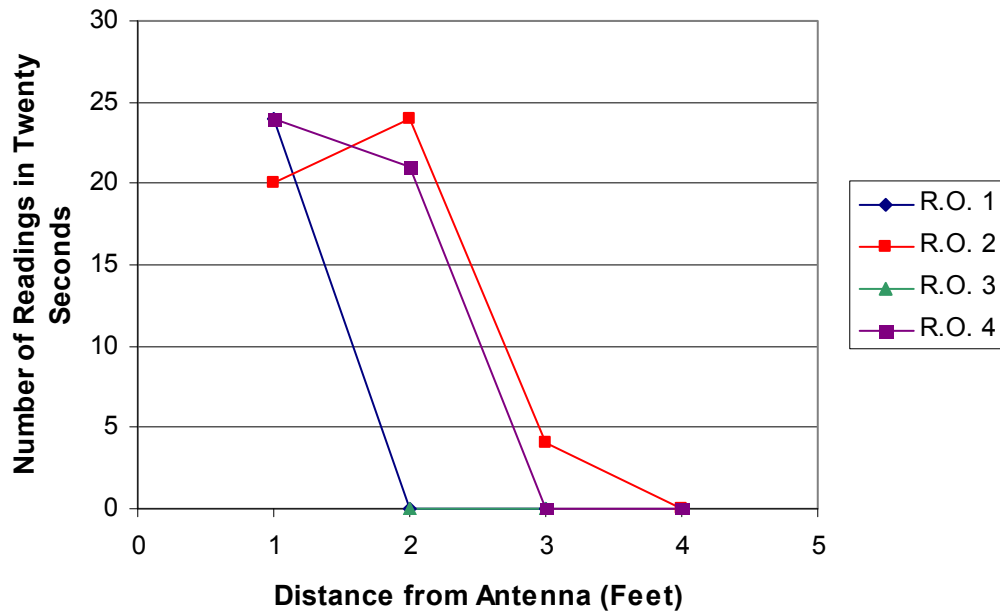
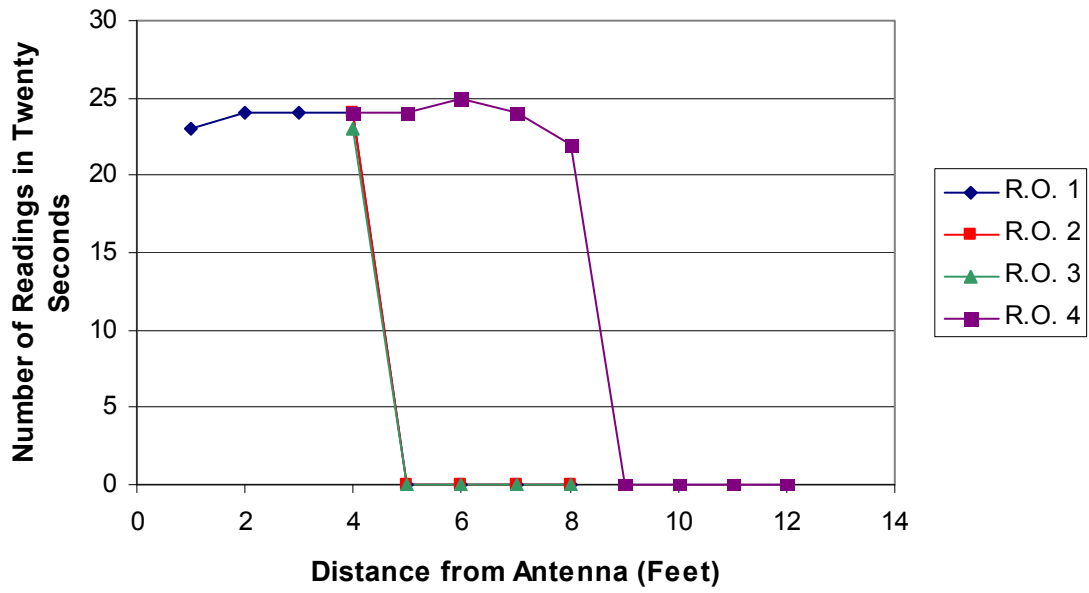## Monopole Tag, Circular Polarization, Orientation #4

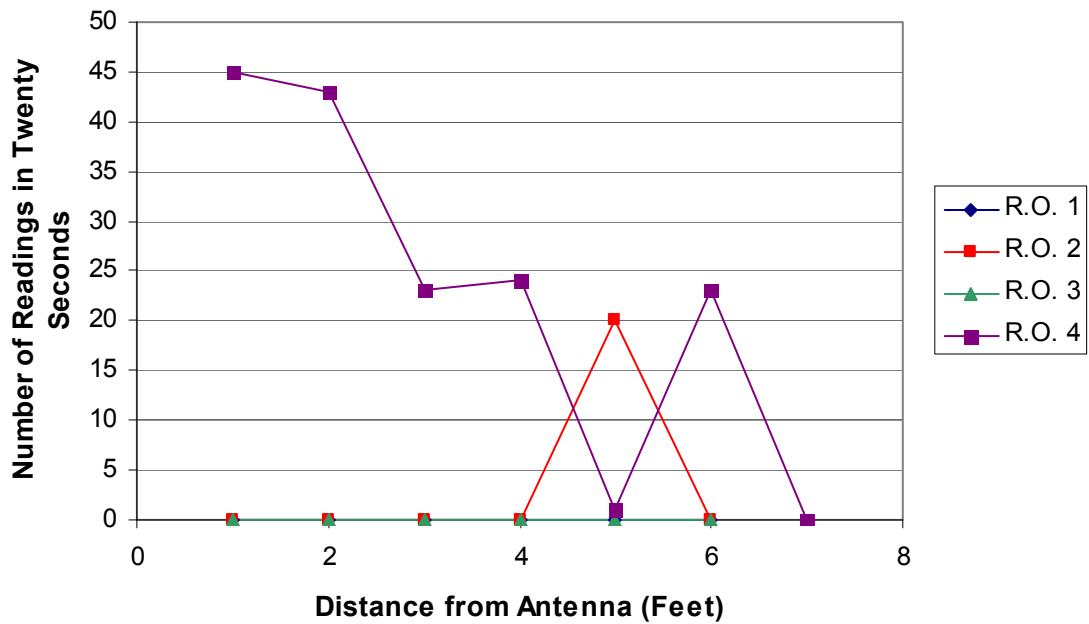**Monopole Tag, Circular Polarization, Orientation #5**

Monopole Tag, Circular Polarization, Orientation #6

Single Patch Tag, Circular Polarization, Orientation #2

Single Patch Tag, Circular Polarization, Orientation #3

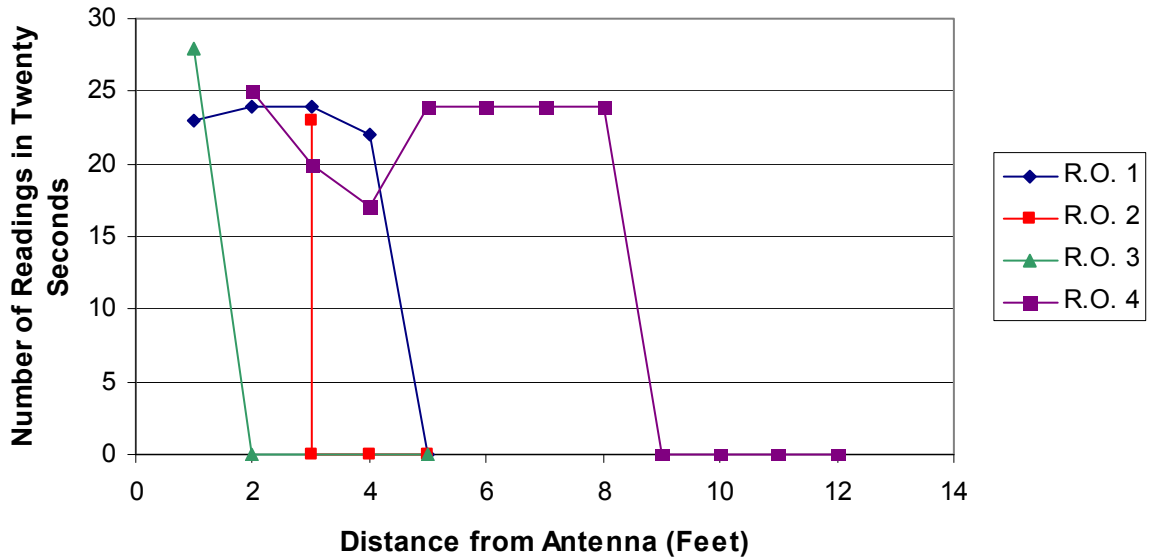## Single Patch Tag, Circular Polarization, Orientation #4

Single Patch Tag, Circular Polarization, Orientation #5
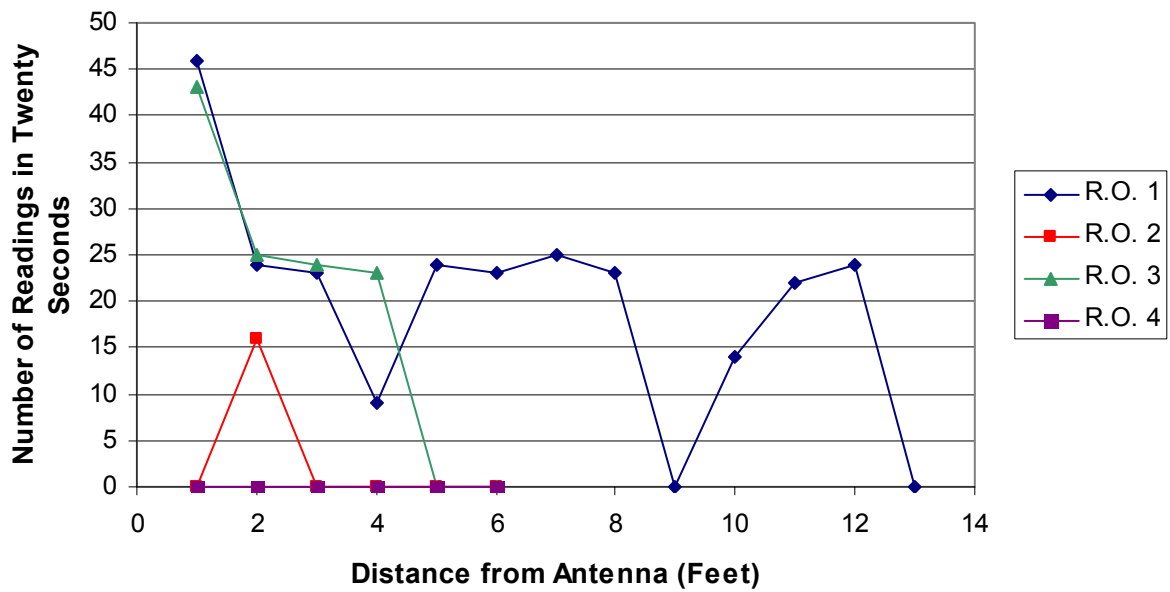
Single Patch Tag, Circular Polarization, Orientation #6
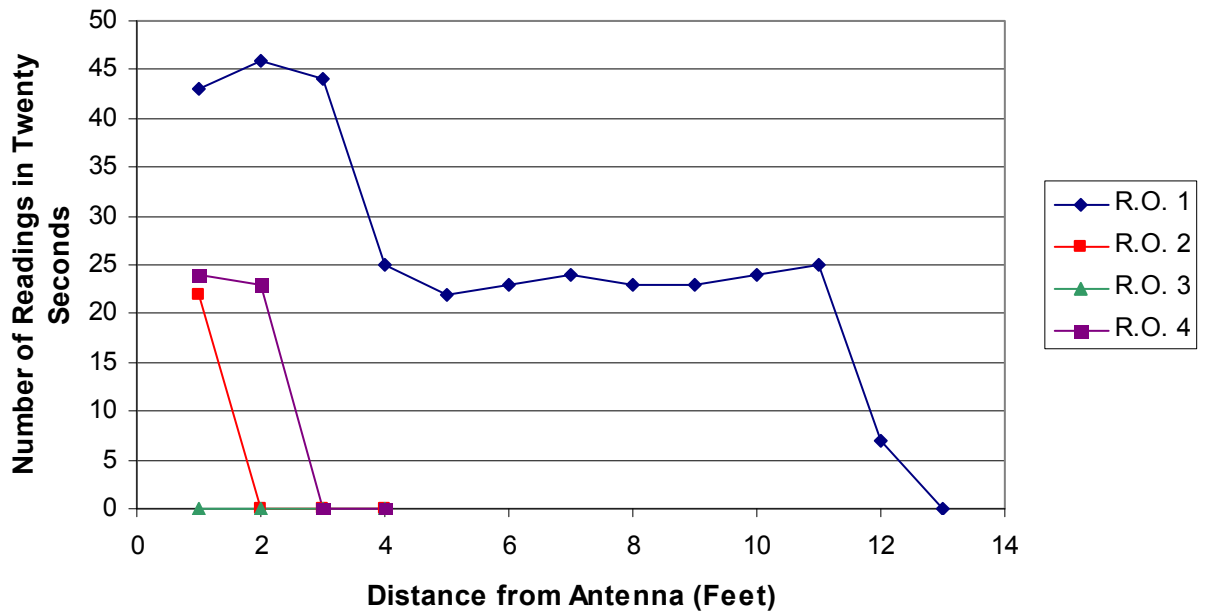
Appendix B

This appendix serves to present work in conjunction with that stated in Chapter 5.

The following figures are from cross-section A-D-F-H:

A-D-F-H (Bottom of Mat)
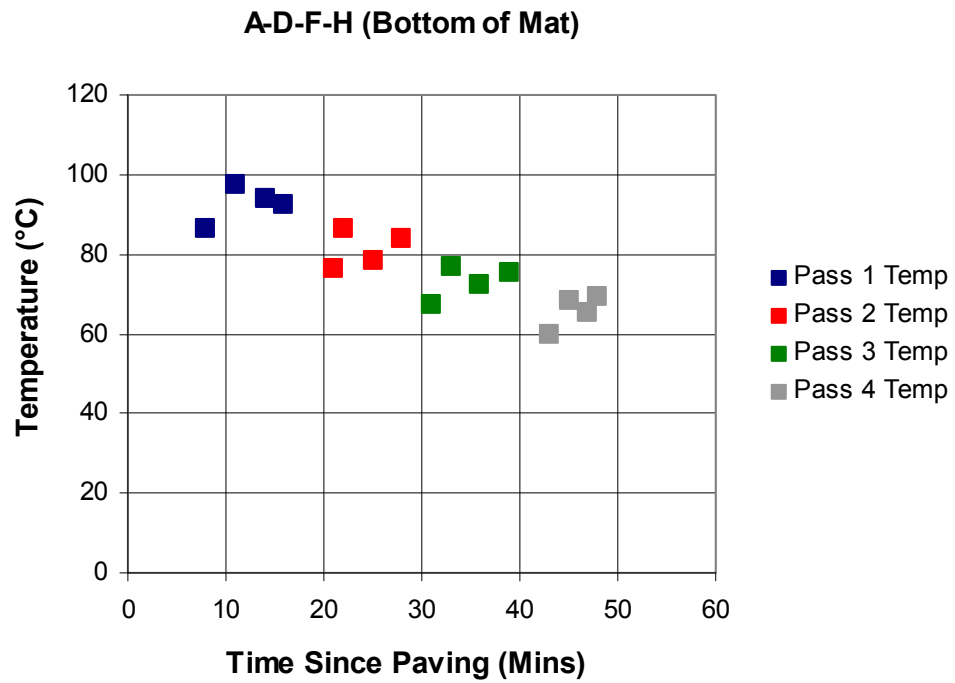
A-D-F-H (Middle of Mat)
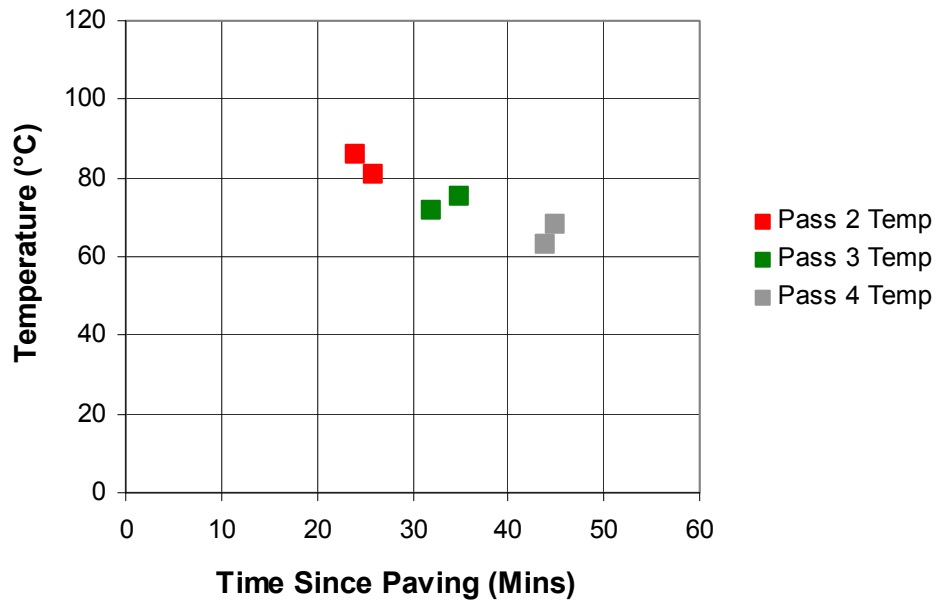
A-D-F-H (Surface of Mat)
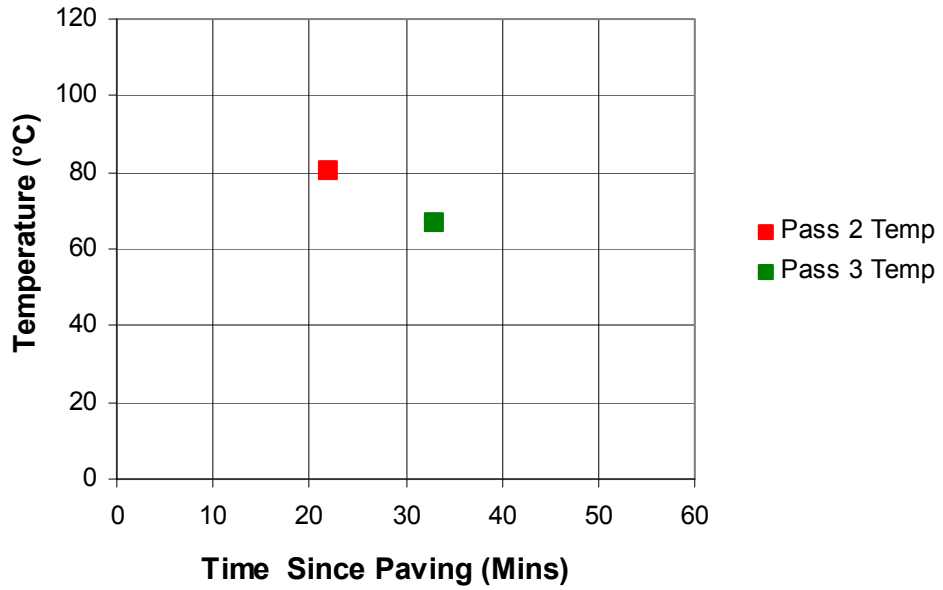
A-D-F-H (Depth of Section; Temperature Vs. Time)

$y = 101.47e^{-0.0093x}$

$R^2 = 0.7521$

$y = 110.39e^{-0.0117x}$

$R^2 = 0.8553$
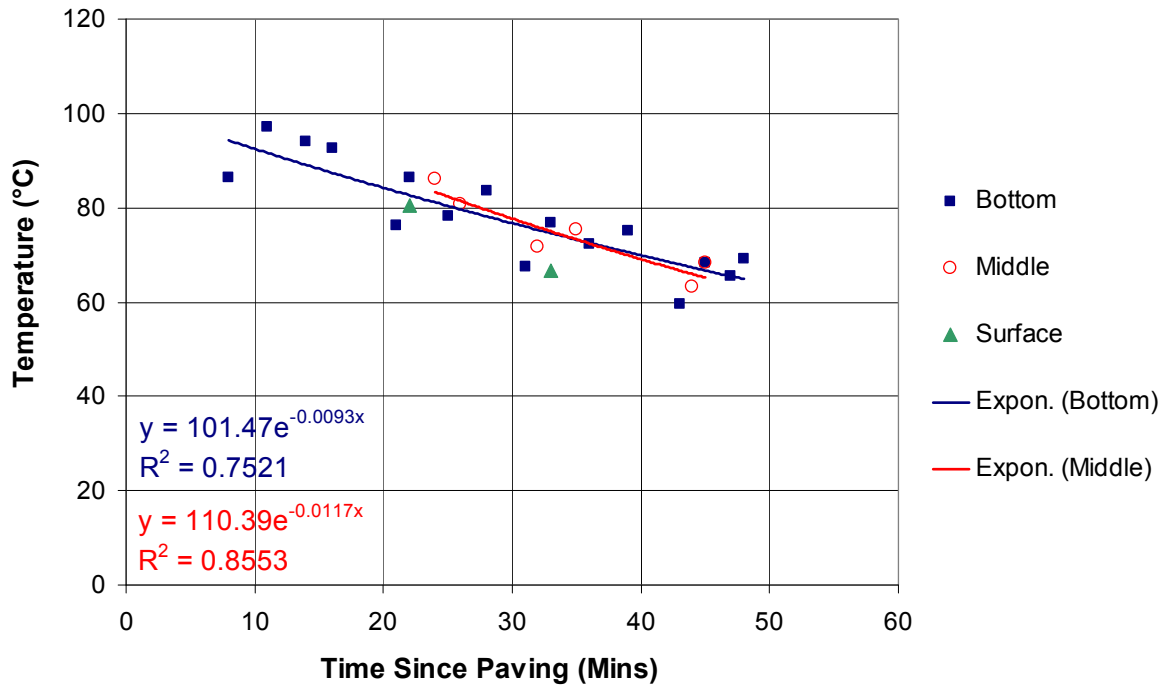
A-D-F-H (Depth of Section; All Temperatures Read)

$y = 101.87e^{-0.0096x}$
$R^2 = 0.7504$

- Time Since Paving (Mins)
- Temperature (°C)

■ All Pts A-D-F-H

— Expon. (All Pts A-D-F-H)
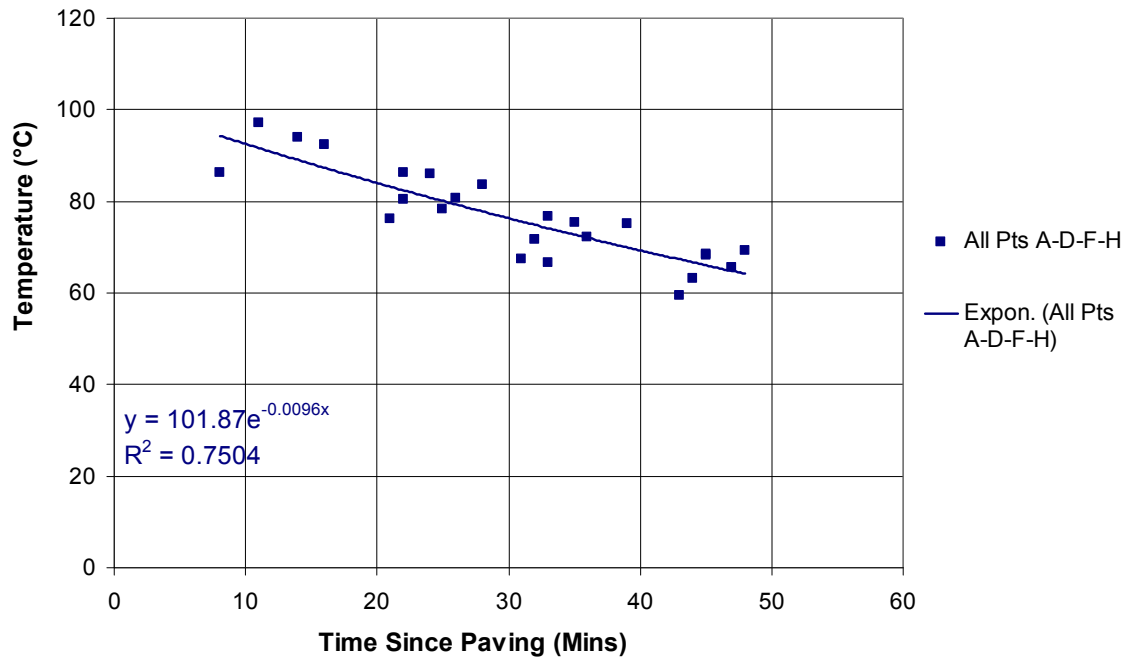
The following tables are the raw-collected in-field test data:

Group A	Single Patch 0ACF	Monopole 03A8	Elev. Mono. 0A32	Surface 0A36	Time (min)			
Pre-Paving	25.7	24.3	28.4		0	0	0	
Pass 1	86.3				8			
Pass 2	76.1	74.7		80.5	21	21		22
Pass 3	67.4	65	71.6	66.7	31	31	32	33
Pass 4	59.6	57	63.3		43	43	44	

Group B	Single Patch 09FE	Monopole 09FB	Elev. Mono. 0508	Surface 09D8	Time (min)			
Pre-Paving	25.4		24.9		0		0	
Pass 1	91.9				8			
Pass 2	75.2			66.3	21			22
Pass 3	64.9	64.7	64.2	55	31	32	32	33
Pass 4	56.9		56.4	44.2	43		44	44

Group C	Single Patch 0AEC	Monopole 05FC	Elev. Mono. 002D	Surface 08C8	Time (min)			
Pre-Paving	25.4		23.1		0		0	
Pass 1								
Pass 2								
Pass 3								
Pass 4								

	Single Patch	Monopole	Elev. Mono.	Surface	Time (min)			
Group D	0C14	02BD	0BE9	051A				
Pre-Paving	30.4		27.7		0		0	
Pass 1	97.2				11			
Pass 2	86.3		86		22		24	
Pass 3	76.7		75.3		33		35	
Pass 4	68.4	67.7	68.3		45	45	45	

	Single Patch	Monopole	Elev. Mono.	Surface	Time (min)			
Group E	0BB9	0A29	0BE3	03E2				
Pre-Paving	24.5	30.2	25.1		0	0	0	
Pass 1	83.5		93.3	104.4	11		12	13
Pass 2	75.9		80	76.5	23		24	25
Pass 3	67.3		69.4	65.4	33		35	36
Pass 4	59.6		61.9	57	45		46	46

Group F

	Single Patch	Monopole	Elev. Mono.	Surface	Time (min)		
	0916	0AB2	03EF	06E2			
Pre-Paving	28.6	27.2	22.3		0	0	0
Pass 1	93.9				14		
Pass 2		78.2	80.8			25	26
Pass 3	72.2	69.5			36	36	
Pass 4	65.5	63.1			47	47	

Group G

	Single Patch	Monopole	Elev. Mono.	Surface	Time (min)		
	09F0	01CA	09C8	0941			
Pre-Paving	25.5		28		0		0
Pass 1							
Pass 2	78.8				25		
Pass 3	68.3				36		
Pass 4	60.9				47		

Group H

	Single Patch	Monopole	Elev. Mono.	Surface	Time (min)		
	09CC	0BBB	013C	0645			
Pre-Paving	31	26.4			0	0	
Pass 1	92.5				16		
Pass 2	83.7	76.2			28	28	
Pass 3	75.1	68.2			39	39	
Pass 4	69.3	62.7			48	48	

	Single Patch	Monopole	Elev. Mono.	Surface			
Group I	0BA7	0B32	013C	0214	Time (min)		
Pre-Paving	26.7	27.7	22.2		0	0	0
Pass 1	82.3				17		
Pass 2	73.1	75.3	80		28	28	28
Pass 3	64.5	67.7	69.3		39	39	39
Pass 4	58.7	61.9	62.2		48	49	49

	Single Patch	Monopole	Elev. Mono.	Surface			
Group J	08EE	04A7	0248	0423	Time (min)		
Pre-Paving	28.6	25.9	21.2		0	0	0
Pass 1	89.9		97.8		17		18
Pass 2			74				29
Pass 3			63.6				40
Pass 4			56.9				50

Chapter 8: References

Colony, D.C. and Wolfe, R.K., (1978), "Initial Cooling of Asphalt Concrete Mats,"

      Transportation Engineering Journal, ASCE, Vol. 104, No. TE3, pp. 295-310.

Corlew, J.S. and Dickson, P.F., (1968), "Methods for Calculating Temperature Profiles of Hot-

      Mix Asphalt Concrete as Related to the Construction of Asphalt Pavements," The

      Association of Asphalt Paving Technologists.

Holman, (2001), <u>Heat Transfer</u>, Ninth Edition, McGraw-Hill.

Jordan, P.G. and Thomas, M.E., (1976), "Prediction of Cooling Curves for Hot-Mix Paving

      Materials by a Computer Program," Department of the Environment TRRL Report LR

      729, Transport and Road Research Laboratory.

Kreith, F. and W.Z. Black, (1980), <u>Basic Heat Transfer</u>, Harper & Row, New York.

Luca, Joseph and Mrawira, Donath, (2005), "New Measurement of Thermal Properties of

      Superpave Asphalt Concrete," Journal of Materials in Civil Engineering, ASCE, Vol. 17,

      No. 1.

RF SAW, Inc., (2010), "RF SAW – One Tag Worldwide," <http://www.rfsaw.com/>

Schwartz, C.W. and Khan, J.S., (2008), "Tracking HMA Placement Using RFID Technology,"

      Department of Civil and Environmental Engineering, University of Maryland.

The Transtec Group, Inc. (TGI), (2010), "Intelligent Compaction,"

      <http://www.intelligentcompaction.com/>

V.R. Voller, et al, (1998), "A Computer Tool for Predicting the Cooling of Asphalt Pavements," Proceedings of the International Conference on Cold Regions Engineering.

Wolfe, R.K. and Colony, D.C., (1976), <u>Asphalt Cooling Rates: A Computer Simulation Study</u>, Final Report on Ohio Department of Transportation Project 2844.

Wolfe, R.K., Heath, G.L, and Colony, D.C., (1983), "Cooling Curve Prediction of Asphaltic Concrete," Journal of Transportation Engineering, ASCE, Vol. 109, No. 1.